A MATHEMATICAL MODEL OF COAL-FIRED FLUIDISED BED BOILERS

by

WILTON LAMON MARKS

A THESIS SUBMITTED IN FULFILMENT OF THE REQUIREMENT FOR THE DEGREE OF DOCTOR OF PHILOSOPHY

THE UNIVERSITY OF ASTON IN BIRMINGHAM

APRIL 1973

S U M M A R Y

A mathematical model of a large coal-fired fluidized bed boiler for power generation is synthesised. The effect of variations in the main parameters of the model on variables such as the background carbon concentrations in the bed, and the transient response of heat evolution are studied.

The mechanisms of solids mixing within the bed, combustion and the flow of heat to the boiler tubes are shown to result in a characteristic dynamic response, knowledge of which is essential for the proper control and regulation of a practical system.

A C K N O W L E D G E M E N T

An acknowledgement of gratitude is made to the National Coal Board for permission to submit this thesis.

A great deal of encouragement and assistance was given by colleagues at the Coal Research Establishment, in particular by E. M. Healey, who acted as the University Supervisor throughout this project. Invaluable assistance was given by D. H. Stockwell in much of the formulative stages of discussion and in checking the text. Mrs. A. Setchell developed the computer programs of the model, and carried out the computations that followed.

Any views expressed are those of the author, and not necessarily those of the National Coal Board.

C O N T E N T S

LIST OF FIGURES

C H A P T E R 1

INTRODUCTION

INTRODUCTION

The use of fluidised combustion has been suggested as an alternative to pulverised fuel (p.f.) combustion for electrical power generation. Patent specifications [1, 2] filed in 1957 by Badische Anilin and Soda Faberik, as well as the National Coal Board describes the combustion of gaseous, liquid or fine solid fuel in a fluidised bed of granular refractory. The heat of combustion is used to raise steam in pipes immersed in the fluidised bed. The combustor comprises a shallow bed of ash about 0.75 m in depth. This is fluidised with air through a perforated base and fed with crushed coal (~1.5 mm) at the requisite rate for power generation. The oxygen for combustion is provided by the fluidising air. A good brief outline of the background work on fluidised combustion is given by Skinner [3].

The basic principle employing fluidised combustion for power generation is shown in Figure 1.1. Crushed coal is blown in at the base of the fluidised bed of ash. The fluidising air enters the bed from a plenum chamber through a perforated base. Combustion of 90% of the coal takes place in the fluidised bed at about 850°C. The steam tubes are immersed in the hot ash. Combustion efficiency is increased still further in the freeboard above the fluidised bed and may reach 97-98%. Approximately half the heat evolution is absorbed by the coolant to generate steam, while the other half is carried by the off gases. Heat recovery from the off gases is in two stages. In the first stage (economiser) about half the enthalpy of the gas is transferred to the water in

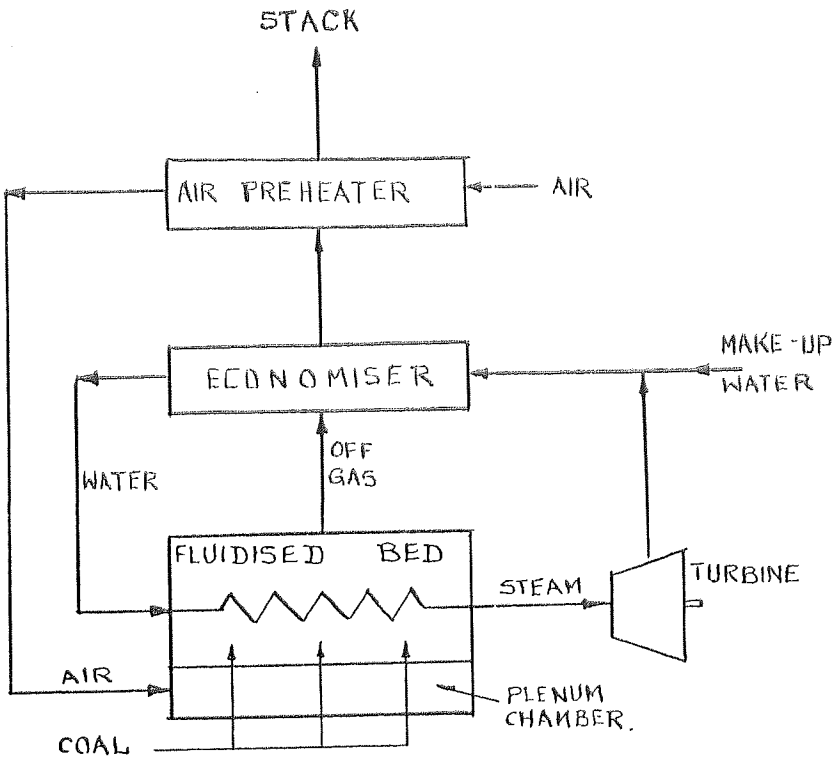

FIGURE 1.1 BLOCK DIAGRAM OF FLUIDISED COMBUSTION SYSTEM FOR POWER GENERATION

the coolant circuit, while in the second stage (heat exchanger) the fluidising air is preheated. Again about half the remaining heat in the off gas is recovered, leaving about 12.5% of the heat evolution as stack losses in the gas.

The essential merit of the process is the exploitation of the high heat transfer coefficient from bed to coolant. Heat transfer fluxes between three and five times greater than those obtained in the convective passes of a conventional boiler can be expected from a fluidised bed system. The relatively low temperature (850^{o}C) of operation of a fluidised bed boiler when compared with flame temperatures of up to 1800^{o}C in a conventional p.f. boiler results in a number of important advantages. At the low combustion temperatures in fluidised beds the vapour pressure of the alkali halides is several orders of magnitude lower than in normal boilers, and hence fouling and corrosion of the steam tubes is minimal. Thus, there is no necessity for 'soot blowing' and the heat transfer coefficients are not impaired by deposits. Because of the absence of corrosion, higher steam temperatures might be economic. Considerable economy and versatility results from the ability to burn high ash content coals, and coals with normal 'viscous' ashes without clinkering. Since the coal size is -1.5 mm rather than pulverised fuel, much of the milling equipment for the coal preparation is obviated. The nature of a fluidised bed with a comparatively long residence time allows the possibility of removal of sulphur by the addition of limestone to reduce pollution. The low combustion temperature also results in lower production of oxides of nitrogen. Finally, the

thermal inertia of the fluidised bed ensures sustained combustion, and offers improved possibilities of regulation and control.

A possible layout for a power generation station using fluidised bed boilers is shown in Figure 1.2. Three sets of turbines together with their fluidised bed boilers and ancilliary equipment are provided to give flexibility for load demand as well as accommodate shut-down of part of the plant for repairs and servicing.

In any project of such a magnitude the essential stages are in order:

(a) the preliminary demonstration of the technical and economic viability of the idea;

(b) the design of the full-scale process;

(c) the design and operation of a pilot plant for experimental and development purposes.

The function of a pilot plant is to provide facilities for engineering development as well as give sufficient confidence in the process to justify commercial investment in a full-scale plant. Thus, the pilot plant must be truly representative of the full-scale process so that there are no problems in scale-up. It is the primary object of this thesis to provide a mathematical model of a fluidised bed boiler so that the problems of scale-up from the pilot plant can be minimised. To achieve this, the model and pilot plant must relate at least to a complete fundamental unit of the process. One design study of a full-scale

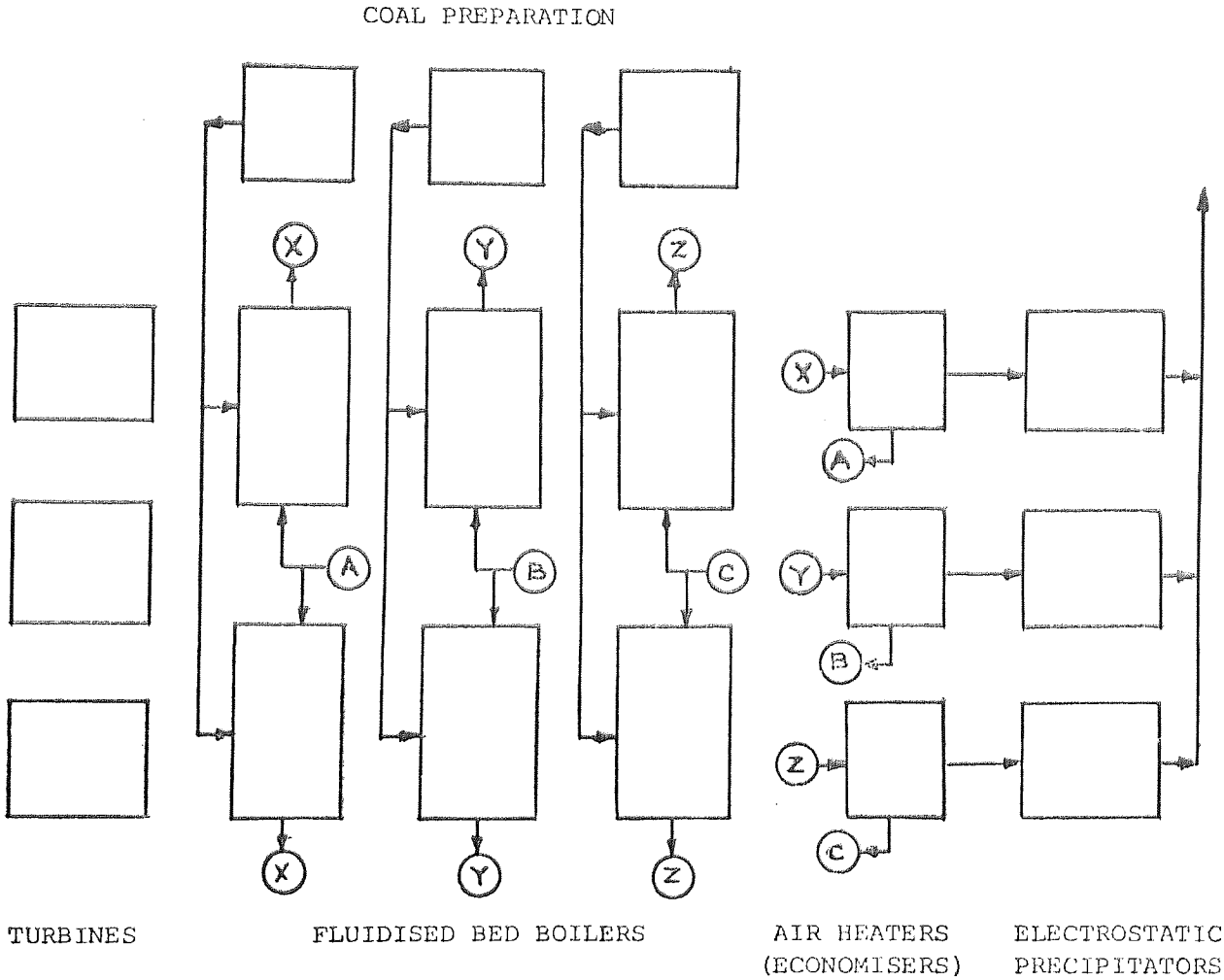

FIGURE 1.2 LAY-OUT FOR POWER GENERATION STATION USING FLUIDISED BED BOILERS

power station suggested that the fluidised bed reactor be constructed as a multiplicity of units of size 6 m x 20 m. Because such a size is transportable, it can be factory assembled instead of constructed at site, keeping capital costs low. A unit of this size is shown in Figure 1.3a. One of the main problems in design is the even distribution of coal and air throughout the fluidised bed. The air is distributed evenly through a very large number of holes in the base of the fluidised bed, which forms the top of a plenum chamber. From engineering and economic considerations the crushed coal cannot be distributed as evenly as the air. At the same time it is necessary to avoid the volatile emission being confined to isolated areas and so starved of oxygen for combustion. In early designs, a multiplicity of point sources was considered, but their number could be prohibitively large in a full-scale plant. An experimental linear feeder of 5 m length[4] was found to distribute coal evenly along its length, and this type of feeder is adopted in the present study in preference to the multi single-point system. The lateral movement of coal through the bed is confined to one dimension - transverse to the feeder, whereas in point feeders the lateral movement is in two dimensions resulting in steeper concentration gradients for the same flow. In the configuration of Figure 1.3a which shows the basic construction unit, the fundamental operational process unit comprises all that area of the fluidised bed served by one linear feeder, and hereafter referred to as a coal feed cell (Figure 1.3b). From the standpoint of combustion efficiency,

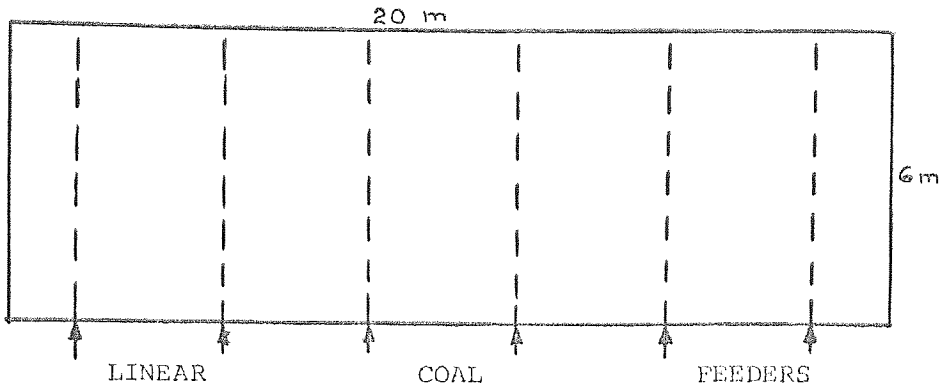

a. PLAN OF PRE-ASSEMBLED FLUIDISED BED

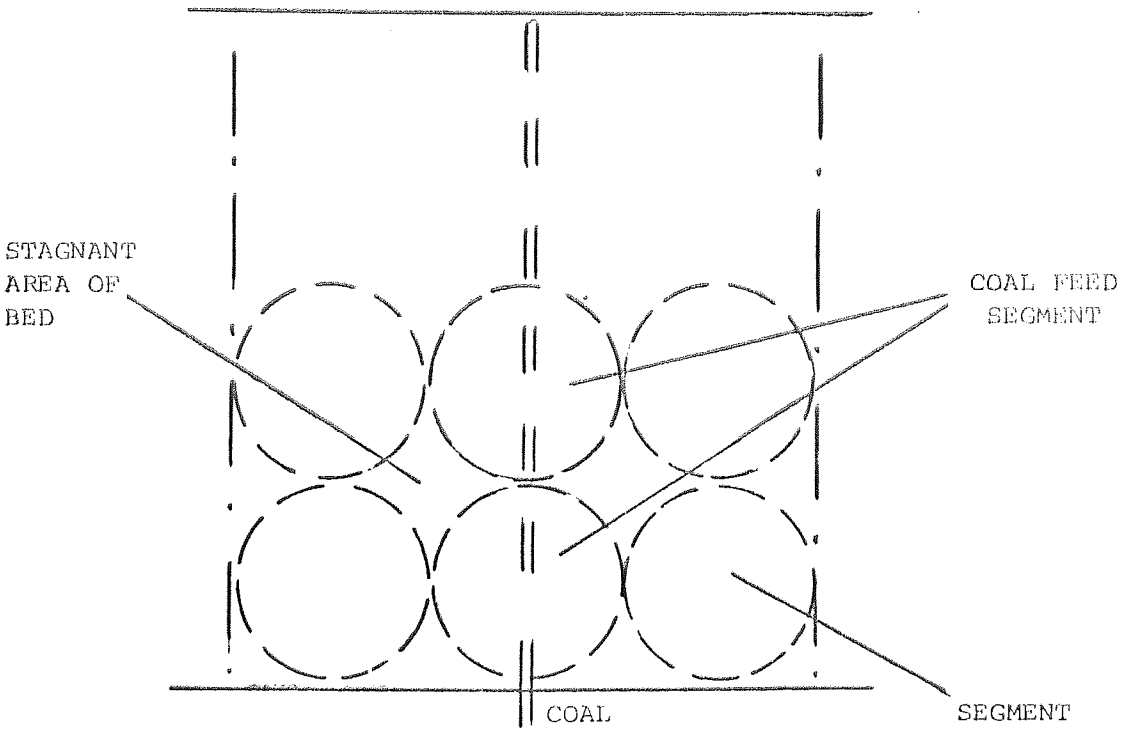

b. PLAN OF COAL FEED CELL

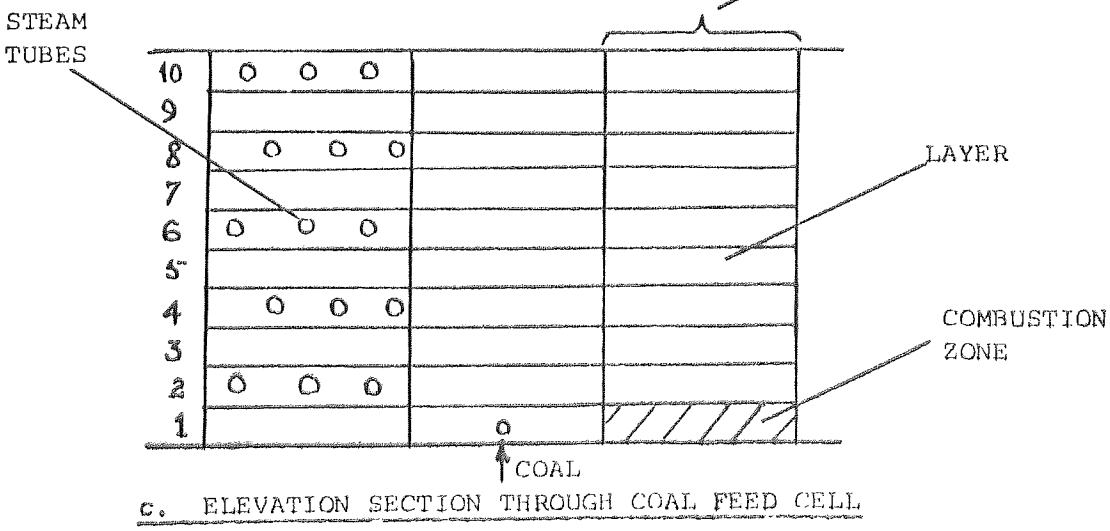

c. ELEVATION SECTION THROUGH COAL FEED CELL

FIGURE 1.3 SEGMENTS AND LAYERS IN A COAL FEED CELL

the pilot plant should extend at least over a single coal feed cell. The basic characteristics of the full-scale plant are the same as those of the coal feed cell since it is composed of multiples of this unit. Other considerations such as mechanics of construction, realistic lay-out of steam tubes, and problems of regulation and control may well tend to increase the size of the pilot plant.

As part of such a project it is very valuable to carry out a theoretical study directed towards the definition of a mathematical model of the process. The synthesis of the model should proceed in parallel with the construction of the pilot plant. The model work indicates areas requiring investigation, and assists in assessing the relative importance of the various factors governing the process. It is also valuable in the planning of experimental programmes on the pilot plant.

When sufficient confidence is obtained in the mathematical model, the need for large numbers of expensive runs on the pilot plant to find optimum operating conditions can be avoided by carrying out computations on the model. Experimental work can be restricted to confirmatory runs within regions investigated theoretically.

A mathematical model is most useful in learning to handle a plant for which there are no 'operator's rules'. The model soon conveys the 'feel' of the gain and dynamic characteristics of the plant. Thus, dependent variables or outputs may be effectively regulated by independent variables or inputs. The next stage in this procedure is the synthesis of a process

controller, so that plant regulation is effected automatically. Here the mathematical model of the process is essential.

In general, the model of a process falls into two complementary parts associated with the need for the plant to be set first at the optimum operating level it is designed for, and then maintained at that operating level. The first requirement calls for a steady-state model defining the operating level. In addition to the required throughput, considerations such as the quality of materials, economics, plant scheduling, etc. are taken into account in the synthesis of this model.

Having set the plant at the required operating level as demanded by the steady-state model, it is necessary to hold the output or finished product within required tolerances. The plant noises cause a drift in the performance and it is necessary to make small compensating corrections continuously about the optimum operating level. This is plant regulation, and requires a knowledge of the dynamic characteristics of the process for its implementation. The dynamic model is synthesised by considering changes, and defining the nature or the mode in which transient responses die down to the steady-state.

This study is a synthesis of a mathematical model to represent combustion in a fluidised bed boiler by simulating the characteristics of a coal feed cell. In particular, the study is aimed at revealing the dynamic characteristic of heat evolution within the fluidised bed and the subsequent transport of this heat within the hot ash to the steam tubes for power generation.

There appears to be little published work on the derivation of a mathematical model to represent combustion in a fluidised bed apart from the work of Highley and Merrick [5] and that by Avedasian [6].

The work by Highley and Merrick was carried out at CRE, Stoke Orchard, concurrent with this study. Their primary concern was to use the mathematical model to assist in the design of a full-scale commercial plant. Experimental results derived from a fluidised bed pilot plant were used in the mathematical model and extrapolations were made to full-scale size. In such an approach the assumption is implied that the likely behaviour of the full-scale plant is the same as that of the pilot plant, and that a uniform mechanism of mixing of solids, represented by diffusion, obtains laterally.

The present study makes assumptions, based on published work, as to the possible non-uniform behaviour of large scale plant, in particular that of segmentation and stagnant areas as shown in Figure 1.3b. These assumptions together with those on combustion are dealt with in detail in Chapters 2, 3 and 4. Bubble coalescence in fluidised beds is assumed to give rise to segmentation, where each large bubble breaking on the surface is derived from small bubbles at the base of the bed over a catchment. Within a segment, rapid lateral mixing is taken to occur since there is a continuous exchange of solids material between bubbles in a given segment. The exchange of solids material between adjacent segments is slow, and is assumed to be restricted to the surface where the wake of large bubbles is

shed. Furthermore, it is conjectured that the combustion of volatiles is restricted to the coal feed segment because of the speed with which these are liberated on heating, and the much higher reaction rate of volatiles when compared with carbon. It follows that combustion in the outer segments of a coal feed cell is restricted to carbon only. Moreover, because of the very thorough gas-solids contacting in fluidisation, the uptake of oxygen is assumed to occur within 0.1 m of the base of the bed.

Ideally, experimental observations should be carried out in a large enough pilot plant to investigate and confirm such assumed characteristic behaviour. Alternatively, where the pilot plant is smaller than the full-scale plant, experimental observations might be made under conditions that prevail at locations successively positioned laterally from the coal feeder at the centre to the periphery of a coal feed cell. The experimental observations conducted on the pilot plant were based on the implied premise that the pilot plant be used to investigate the area around the coal feeder, and that extrapolations be made therefrom. The application of such experimental data to this study is made with due regard to the underlying assumptions of segmentation and the limitations of the direct application of some of the experimental findings are discussed in Section 4.1. This procedure is deliberately followed in an attempt to avoid the problems that might result in the scale-up from pilot plant to full-scale.

Implicit in the above assumptions is the fact that

combustion in the coal feed segment is largely dictated by the volatile content of the coal. It follows that the volatile content of the coal has an important bearing on the coal feeder spacing, and this study takes this factor into account. The effect of altering the volatile content of the coal feed for a fixed coal feeder spacing is also discussed in Section 7.1.1.

The work by Avedasian was directed to determining the kinetics of char combustion in a fluidised bed after devolatalisation of coal. He was not concerned with operating the 75 mm bed to represent sections of a large fluidised bed spaced laterally away from a coal feeder.

Fan et al developed an interesting generalised progression model [7] to represent flow systems with varying degree and mode of mixing as may arise in segments in a shallow fluidised bed, radial flow reactor, or short tubular reactors. The work is limited to the deduction of expressions to represent the residence time distributions of the progression models concerned. No consideration is given to the application of the fluidised bed system for combustion or heat transfer.

C H A P T E R 2

THE PRINCIPLE OF FLUIDISED COMBUSTION

THE PRINCIPLE OF FLUIDISED COMBUSTION

2.1 General

The process of fluidised combustion is governed by simultaneous conditions of mass and heat flows within the reactor. The basic nature of these flows is set out in Figure 2.1 which shows a pair of simultaneous three input-three output matrices. The mass and heat flow in the coal (fuel), air and water (coolant) are the independent variables or inputs and upon the settings of these depend the outputs or dependent variables, i.e. the mass and heat flows in the ash, off-gas and steam respectively.

In Figure 2.1a the only cross coupling term is the mass transfer of carbonaceous material from the solids stream to the gaseous stream during combustion. This results in the a matrix of transforms linking the outputs and inputs as shown.

In Figure 2.1b it is suggested that heat transfer is from the solids stream rather than from the gas stream to the coolant, resulting in the b matrix of transforms indicated. This is borne out by the result[8] that the heat transfer coefficient initially increases with fluidising velocity and then falls off. The initial increase in fluidising velocity causes increased agitation of particles in the particulate phase. The duration of contact with the heat transfer surface decreases while the frequency of contact increases. This results in an increase in the heat transfer coefficient. At higher fluidising velocities, when more of the fluidising gas passes through the bed in bubbles, particle contact with the heat transfer surface is denied whilst bubbles are in contact with that surface. This results in a fall in the heat transfer coefficient. Thus, it is reasonable to assume that heat

$\dot{W}$ = mass flow

$\dot{H}$ = heat flow

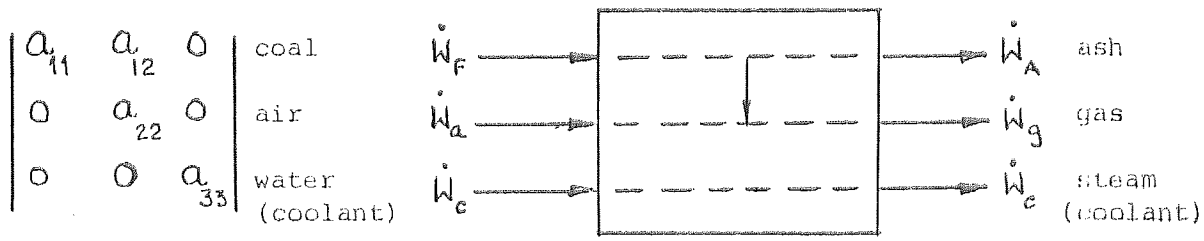

a. Mass Flow

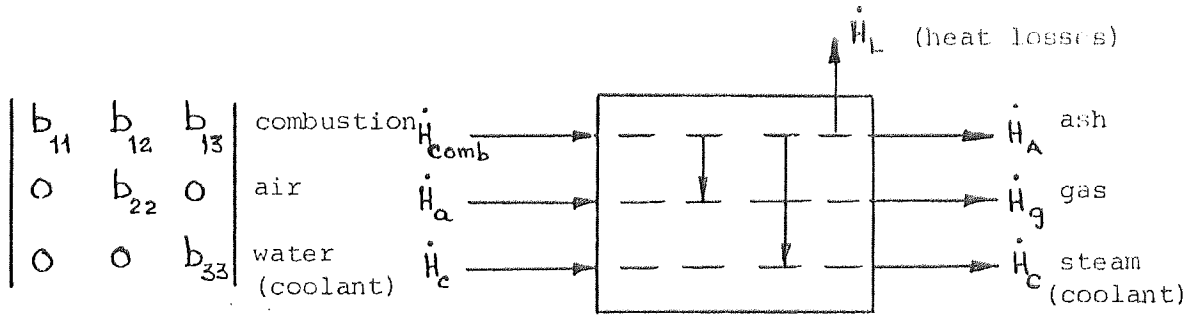

b. Heat Flow

FIGURE 2.1. BASIC SIMULTANEOUS MASS AND HEAT FLOWS

is transferred from the solids stream to the coolant.

It is fortunate that both the transfer matrices have triangles of zeros making them easy to manipulate. Each of the terms of the matrices has two constituents - a gain constant or differential coefficient and a dynamic term. The gain constant relates the magnitude of a change in an output variable to that of a particular input variable. Thus, if an input variable is changed in value the corresponding output variable will also change, and it is the gain constant that relates the new steady-state of the output to the initial change in the input. The dynamic component relates the way in which the output follows the input during such changes. This component defines the plant behaviour during transients and is characteristic of the particular stream.

2.2 Definition of the Synthesis Problem

Having set down the basic simultaneous mass and heat flow matrices, it is possible to translate the plant layout of Figure 1.1 into the schematic principle of Figure 2.2. This shows the three stages of reactor, economiser and air preheater.

There are seven distinct phenomena occurring within the system. These define the solids and gas flows, the various heating and heat release mechanisms and the transfer of heat to the coolant. The entire functioning of the process can be defined by considering the interactions of the kinetics of the following individual mechanisms:

1. Movement of solids
2. Movement of gases through the bed height
3. Heating of coal and volatile evolution

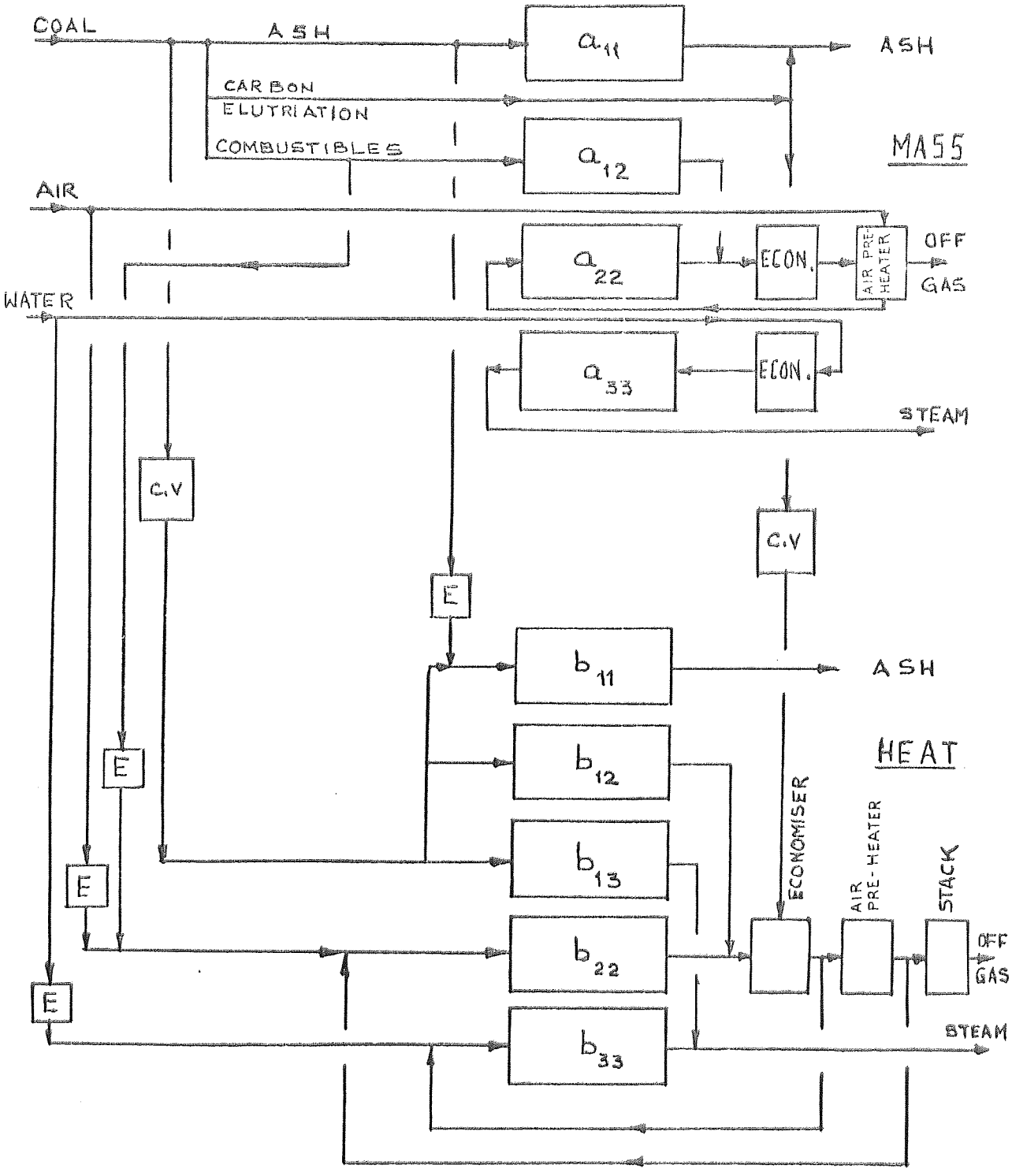

FIGURE 2.2 SCHEMATIC PRINCIPLE FOR A MATHEMATICAL MODEL OF A FLUIDISED BED

4. Combustion of volatiles

5. Combustion of non-volatiles

6. Heating of gases

7. Heat flow within the ash plasma to steam tubes

The heating time and time for volatile evolution are of the order of a second, while that for the combustion of volatiles is a fraction of a second. Due to the excellent gas/particle contacting in fluidisation, the heating of gases is almost instantaneous. Hence, in this study these three mechanisms (3, 4 and 6) are assumed to be instantaneous.

Each of the terms of the simultaneous mass and heat transfer matrices has two constituents, a gain constant or differential coefficient and a dynamic term. The gain constant is best obtained by differentiating the relevant equations in the steady-state model [9]. This is done in Appendix 1, where the partial differentials, four defining mass flow and five defining heat flow, are extracted.

In the synthesis of the model the determination of the dynamic constituents is a problem of some proportion. Quite apart from the strategy adopted in making the synthesis, much judgement is called for in making simplifications, incorporating observed mechanics, and having some regard to the degree of mathematical complexity of the expressions and indeed that of the solution. Each one of these factors imposes its own distortion and these are tolerated to the extent that the original is not fundamentally altered in nature. An assumption or simplification which results in a behaviour being substantially

unrepresentative of that which obtains in practice must be avoided. At the same time, coarse approximations are quite legitimate, for a sacrifice in resolution usually results in a simplified expression.

Of the terms in the mass and heat flow transfer matrices the term b_{13} is the most important since it represents the heat evolution and its flow to the steam tubes - the primary function of the process. The dynamics of this term are a cascade of two components. The first component is the dynamic of heat evolution as the coal is burned in the combustion zone while mixing under the influence of the mechanics of solids flow that obtain within the bed, while the second component is the dynamic of the flow of this heat evolution from the combustion zone to the steam tubes also under the mechanics of mixing.

The dynamic constituents of the other terms in the two transfer matrices are either simple to approximate or are derived analogous to one or other of the two components of b_{13}.

The dynamics of a_{22} and b_{22} represent the plug flow time of the air through the bed height, while that of a_{33} and b_{33} represent the plug flow time of the coolant in the steam tubes.

The dynamic constituent of b_{12}, the heating of gases within the bed, may be assumed instantaneous. That of a_{12} which represents the transfer of carbon from the fuel to the gaseous stream due to combustion is the same as that of heat evolution, the first of two components of b_{13}, since heat evolution results in the carbon being oxidised to gas and joining the gas stream.

The dynamic constituents of a_{11} and b_{11}, the mass and heat flows in the ash stream, are identical. Now the ash leaves

the bed in two sub-streams - by elutriation from each coal feed cell, as well as overflow at the wier of the bed. The dynamics of the ash sub-stream that is elutriated may be assumed to be instantaneous, while that of the overflow sub-stream may be approximated to an exponential decay. The exponential time-constant is given by:

time-constant = total mass of ash in the bed/mass flow of ash over the wier

In particular, this study is concerned with the synthesis of the dynamic component of the term b_{13} in the heat transfer matrix. The other terms either follow from this synthesis or are derived by approximation as suggested above.

Before outlining the procedure to be followed in the synthesis of the dynamic characteristic of b_{13}, it is worth defining more closely the structure of the coal feed cell which comprises all that area of the fluidised bed served by a single coal feeder, since the synthesis procedure is based on it.

Whitehead and Young [10] have shown that large fluidized beds exhibit an alveolate or cell-like structure of segments. These segments are due to bubble coalescence, a characteristic of fluidisation. Using bed height and fluidizing velocity as independent variables they were able to induce in a large fluidised bed a sharp resonance corresponding to a stationary pattern of large bubbles bursting on the surface. Each bubble at the surface is derived by the coalescence, at successive bed heights, of bubbles originating from a catchment at the base. Thus the bubbles increase in size with bed height, though the

total volume flow of gas in the bubbles remains constant with height. They found that the size of the catchment or segment increases with both bed height as in Figure 2.3 and with fluidising velocity as in Figure 2.4. It was also shown that the space in between a pattern of segments is remarkably stagnant, since no bubbles pass through such spaces.

In a practical configuration for a fluidised bed boiler the steam tubes may interfere with or distort the coalescing bubble pattern and tend to weaken the segment structure. In the absence of an experimental investigation to study the effect and implication of such impedimenta, it was decided to incorporate the concept of segments in the coal feed cell, and to synthesise the theoretical model such that the coal feed cell extends over an integral number of segments as shown in Figure 1.2b. The investigation covers a range of coal feed cell sizes that extends from two to seven segments with three being the most likely size in a commercial application. The number of segments of which the coal feed cell is composed is a measure of the width of the cell or the distance over which the lateral flow of carbon occurs. This distance is a function of the type of coal used.

The distance, transverse to the linear coal feeder in Figure 1.2b, over which the lateral flow of coal extends may be estimated by considering the feed coal as composed of volatiles, fines and coarse carbon particles. On meeting the hot ash plasma at 800^{o}C in the bed, the feed coal particles may be assumed to reach devolatilization temperatures of around 400^{o}C in a second or two, with the result that all volatile evolution may be said

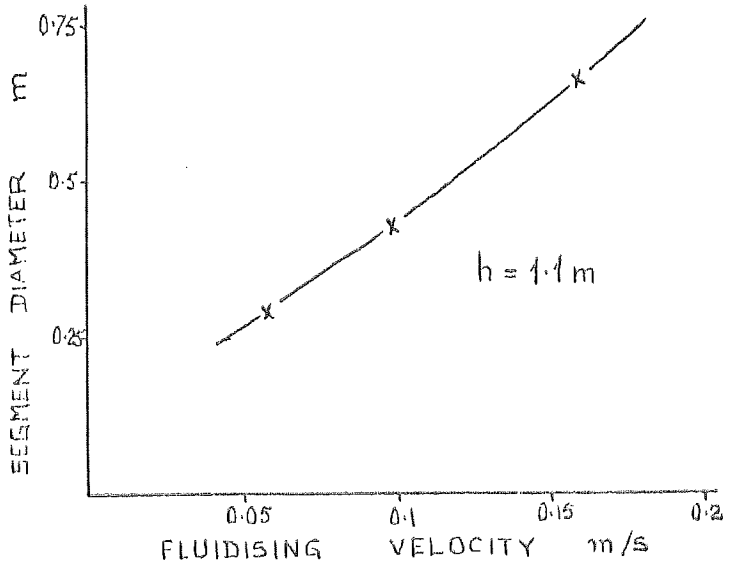

FIGURE 2.3 EFFECT OF FLUIDISING VELOCITY ON SEGMENT SIZE

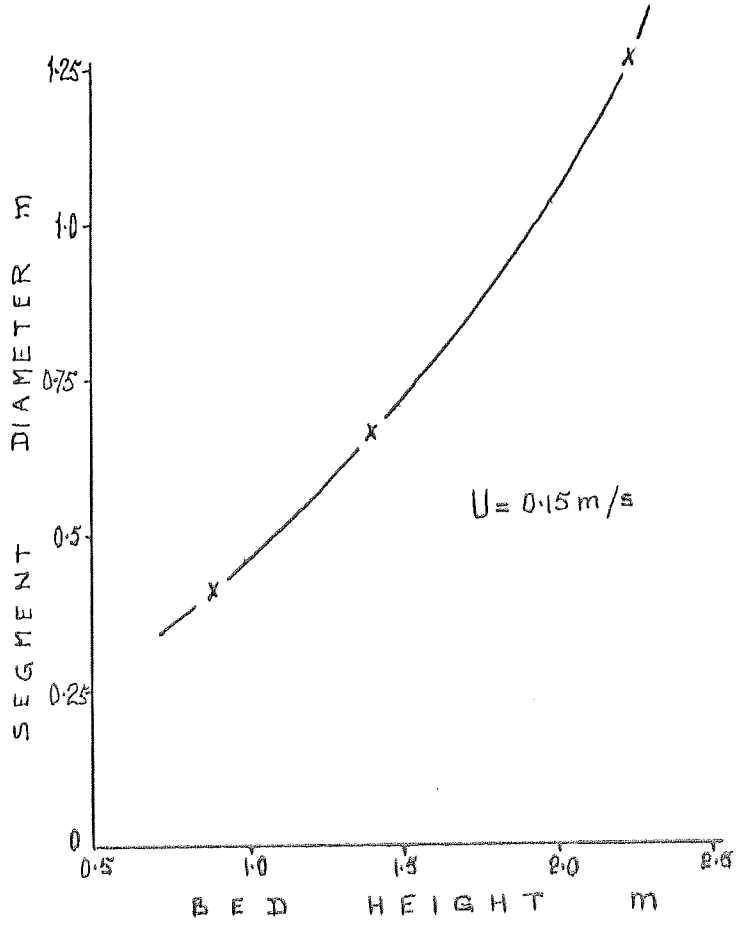

FIGURE 2.4 EFFECT OF BED HEIGHT ON SEGMENT SIZE

to take place near the base of the coal feed segment. Koslov[11] has shown that the rate of combustion of volatiles (methane) is some 10^4 to 10^5 times faster than that of carbon, leading to the conclusion that the volatiles react preferentially with oxygen in the coal feed segment.

Inevitably, the coal feed, which consists of particles up to 1.5 mm for a fluidising velocity of 0.6 - 0.9 m/s, contains a proportion of fines. Fines may be considered to comprise all those particles below a critical size x_c at which buoyancy occurs at fluidising velocity. Such particles are assumed to move through the bed height in the plug flow time of the air and do not obey the normal laws of vertical and lateral flows of solid particles that obtain within the bed. These feed fines, by reason of their size, are some ten times more reactive than the coarse carbon particles because of their increased surface to weight ratio.

In view of the fact that in the coal feed segment there is a release of all the volatiles together with the ingress of feed fines which may run to about 20% of the feed, both of which are more reactive than coarse carbon particles, it is assumed that all the available oxygen in the coal feed segment is absorbed first by the volatiles and then by the feed fines. Experimental evidence indicates near perfect combustion of volatile matter with about 20% of the feed fines burning within the bed.

The primary effect of an increase in volatile content of coal is to leave less carbon in the feed for the remainder of the

coal feed cell, resulting in a decrease in its size because of decreased effective lateral flow. The number N of segments that comprise the coal feed cell is thus inversely proportional to the total combustion in the coal feed segment. Hence:

$$N = 1/(.01V + .2 \text{ feed fines}) \qquad 2.1$$

where all the volatiles V% and 20% of the feed fines burns in the coal feed cell. It is further assumed that volatiles use the same ratio of air as carbon. The relationship from equation 2.1 plotted in Figure 2.5 shows the effect of volatile content of coal on the number N of segments of which the coal feed cell is composed.

For a fluidising velocity of 0.6 - 0.9 m/s and a bed depth of 0.75 m the segment is about 0.75 m in diameter, and comprises about 500 kg of ash (density of ash 800 kg/m^3).

Each segment is subdivided into layers through the bed height as in Figure 1.2c. The size of the layer is set by the conditions of operation of the bed, in particular the fluidizing velocity so as to simplify the expressions for vertical mixing deduced in Appendices 3 and 4.

Steam tubes are packed in an array in the upper layers of the bed to give the most effective heat transfer consistent with the proper functioning of the process.

The procedure to be followed in the synthesis of the dynamic component of the transform b_{13} in the heat transfer matrix consists of first defining the mechanisisms of solids mixing in a fluidised bed, and then applying these to trace the

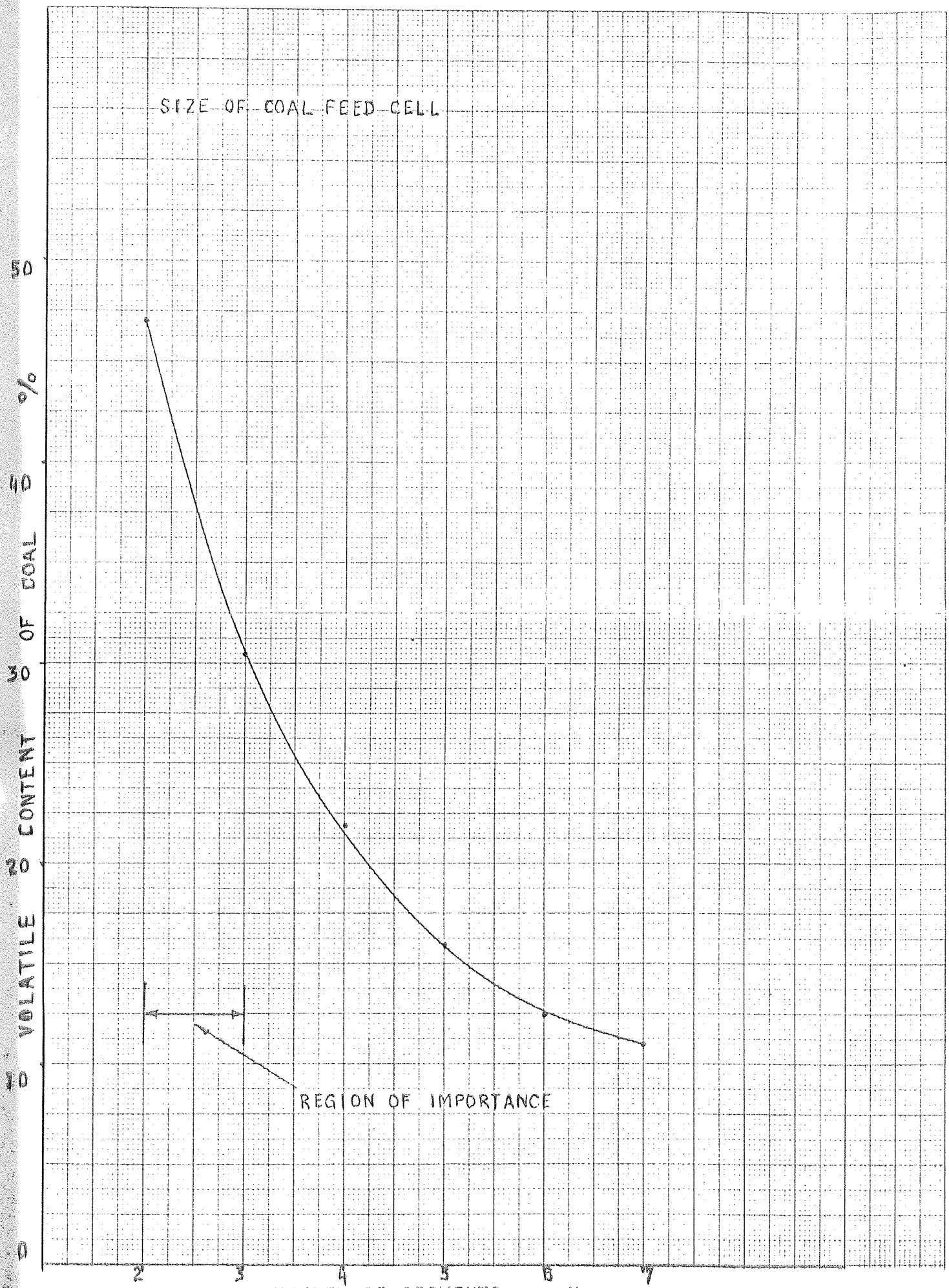

FIG. 2.5 EFFECT OF COAL QUALITY ON THE NUMBER N OF SEGMENTS IN THE COAL FEED CELL

space-time history of coal in the lattice of segments and layers of Figure 1.2c of the coal feed cell. Meanwhile, the carbon particles suffer some reduction due to combustion and abrasion, thus continuously altering their size distribution. Under equilibrium conditions the amount of carbon leaving the coal feed cell as products of combustion and as elutriated carbon loss must be the same as the feed to the entire cell. Having attained equilibrium, a step change in coal and air is made, and the transients, corresponding to the resultant change in heat evolution together with the change in heat transferred within the hot ash plasma to the steam tubes are deduced by following the space-time history referred to above. These transients are fitted with time trajectories, the transforms of which are known, to reveal the desired dynamic component of b_{13}.

It now remains for the mechanics of motion within the fluidised bed to be defined. The kinetics of solids and gas flow, and of mixing are synthesised using difference equations to represent the fundamental phenomena observed within a fluidised bed.

CHAPTER 3

FUNDAMENTAL PHENOMENA OF FLUIDISATION

FUNDAMENTAL PHENOMENA OF FLUIDISATION

3.1 General

In order to represent the behaviour of fluidisation mechanistically, it is necessary first to define the fundamental phenomena of fluidisation. These mechanisms are then used to devise a gross pattern that represents the effect of the fundamental phenomena. [12] - [18]

The process of mixing in fluidised beds is by bubble transport and not by diffusion. The theory developed in [12] and [13] is intimately concerned with the hydrodynamics around a bubble, and defines the motion of particles affected by the bubble. By contrast, the present study is concerned with the overall problem of mixing and mass flow in a fluidised bed of ash containing about 0.1 - 1% of coal which is being burned. The bubble transport theory is used to synthesise expressions for the overall solids and gas flows through the bed.

Simplifying assumptions are made throughout in view of the imprecise nature of the effects of repeated bubble transport and its associated interactions. The relevant results of previous work [14] - [18] are summarised in sub-sections 3.2 and 3.3.

3.2 Fundamental Phenomena of Solids Movement

A single bubble gathers material from the bottom layer of the bed in its wake and transports it to the surface (Figure 3.1). During the ascent of the bubble some of the wake material is shed. As the wake rotates (Figure 3.2), grows in size and becomes unstable, a torus of D section is sliced off (Figure 3.3). When

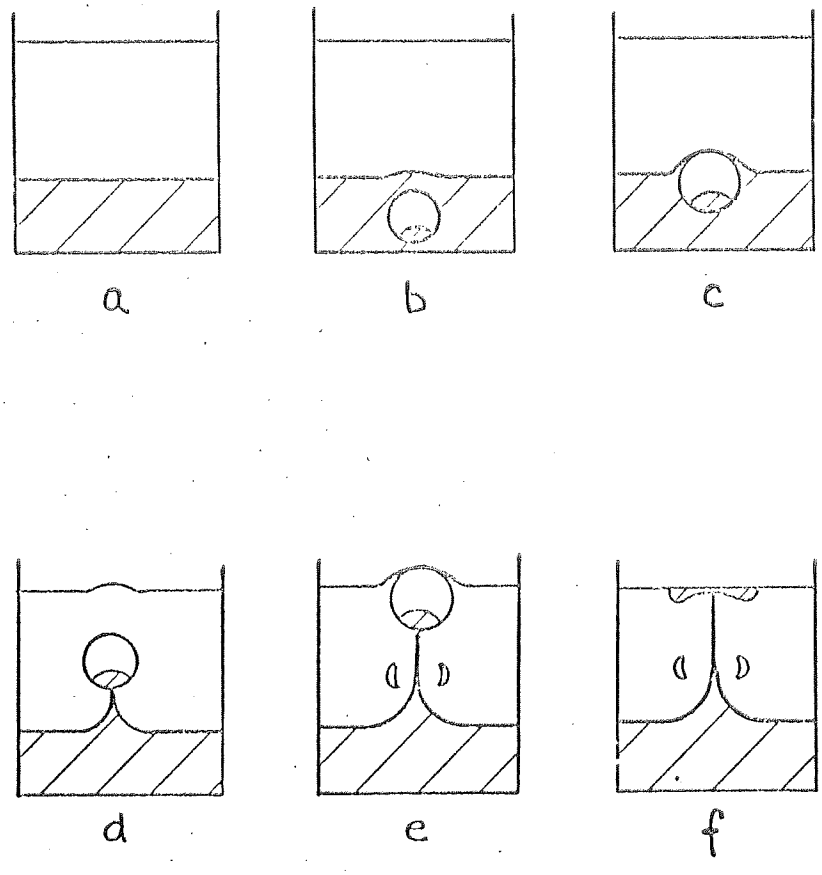

FIGURE 3.1 BUBBLE TRANSPORT OF SOLIDS

N.B. Taken from Reference 14.

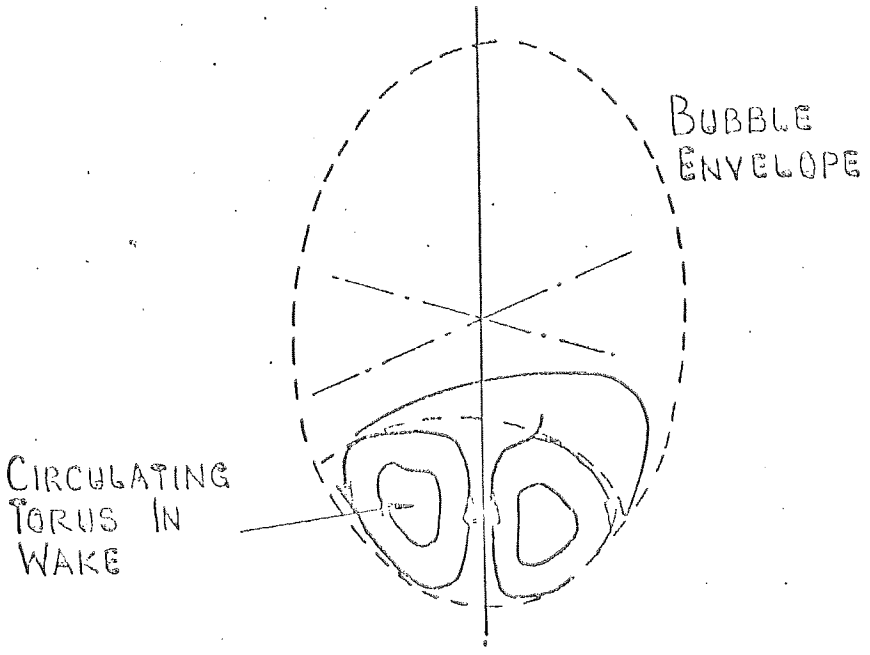

FIG. 3.2 SECTION THROUGH BUBBLE.

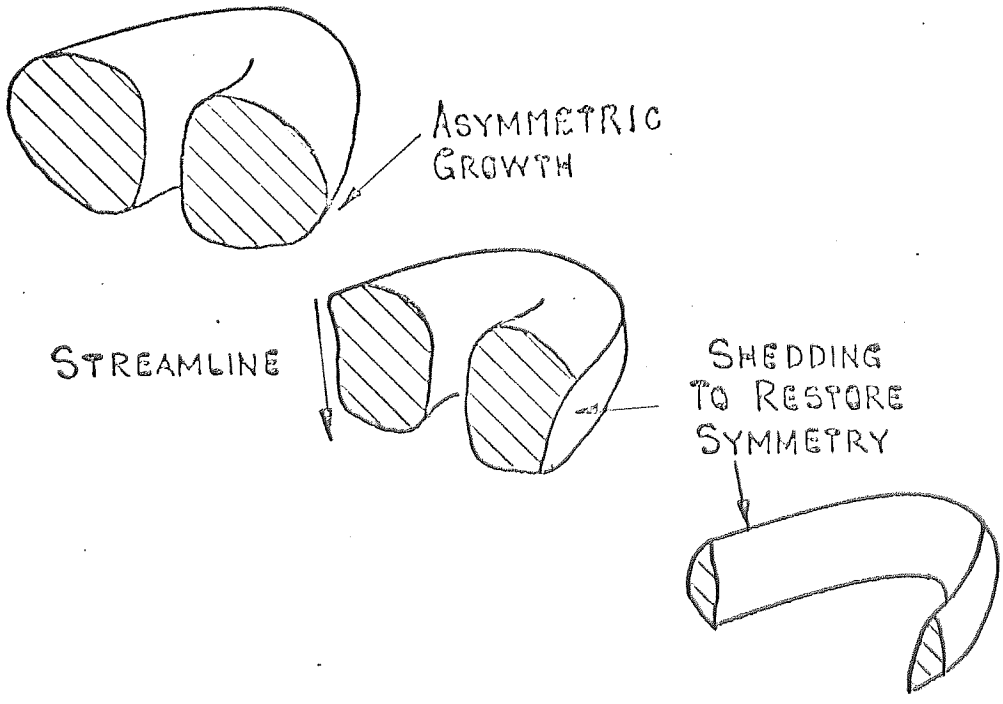

FIG. 3.3 WAKE SHEDDING BY BUBBLE.

N.B. Taken from Reference 14.

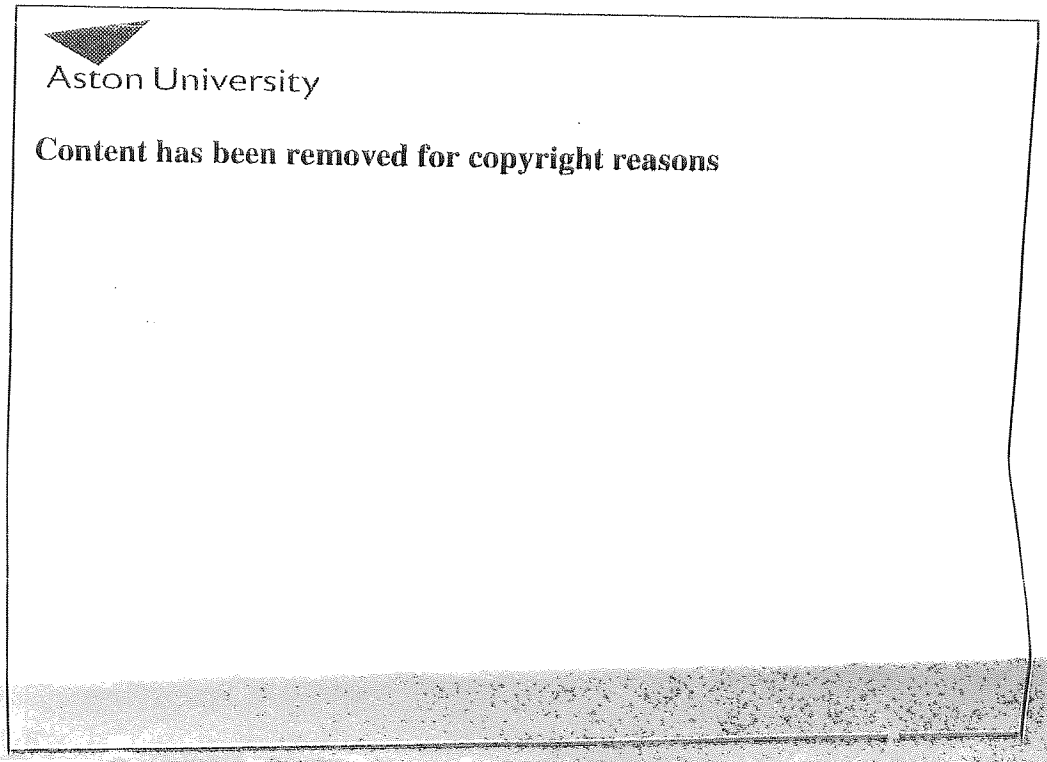

FIG. 3.3 WAKE SHEDDING BY BUBBLE.

N.B. Taken from Reference 14.

the bubble reaches the surface, the remainder of the wake is deposited as a disc on the surface (Figure 3.1f).

Figure 3.4 shows the effect of bubble transport on successive layers from the base. Material within half a bubble diameter from the base is carried up in the initial wake, and shed during ascent as indicated above. Material beyond a half bubble diameter does not appear to be caught up in the initial wake to any appreciable degree for a single bubble. The wake comprises about a quarter of the total bubble volume.

The effect of successive bubbles is seen in Figure 3.5. It is assumed that the bed consists originally of a bottom layer of dark material and a top layer of light material. The sequence of events is related to the number of bubbles and not to the passage of time, as the interval between bubbles does not contribute to material transport and hence mixing. The boundary separating the dark and light layers moves progressively down the bed followed by the partially mixed material. In a practical case, where the bed is fluidised at a given gas flow-rate, bubbles form continuously so that mixing progresses uniformly with time proportional to the gas flow-rate. This latter determines the bubble size and frequency.

Poorer mixing results from a pattern of multiple bubbles as seen in Figure 3.6. The mixing due to 10 x 7 bubbles compares poorly with the effect of the fifty successive bubbles of Figure 3.5c. It appears that, where the bubbles are in close lateral proximity, the transport mechanism of individual bubbles is partially cancelled. In effect, the degree of wake shedding is increased.

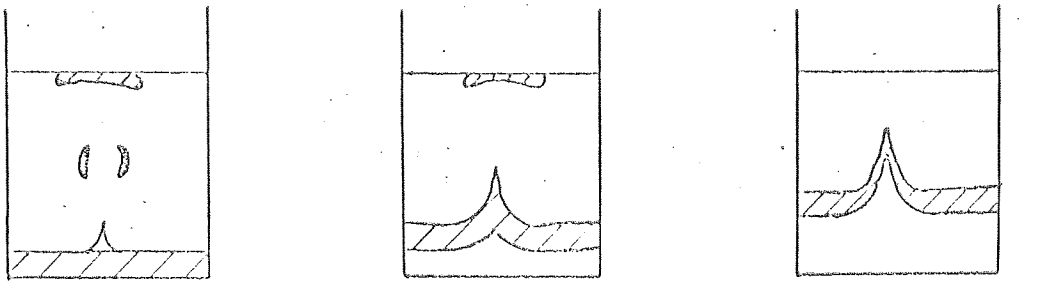

(a) Carried In Wake. (b) Only Just Caught In Wake. (c) Passed Through.

Fig. 3.4 Effect Of Bubble Transport On Successive Layers At Half Bubble Diameter From Bottom.

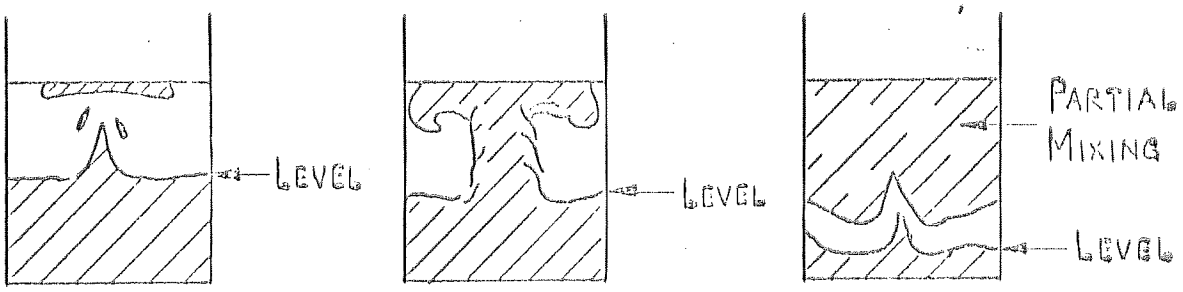

(a) One Bubble. (b) Ten Bubbles. (c) Fifty Bubbles.

Fig. 3.5 Effect Of Successive Bubbles On Mixing & Separation Level.

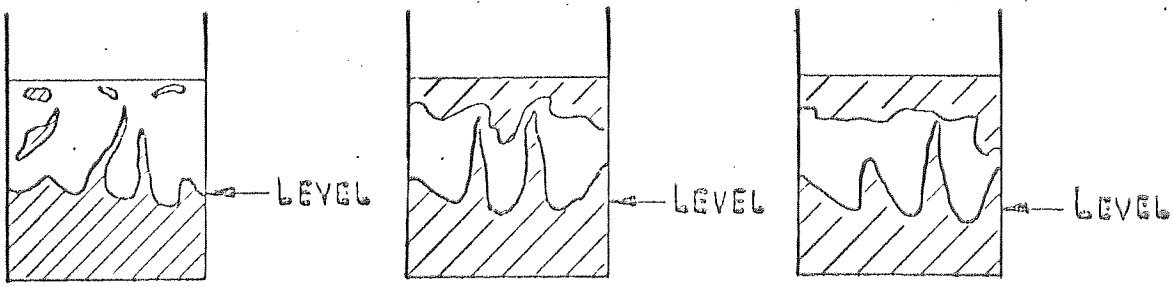

(a) 1x7 Bubbles. (b) 5x7 Bubbles. (c) 10x7 Bubbles.

Fig. 3.6 Poor Mixing Due To Multiple Bubbles.

N.B. Taken from Reference 15.

In the synthesis of an algorithm of expressions to simulate the vertical movement of solids material this pattern of vertical transport of solids in the wake of bubbles through the layers of a segment is followed. Due mainly to bubble coalescence the wake is continuously shed and replenished so that it is maintained constant with the movement of bubbles from base to surface. Instantaneous mixing is assumed within the wake between replenished material and the compliment of the material shed. Accompanying this rapid upward movement of solids at bubble velocity is a slow downward movement of solids from layer to layer by displacement for mass conservation. Both the upward movement of solids and the accompanying downward movement are assumed to occur uniformly over the segment width.

These two movements of solids brought about by bubble transport constitute an asymmetrical mixing in each layer which is characteristic of fluidization. The vertical mixing is asymmetrical in that a given layer receives material from all layers below it by bubble transport but only from the layer above it by downward displacement in the time that it takes for bubbles to travel through the bed height. This is because the velocities of the two flows are not the same, though the amounts are.

The shedding of the wake of bubbles bursting on the surface results in a spreading of wake material along the surface. This mechanism provides the basis for defining the lateral flow as a solids exchange between surface layers of adjacent segments.

3.3 Fundamental Phenomena of Gas Flows

The air supplied to a fluidised bed may be thought of as

forming bubbles and a particulate constituent. The particulate constituent may be further divided into low velocity particulate phase gas and bubble 'cloud' gas travelling at bubble velocity.

Clouds are intimately associated with bubbles as shown in Figure 3.7, and their existence can be explained in the following way. Since the velocity of bubbles is greater than that of gas in the particulate phase, that particulate phase gas immediately below a bubble sees the bubble as a void, and, as it were, rises through the bubble much faster than through an equivalent bed height of the particulate phase. On rising through and beyond the bubble, this gas re-enters the particulate phase, is slowed down, and finally overtaken by the bubble. During this overtaking the gas flows in a streamline around the bubble. When it returns below the bubble it is once again in a position to pass through the bubble. Thus, each bubble has associated with it an amount of particulate phase gas in the form of a cloud [16] - [18]. A bubble may be considered as transporting not only solid material in its wake, but also gas in excess of that within the bubble.

That component of the particulate phase gas which is cloud rises through the bed at the average bubble velocity which is greater than that of the slower moving particulate phase gas. Because of the close association between clouds and bubbles, and the difference in velocity between cloud and particulate phase gas, the cloud gas stream is lumped with the bubble gas stream in the subsequent analysis.

In sub-sections 3.4 and 3.5, gross patterns of gas and solids flows are described to represent the effects of the

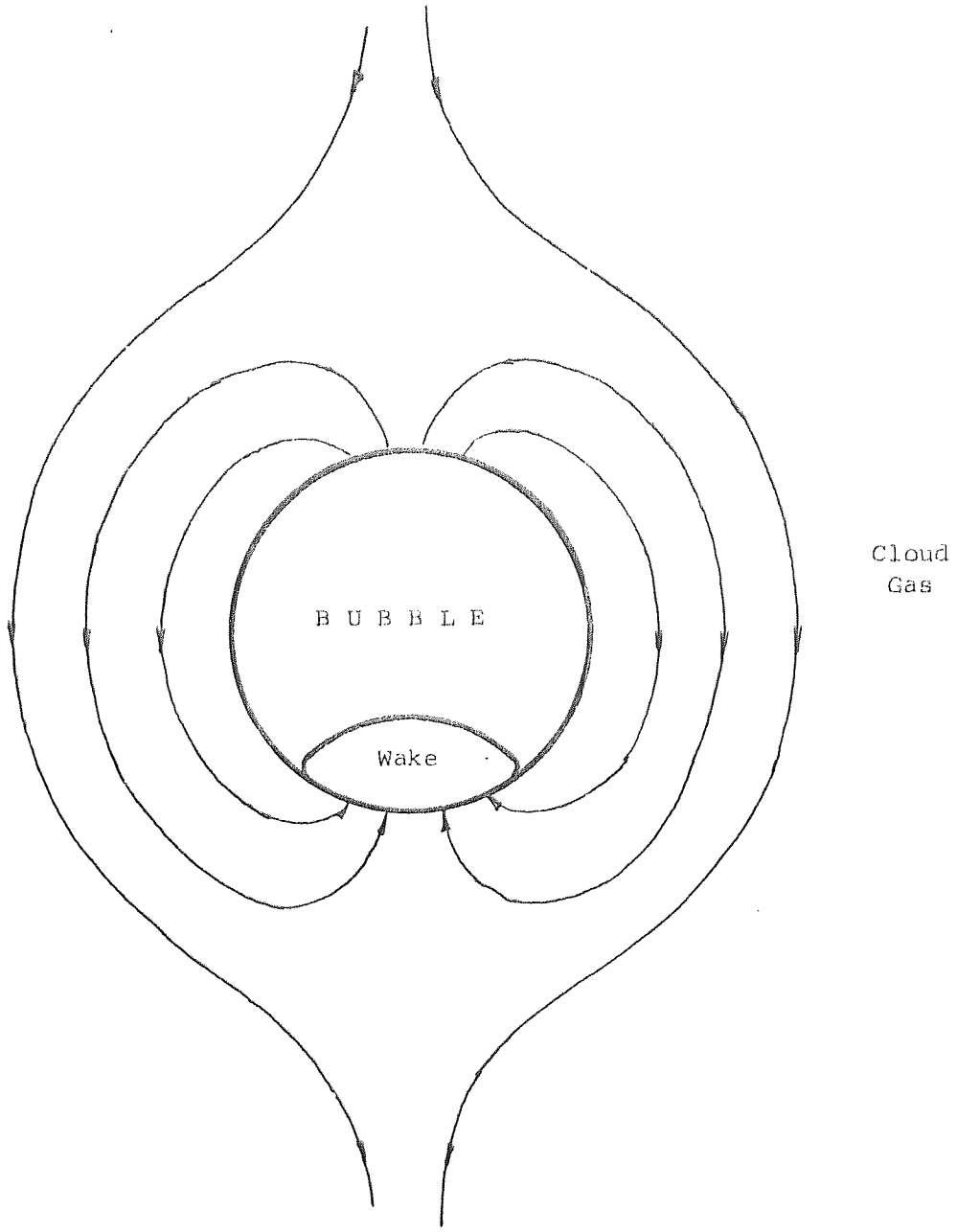

FIGURE 3.7 STREAMLINE FLOW AROUND A BUBBLE SHOWING CLOUD GAS ASSOCIATED WITH THE BUBBLE

fundamental phenomena outlined in sub-sections 3.2 and 3.3. These patterns are used to define expressions for the composition of the gas in the layers of segments, as well as the solids flows that result in mixing in the segments of the cell.

3.4 Gross Pattern of Gas Flow

The synthesis of expressions defining the mixing and flow of gases is facilitated by the subdivision of the segments into horizontal layers as in Figure 1.2c. The thickness of the horizontal layer for gas flow differs from that for solids movement.

In addition to the subdivision of the segments into horizontal gas layers, it is convenient to subdivide each segment into vertical profiles, which depend upon the conditions under which the bed in run. For incipient fluidisation, the fluidised bed may be divided into profiles of solids and particulate phase gas only as in Figure 3.8a. In an effervescent bed with bubbles, three vertical profiles require consideration, i.e. solids, particulate phase gas and cloud/bubble gas. These are shown in Figure 3.8b. The profiles are dependant upon the air flow at which the bed is operated.

In the plug flow time T of bubbles through the bed height the entire bubble stream within the bed is renewed. The gas layer thickness is so chosen that in this same time the particulate phase gas of slower velocity U_p moves through one layer. Thus, there is particulate phase gas which entered the bed in different intervals of time T indicated in the successive layers of Figure 3.8b, whereas the bubble stream

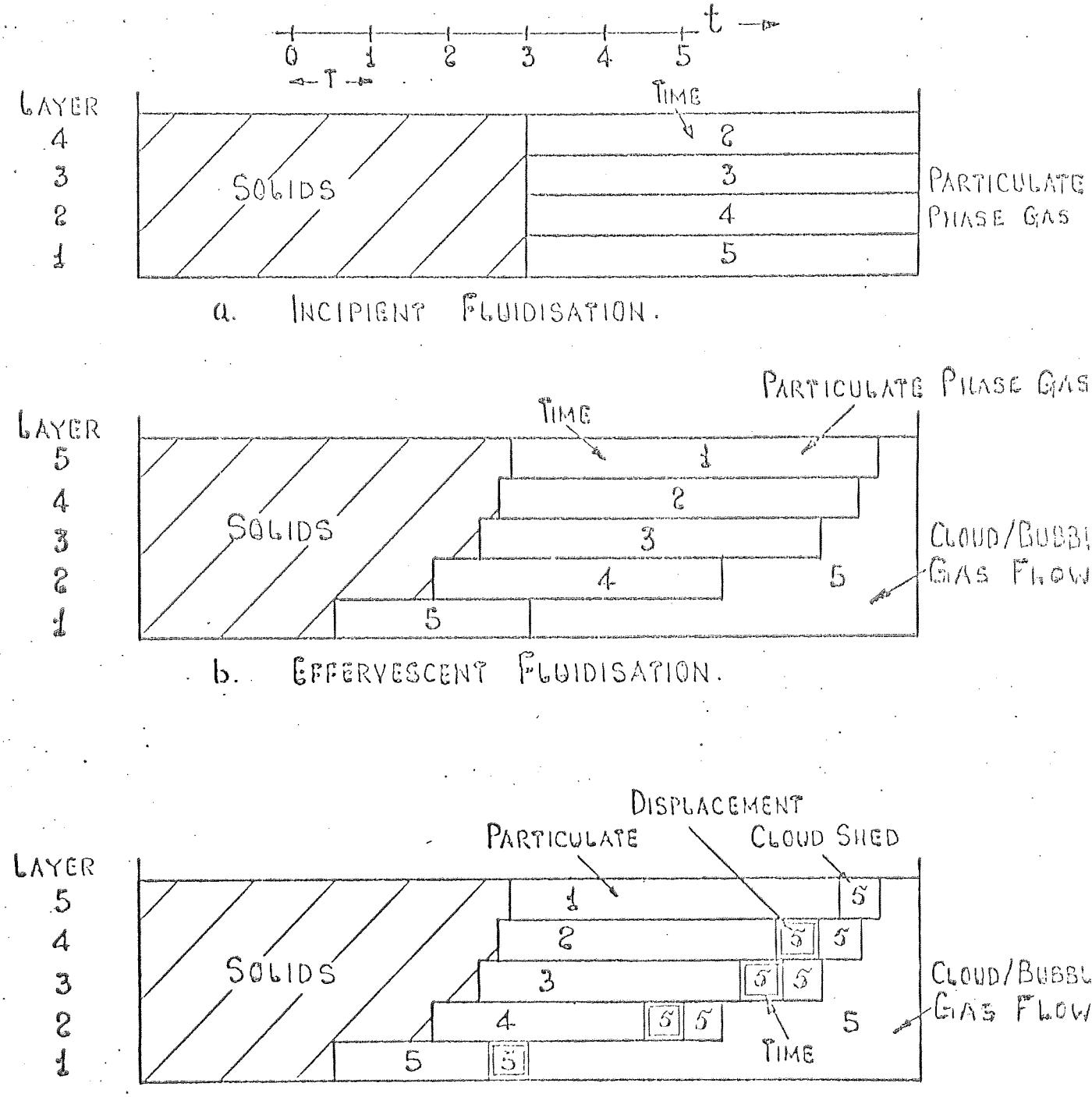

FIGURE 3.8 LINEATION OF SEGMENT OF FLUIDISED BED

(The numbers indicate the time interval at which the gas enters the segment)

originates in only one time interval - the most recent (T = 5).

In Appendix 2 a set of four equations A2.01, A2.05, A2.06 and A2.07 define the areas of cross-section, at different heights in the bed, occupied by the solids phase and the various gas phases of particulate, bubble, cloud and wake gas. Solutions to these equations are given in equations A2.08 to A2.11 to define the vertical profiles of the various states shown in principle in Figure 3.8c.

The profiles of these states alters with bed height since cloud shedding occurs as the bubbles rise from base to surface. These profiles are defined with respect to a gas layer which is defined in equation A2.14 as the height through which the slow moving particulate phase gas rises in the same time T that the fast bubble phase gas rises through the entire bed height.

A profile of the various phases is shown in Figure 3.9a for a fluidising velocity of 0.9m/s. It is of interest to note that at this fluidising velocity no particulate phase gas enters the bed in layer 1. In fact, the cloud requirement for the first two layers is in excess of the available particulate phase gas. It is only above layer 2 that cloud shed gives rise to slow moving particulate phase gas at a fluidising velocity of 0.9m/s.

Now consider the flow of the gas phases in further detail. The expressions for the kinetics of gas flow are deduced in Appendix 3.

The cloud/bubble flow is one of simple plug flow as set down in equation A3.1.

The particulate phase gas consists of three constituents

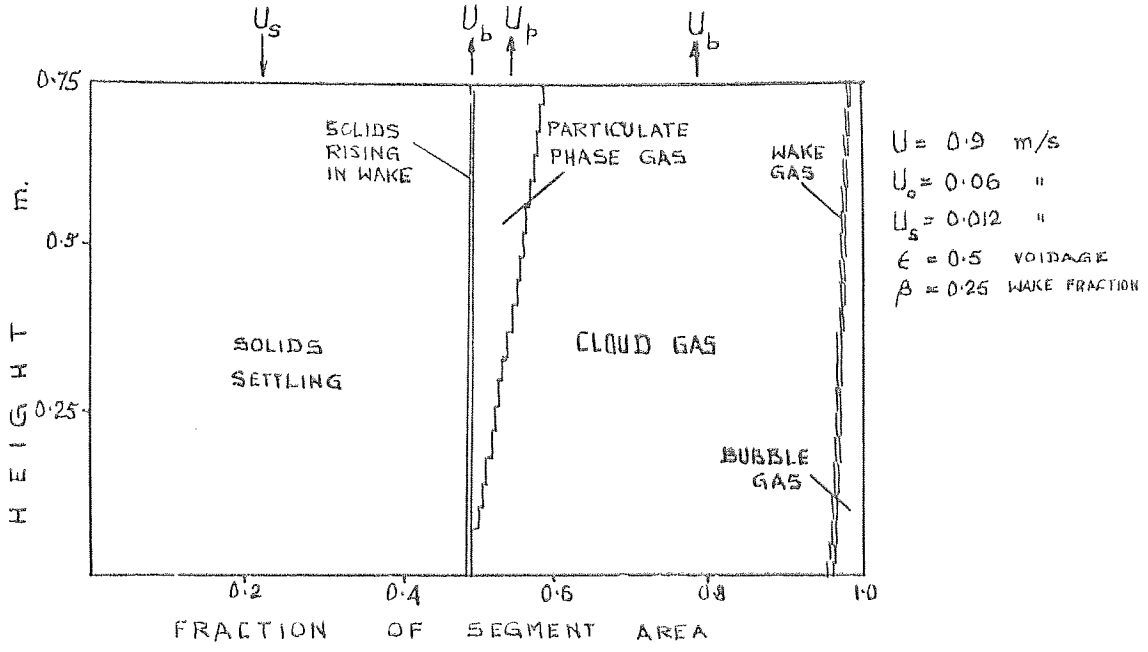

a. Proportions of solids and gas states in a segment.

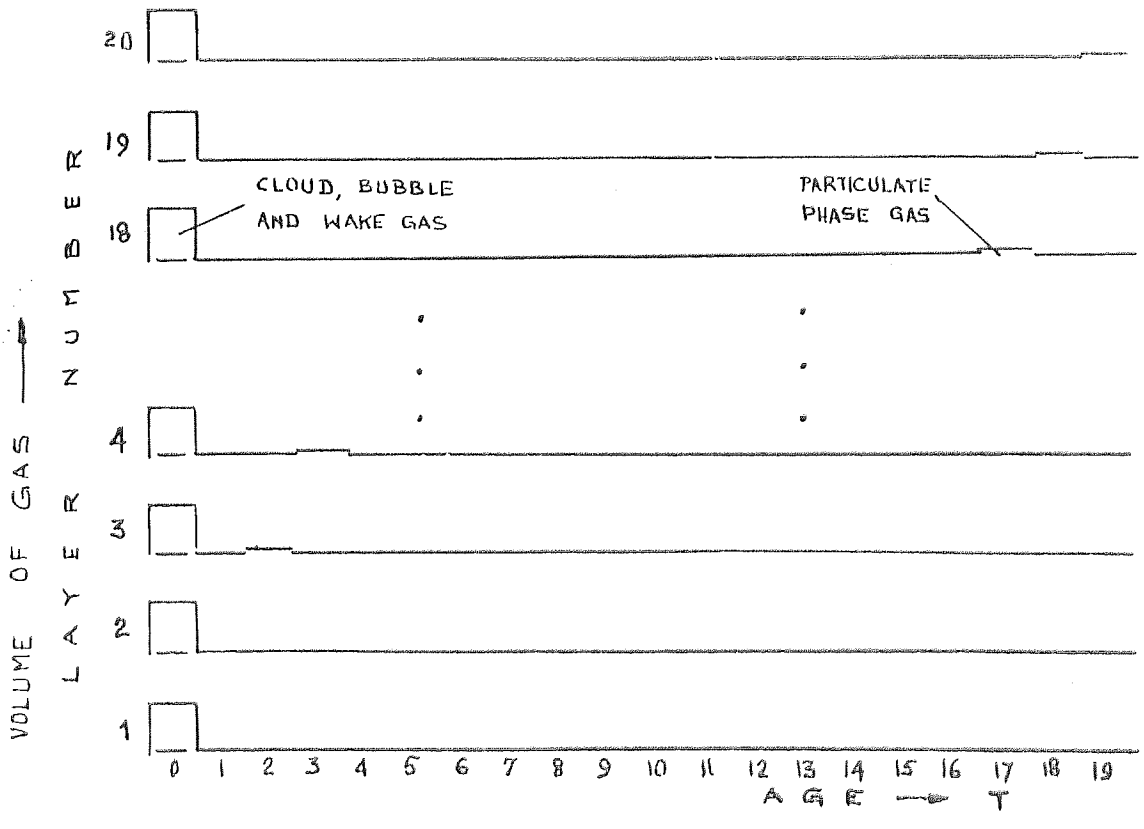

b. Gas residence time distribution in layers.

FIGURE 3.9 GAS FLOW IN A SEGMENT

as shown in Figure 3.8c. A particulate constituent A_p enters the base at each interval of time and progresses to the surface in plug flow. A displacement constituent A_d moves downward to replace that transported upwards by bubbles in their wake, and a third constituent A_{cs} is due to cloud shedding as bubbles coalesce during ascent. The intervals of time T during which the three mechanisms of plug flow, displacement and cloud shedding occur in the several layers are indicated in Figure 3.8c. This same pattern is set down as an expression of terms in A3.2 defining the areas of cross-section occupied by the various constituents of particulate, bubble/cloud, cloud shed and displacement gas in the layers.

An algorithm is deduced in equations A3.3 and A3.6 that defines the movement of these constituents with time, with the proviso that the boundary conditions attaching to the bottom and surface layers are as defined in equations A3.7 and A3.8.

Equations A2.08 to A2.11 from Appendix 2 are programmed in Listing A2.1 and are used to calculate the profiles of Figure 3.9a. Simplifications of the equations A3.3 and A3.6 are used to give the gas residence time distribution for each layer. The results for a fluidising velocity of U = 0.9m/s is shown graphically in Figure 3.9b. These results indicate that for all practical purposes the gas flow may be considered to be of single phase with a plug flow time T = 1 second, the same as that of the bubble phase through the bed height.

3.5 Gross Pattern of Solids Flow

In this study the vertical flow of solids through the layers of a segment is assumed to result in lateral homogeneity in each layer, and it is further assumed that the asymmetrical pattern of mixing deduced in Appendix 4 is analogous to that produced by wake transport of solids by bubbles. In the case of lateral mixing, solids exchange occurs only between surface layers of adjacent segments.

3.5.1 The Vertical Flow of Solids

The synthesis of expressions that define the vertical flow of solids is facilitated by the sub-division of the segments of Figure 1.3c into horizontal layers. The thickness of a layer is such that it contains an amount of material equal to the total wake capacity of all the bubbles generated during T, the plug flow time of the bubble phase through the bed height. Thus, the total ash/carbon content of a layer is potentially portable with each renewal of air through the bed height for perfect bubble transport, i.e. no wake shedding of solids. In that event all the material from layer 1 at the base of the bed is carried in time T to the surface to form the surface layer, and each layer moves down one by displacement. This simple flow pattern is used in Appendix 9 to derive an initial value for the background carbon in the segments. These initial values of background carbon are a remarkably good approximation from which to commence an iterative calculation of the process of combustion and elutriation. The close proximity of an initial value of a

target to its final value ensures stability and rapidity of convergence.

In fact, bubble transport is not perfect and wake shedding and replenishment of solids occurs continuously in the passage of bubbles through the successive layers. Accompanying this upward movement of material is a downward displacement of solids for mass conservation. Thus, in an interval of time T any layer receives material from both above by displacement and from below by bubble transport. Whereas, the material obtained by displacement is from the layer immediately above, that obtained by bubble shed contains material from the layers below, giving rise to an asymmetrical pattern of mixing which is characteristic of fluidisation.

In Appendix 4, this pattern of bubble transport, wake shed and downward displacement is assumed to occur in discreet steps from layer to layer. A bubble shedding factor f of value $0 < f < 1$ determines the fraction of the wake that is shed in passage from one layer to the next, and this factor is assumed to be constant through the bed height. The wake carrying capacity of bubbles is also assumed to be constant through the bed height. Commencing with a given pattern defining the carbon content of layers as C_1 to C_5 in a bed of say five layers at time m T shown in Table A4.1, the mechanisms of bubble transport, wake shed and downward displacement described above are applied to deduce the composition of the carbon in the layers at time $\overline{m + 1}$ T in terms of the carbon contents C_1 to C_5 of the layers at time m T. From this pattern is deduced the algorithm of

equations defined in A4.4 that define the composition of the general layer r. The composition of the surface layer is defined in equation A4.5.

3.5.2 The Lateral Flow of Solids

Because of bubble coalesence, material within a segment is constantly directed towards the centre of the segment at the surface. In view of this, it is assumed that no solids material interchange between segments occurs through the bed height except between surface layers. This is because of the surface spreading of solids as bubbles burst on the surface. From any given segment a fraction B of value $0 < B < 0.5$ of the material in the surface layer flows laterally to each of the two adjacent segments in the case of lateral flow transverse to a linear coal feeder. Knowing the content of surface layers of segment j and its adjacent ones j + 1 and j - 1 at time m T, the composition of the surface layer in segment j at time $\overline{m + 1}$ T is defined by equation A4.6. Boundary conditions at the centre of the coal feed cell and at its periphery are set down in equations A4.7 and A4.8.

C H A P T E R 4

COMBUSTION AND ELUTRIATION

COMBUSTION AND ELUTRIATION

4.1 General

It has been pointed out in sub-section 2.2 that the volatile content of the coal that is fired may have a direct bearing on the size of the coal feed cell, and hence the number of segments of which it comprises. Figure 2.5 shows a relationship between the number of segments over which the coal spreads for stoichiometric combustion, and the volatile content of the coal fired. This is based on the assumption that all the volatiles are evolved in the coal feed segment and that these burn in the segment with some of the available oxygen. Over and above this, 20% of the feed fines is assumed to burn in the coal feed segment. Both these latter assumptions are deduced indirectly from data plotted in Figures 4.1a, b and c, based on experimental results from a fluidised bed combustor.

In the characteristics of Figures 4.1a, b and c, which show the quality of combustion obtained experimentally when the fuel feed conditions are altered from excess air (positive stoichiometric) to excess coal (negative stoichiometric) these results show non-linear changes in both carbon concentration in the bed (Figure 4.1a) and in carbon elutriation loss (Figure 4.1b). In addition, Figure 4.1c shows some incomplete combustion indicated by the presence of CO and CH_4.
In the experimental investigation a feed rate was set and maintained for four hours, during which transients were assumed to reach steady-state before readings were taken. It may be argued that the implications of this procedure can lead to

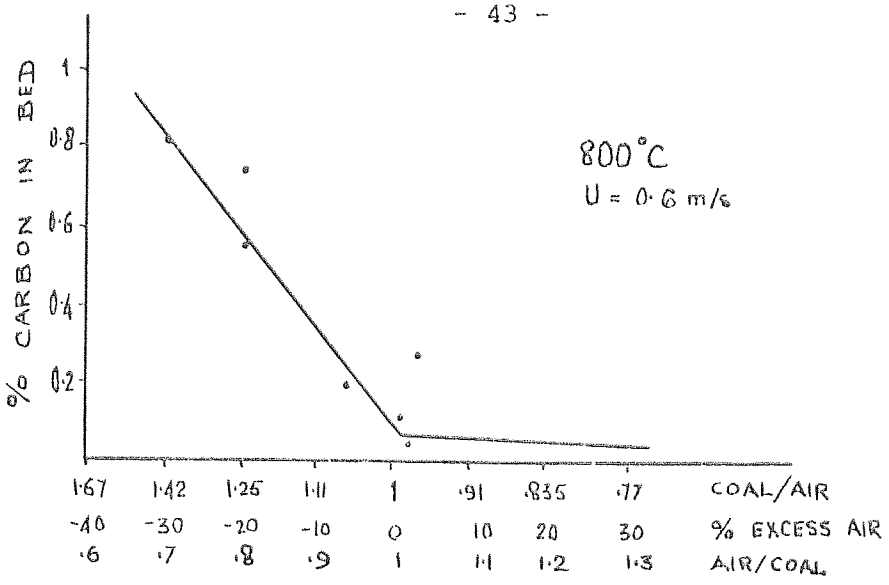

a. Carbon Content of Bed

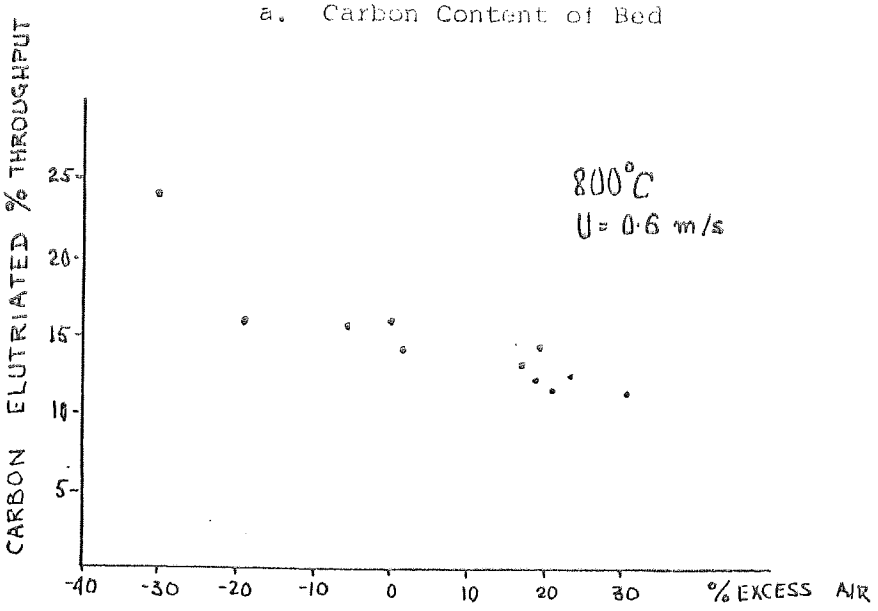

b. Carbon Elutriated from Bed

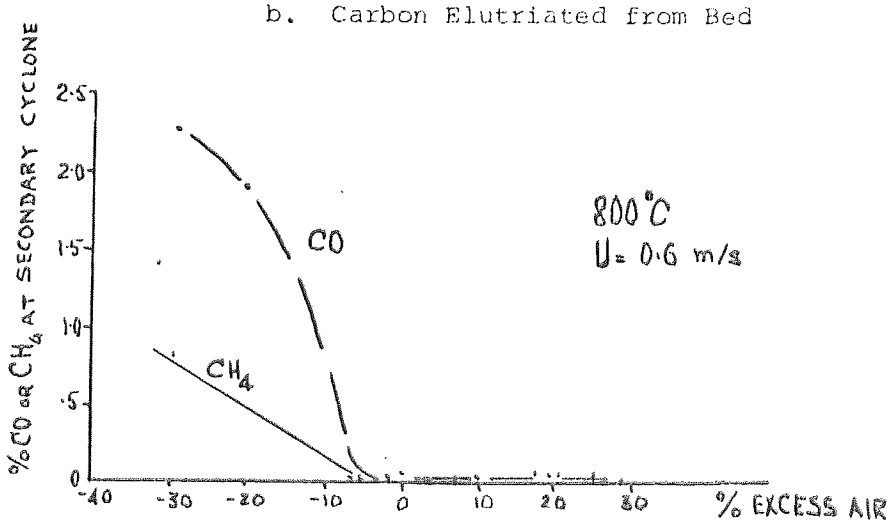

c. Incomplete combustion with excess coal

FIGURE 4.1 EXPERIMENTAL RESULTS FROM A FLUIDISED BED COMBUSTOR

inferences which may be misleading, in particular with excess coal feed.

Thus, within the confines of the experimental combustor, there is not enough air to burn with the coal fired. However, steady-state conditions require that the carbon leaving the bed must be equal to the carbon supplied. The excess coal feed builds up in the bed to a level at which the abrasion loss is the same as the excess coal supplied. This explains the sudden increase in carbon concentration (Figure 4.1a) as well as the excessive carbon elutriation loss (Figure 4.1b) with excess coal feed. The long residence time of the carbon in the bed must decrease its size distribution unrealistically so that the elutriation rate is artificially high for a given carbon concentration. The high carbon concentration together with the large proportion of reactive fines not only competes with the volatiles for the available oxygen in the combustion zone, but may result in some conversion of CO_2 into CO through the bed height. This explains the incomplete combustion shown in Figure 4.1c.

In a large bed the apparent excess carbon fed to a central segment of a coal feed cell moves laterally into outer segments where it burns. Thus, in this study it is assumed that the carbon concentrations in the segments arise from the requirements of lateral flow alone. Furthermore, no incomplete combustion is allowed for as in Figure 4.1c, and the quantity of feed fines elutriated in a coal feed segment is assumed to be a constant proportion of the coal throughput. From Figure 4.1b the proportion of fines elutriated is about 14% of the throughput

under stoichiometric coal and air feed conditions. A critical elutriation size of 0.125 mm is equivalent to about 18% of fines in the coal feed. If a proportion of 0.2 of this is assumed to burn in the coal feed segment, the elutriation is 14% of the throughput which is in close agreement with the experimental results.

Further assumptions of the present study that affect the pattern of combustion are as follows:

Lateral uniformity is assumed in a segment.

Combustion is largely confined to the bottom layer of each segment where there is oxygen uptake[19]. In support of this it was observed that the oxygen by-pass of the bed did not vary substantially when the bed height was varied from 1 m down to 0.1 m. Any oxygen not burnt after the first layer is assumed to by-pass the bed.

Combustion together with abrasion reduces the diameter of carbon particles at a zero order rate with respect to the particle size - k_1 for combustion and k_2 for abrasion. All abrasion fines are assumed to be below the critical elutriation size. The rate of size reduction of carbon particles due to combustion is a function of the background carbon, the size distribution of the carbon particles, and the oxygen available for combustion in the segment in question.

The coal feed particles are assumed to have a size distribution given by the Rosin-Rammler relation A5.1 in Appendix 5, and shown in Figure 4.2. It is assumed that there is no change in size distribution of the particles due to decrepitation,

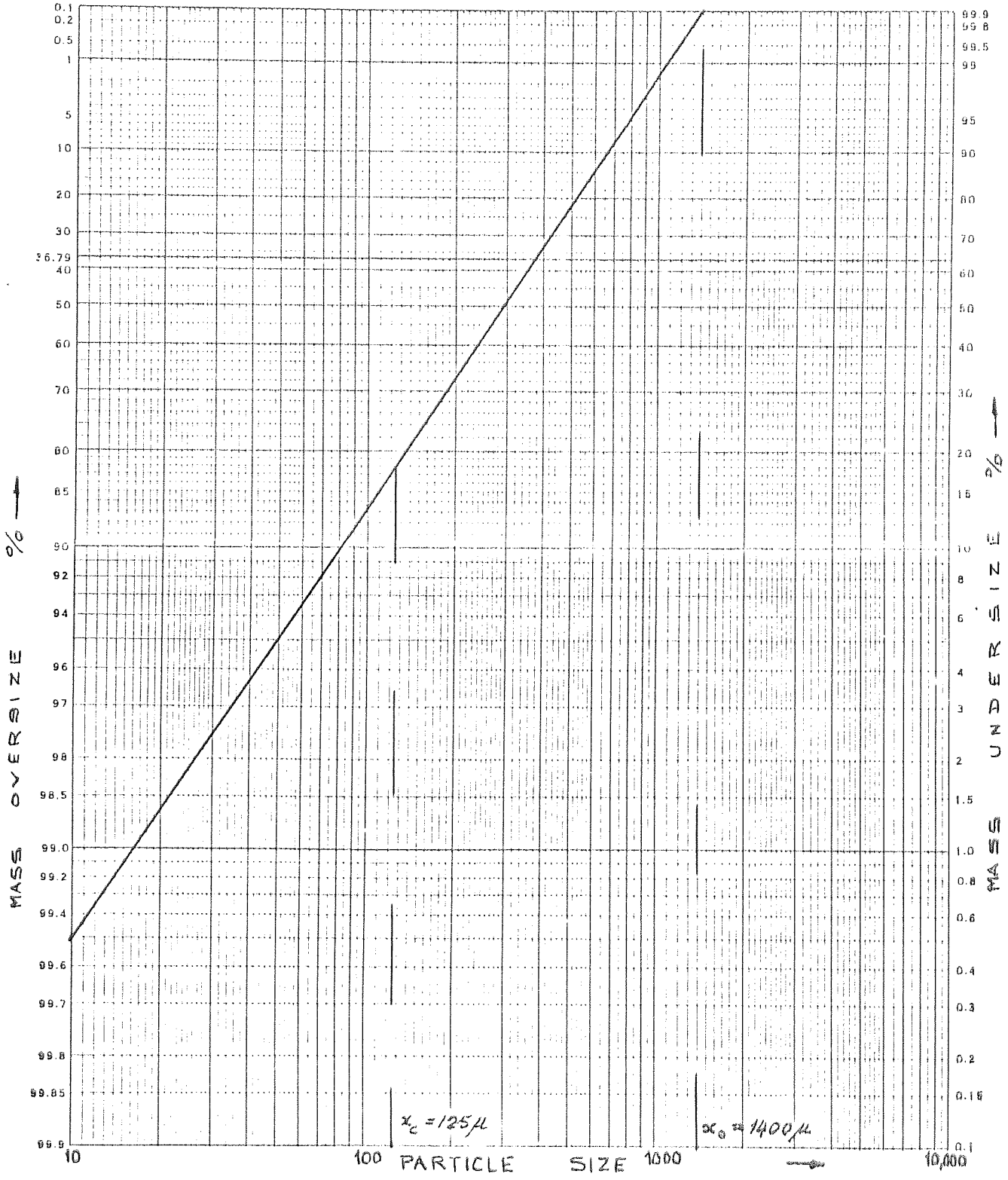

FIGURE 4.2 ROSIN-RAMMLER SIZE DISTRIBUTION OF COAL FEED

swelling or volatile emission. The feed fines consist of that fraction of the feed below the critical elutriation size, x_c, remembering that these fines loose their volatile content immediately on meeting the hot ash plasma of the bed. Expression A5.2 and A5.3 respectively may be written for the feed fines burnt within the bed, and the remainder which is elutriated from the bed, based on the assumption that a fraction ϕ_o of the feed fines burns within the bed.

4.2 Steady-state Mass Loss of Carbon from a Segment

Steady-state combustion and abrasion, which result in carbon particle size reduction, are dealt with in Appendix 6. Assuming zero order reduction rates, with respect to size, for both combustion and abrasion, a change Δx in size in the incremental time T (plug flow time of bubbles gas through the bed height) may be defined as in equation A6.02. The size range of the feed may be expressed as a series of μ mono-sizes, each mono-size differing from the next by Δx. In this way the combined effects of combustion and abrassion which together result in a size reduction of Δx in time T, may conveniently be expressed by each mono-size decreasing one size. Such a concept contains the essentials of a mechanistic approach to represent the effect of combustion, and will be discussed later.

The basic assumption that the combustion is of zero order with respect to particle size is shown to lead in equation A6.07.to an expression that defines the change in mass of a particle due to combustion as a function of its surface

area, i.e. x^2. It is a widely held view that combustion for solid fuels is a surface phenomena. It is fortuitous that this same assumption, that combustion and abrasion are of zero order with respect to size, allow the mass reduction due to combustion to be separately expressed from that due to abrasion, in spite of the two being lumped together to produce a common size reduction Δx in time T. The form of this expression is given in equation A6.10 and is common to both combustion and abrasion. One set of constants l_1, p_1, q_1 is used to derive the mass reduction of each monosize for combustion, while a second set of constants l_2, p_2, q_2 is used to derive the mass reduction of each monosize for abrasion. In this way the effects of combustion and abrasion may be accounted for separately.

Now, the background carbon varies from segment to segment, while the air available for combustion is more or less constant for all segments. This gives rise to a change in the rate of particle size reduction from one segment to the next. In turn, this results in a different particle size distribution in each segment. Since combustion is a surface phenomenon, the rate of particle size reduction due to combustion is itself effected by the total surface area of all the carbon particles in a segment. The relationship between $\dot{x}$, the rate of size reduction of particles, S, the total surface area of the carbon particles, and the net air available for combustion of carbon particles in a segment is given in equation A6.14. $\dot{x}$ is inversely proportional to S and directly proportional to the net air for combustion. Using this relationship it is possible to derive the rate $\dot{x}^j$ of

particle size reduction in the jth segment knowing $\dot{x}^s$ for the periphery segment s as set down in equation A6.17.

It is appropriate at this stage to define the units in which carbon and air are expressed in this study. The coal feed cell, composed of several segments, is considered to be operated at stoichiometric coal and air throughput. All amounts of carbon and air are expressed as fractions or multiples of the cell throughput, here regarded as unity.

Such a unit is consistent with the operation of a fluidised bed which is concerned with the rates of carbon feed to and removal from the cell. Where the rate of carbon loss or air usage is a fraction of the cell throughput, such as mass loss due to combustion and elutriation, or to excess air etc, the rate is expressed as a fraction of the 'cell throughput'. On the other hand the background carbon in a segment represents a potential combustion inertia that has the dimension of time. Hence:

$$\begin{array}{l}\text{background carbon or}\\ \text{potential combustion}\\ \text{inertia in segment}\\ \text{(seconds)}\end{array} = \frac{\text{background carbon in segment (kg)}}{\text{carbon throughput for entire cell (kg/s)}}$$

This unit of time gives an indication of the integral of throughput accumulated or the time for which the carbon in the segment will support combustion. A meaningful comparison of the background carbon in segments from cells of different size is possible in terms of the duration for which the carbon in the segments will support combustion. In Figure 7.01, the combustion inertia is expressed in seconds of cell throughput. For a cell

composed of three segments, the combustion inertia in the central or coal feed segment is an accumulation of 42 seconds of cell throughput, while the combustion inertia in each of the outer segments is 23 seconds of cell throughput. The duration for which the total carbon in the cell will support combustion is 88 seconds - there being one segment of 42 seconds and two each of 23 seconds of throughput. A direct comparison may be made with the combustion inertia for a cell of two segments where, from Figure 7.01, the combustion inertia in the central segment is 50 seconds, while the combustion inertia in the two flanking half segments together is 34.5 seconds. The total combustion inertia in the cell of two segments is 84.5 seconds as compared with 88 seconds for a cell of three segments.

The value of expressing the background carbon as combustion inertia is appreciated by comparing the combustion inertia in the central or coal feed segment for the two and three segment cells considered above. The combustion inertia in the central segment for N = 2 will support combustion at the cell throughput for 50 seconds, while the combustion inertia in the central segment for N = 3 will support combustion at its cell throughput for only 42 seconds. This is a meaningful comparison, yet the absolute quantity of background carbon in the central segment for N = 2 is less than that in the corresponding segment for N = 3.

The coal throughput for a segment in a fluidised bed of height 0.75 m, fluidised at U = 0.75 m/s is estimated[9] as 0.016 kg/s. The cell throughput is thus 0.016 N kg/s, where there are N segments in the cell. A segment having a combustion

inertia of C seconds, contains 0.016 NC kg of carbon. With 500 kg of ash per segment, the carbon concentration is 0.0032 NC%. The combustion inertia profiles of Figure 7.01 are plotted in Figure 7.02 using this relationship to give the percentage carbon concentration in the segments for comparison.

Having defined the units (fraction of cell throughput to signify combustion, elutriation, etc, and combustion inertia in seconds to signify background carbon) combustion balances between carbon and air may be expressed as fractions of cell throughput and equated. Typically, such a balance for the jth segment is expressed in equation A6.23, from which may be derived expressions A6.24 and A6.25 for the net air (fraction of air throughput) available for combustion of carbon particles in the jth (general) and sth (periphery) segments of the coal feed cell. These expressions are used in equation A6.17 to define the rate of particle size reduction $\dot{x}^j$ in the jth segment relative to the rate of particle size reduction $\dot{x}^s$ in the periphery segment s.

The different rates of particle size reduction in the segments of a coal feed cell may be said to effect a constant size reduction over different incremental periods of time in the respective segments. If these increments of time for the same size reduction in the segments are arranged to be integers, then the same particle size reduction Δx occurs in the segments at these integers of time respectively. By this ruse the carbon and the carbon particle mass-size distribution in the different segments may be expressed in terms of the identical range of mono-sizes as the feed is subdivided into. Thus, no problem is

encountered in lateral flow in which an exchange of particles between surface layers of adjacent segments occurs, since the same range of mono-sizes is used to define the mass-size distributions in all segments. Equations A6.29, A6.30 and A6.32 relate the incremental time T^j for the jth segment to the incremental time T required to effect the same size reduction Δx in segment s. The ratio T^j/T of these incremental times is finally expressed in equation A6.30 in terms of the known rates of size reduction k_1 due to combustion, and k_2 due to abrasion for the periphery segment s.

The mono-size mass interchange between surface layers of adjacent segments is based on equation A4.6 and is expressed as an algorithm of three equations, A6.31 to A6.33, arranged in three steps. Lateral exchange is applied at increments T of time, and the accumulated mono-size mass over the increment T^j of time is subjected to a single size reduction. In the final step of the algorithm the nomenclature is updated to correspond to the next size down for the subsequent increment T^j of time.

Three boundary conditions apply to the implementation of equation A6.31 at j = 1 the coal feed segment, and j = s the periphery segment for N = odd or even number of segments. These conditions are analogous to reflection at these boundaries, and are defined in equations A6.34 to A6.36.

The product of mono-size mass in segment j and the fractional loss in mass due to combustion and abrasion are expressed in equations A6.38 and A6.39 to give expressions for the carbon loss from each mono-size in the segment due to combustion and

abrasion respectively per incremental time T.

The size reduction to critical elutriation size x_c of the penultimate size x_{c-1} in segment j gives rise to fines, the rate of removal of which, with respect to the incremental time T, is expressed in equation A6.40.

The losses in mass (fraction of cell throughput) of combustion and elutriation expressed in equations A6.38 to A6.40 in terms of each mono-size are integrated over the entire range of mono-sizes to give the carbon loss (fraction of cell throughput) due to combustion and elutriation in the segment. For the coal feed segment the feed fines burnt within the bed and that elutriated from the bed from equations A5.2 and A5.3 respectively are added to these amounts to give the carbon combustion and elutriation in equations A6.41 to A6.43. For segment j the carbon combustion and elutriation losses (fraction of cell throughput) are expressed in equations A6.44 to A6.46

4.3 Steady-State Carbon and Air Combustion Balances in the Cell and in the Freeboard

Steady-state combustion balances both in the cell and in the freeboard above the cell are defined in Appendix 7 in terms of the fraction of throughput of air and carbon. With stoichiometric coal and air feed to the cell, an amount of air (fraction of cell throughput) must by-pass the bed to balance the elutriation of fines from all the segments of the cell in the steady-state. This is set down in equation A7.1.

Now excess fluidising air could be used to increase the combustion of fines within the bed, and thereby tend to reduce

the elutriation of unburnt fines. However, the excess air tends to increase elutriation loss because of the increased fluidising velocity, removes a larger proportion of the heat of combustion as sensible heat in the increased air flow, and results in increased pumping costs. Because of these factors, it may be more effective to introduce directly into the freeboard preheated excess air to increase the combustion of elutriated fines.

All the fines of critical elutriation size x_c must remain in the proximity of the surface in the freeboard until reduced by combustion to airborne size x_e for open tube air flow. In the steady-state the combustion of the fines of size x_c per unit of incremental time T is defined by E_1 of equation A7.3. Of the remaining fines a fraction, E_2, burns in the freeboard (equation A7.4) while the remainder E_o is lost in the stack (equation A7.5) with the corresponding air by-phass (fraction of throughput) expressed in equation A7.8.

4.4 Transient Mass Loss of Carbon from a Segment

In order to determine the dynamic characteristic of heat evolution in the coal feed cell, it is necessary to derive an expression for the mass loss of carbon due to combustion in the segments during a transient in response to a step change in coal and air throughput. This expression is deduced in Appendix 8.

In the steady-state the background carbon in each segment supports both the lateral flow of carbon through the segment as well as the combustion loss that is in balance with the fluidising

air. The combustion mass loss ML^j of carbon in segment j from equation A6.44 may be expressed as the product of the background carbon in the combustion zone and a mean reduction factor $\bar{\gamma}^j$ defined in equation A8.02. Provided the transient does not introduce large relative changes in background carbon in the segments, this value of $\bar{\gamma}^j$, the mean reduction factor, may be assumed to apply over the entire transient. Thus, both before and after the transient, the mean reduction factor, $\bar{\gamma}^j$, gives rise to mass losses which are in combustion balance with the fluidising air, while during the transient as the background carbon in the segment builds up, it provides an instantaneous mass loss which increases in value from that before to that at the end of the transient. Now this instantaneous mass loss of carbon is in combustion balance with only part of the fluidising air during the transient. The remainder of the air may be said to be in instantaneous excess. At the start of the transient this instantaneous excess air is equal to the step increase in air. As the transient progresses it decreases to zero in the steady-state.

During a transient following a step increase in throughput to the cell, combustion imbalances are set up in segments between the net carbon flow in and the fluidising air. There is an immediate increase in air throughput at the step change. The net carbon flow into each segment, however, is established gradually as the background carbon builds up in response to the step increase in coal throughput to the cell.

In each segment the mass loss ML_t^j of carbon due to

combustion during the transient may be considered as the sum of two terms as in equation A8.08. The first term represents the instantaneous mass loss of carbon as the background carbon builds up, while the second term is a function of the difference between the maximum potential and instantaneous mass losses during the transient. This second term is in balance with the instantaneous excess air throughput, and decreases to zero as the transient progresses to steady-state. The instantaneous excess air during a transient may not be expected to have the same efficiency of utilization as that fraction of the fluidizing air, which is in balance with the instantaneous loss of carbon as a result of the build up of the background carbon. The factor e of value $0 < e < 1$ sets the efficiency of utilization of the instantaneous excess air during the transient in equation A8.08. The mass loss of carbon due to this second term is effective immediately as the step increase of air throughput, and depletes the background carbon in the segment. As the transient progresses the lateral flow of carbon overcomes this depletion to give a build up of background carbon.

Since combustion is assumed to occur at the surface of carbon particles, and since e is a function of part of the combustion air uptake, the parameter e^j is directly proportional to s^j the surface area of all the carbon particles in segment j as in equation A8.07. This equation may be used to relate the values of e^j for the successive segments of the cell.

During the transient the fines burnt in the segments are assumed to increase in the ratio of the total mass loss to the

mass loss ML^j of equation A6.44 prior to the transient. The proportionality factor defining the increase in fines burnt is given in expression A8.10.

C H A P T E R 5

DEVELOPMENT OF COMPUTER PROGRAM OF THE MODEL

DEVELOPMENT OF COMPUTER PROGRAM OF THE MODEL

5.1 General

The mechanisms and algorithms synthesised in Appendices 4 to 9 that define the vertical and lateral mixing of solids within a fluidised bed and the size distribution, combustion and elutriation of carbon from segments must be assembled into a sequence to simulate a fluidised bed boiler.

Due to the limitation of storage space available in the computer, it was not possible to assign a unique mass-size distribution to the carbon particles in each layer of all the segments of the coal feed cell. This called for a compromise in which a two-stage solution is adopted. In the first stage no differentiation is made within a segment in terms of layers and a steady-state simulation is carried out. All the carbon particles within a given segment are subjected to a uniform rate of size reduction to determine mass losses due to combustion and elutriation, combustion inertia and carbon particle mass-size distributions in the segments. The values obtained from this steady-state simulation, in particular the mass losses due to combustion and elutriation, and the combustion inertia in the segments are used in a second stage solution in which distinction is made between layers of segments and a transient solution effected. In this second stage solution these steady-state values deduced from the first stage are used, together with vertical and lateral mixing and the mechanism of mass loss of carbon due to combustion during a transient (Appendix 8) to determine the mass loss of carbon as a consequence of transient

heat evolution.

5.2 Initial Values of Background Carbon, and Carbon Mass-Size Distribution in Segments

In programming the model an iterative procedure for computation is inevitable.

The incremental time to effect a fixed size reduction in the several segments of a cell are functions of factors such as combustion inertia, size reduction, fines burnt, etc. However, in the various segments, these latter factors are in themselves functions of the former increments of time to effect a size reduction which defines combustion, elutriation, background carbon and mass-size distribution of particles etc. Such an interdependence calls for an iterative computation.

Commencing the computations with initial values which are close to the final values of the combustion inertia and mass-size distribution of carbon particles in the several segments of the coal feed cell ensures the rapid and stable convergence of the iterative procedure. Moreover, if these initial values are derived by simple rough-and-ready estimates, they form a useful cross-check on the more involved treatment by the model. Expressions are derived in Appendix 9 to define both the background carbon (seconds) and the mass-size distribution of carbon particles (fraction of throughput) in the various segments of the cell, using simple rough-and-ready methods for the estimation.

The estimates of background carbon are made starting with the periphery segment of the cell and proceeding to the coal

feed segment. The potential between the background carbon in adjacent segments must be sufficient to effect the necessary lateral flow of carbon from the centre to the periphery of the cell (equation A9.3). This relates the background carbon in adjacent segments. The background carbon in the periphery segment of the cell is estimated by considering the rate of removal of carbon by combustion, the rate of mixing, and the average burning time of carbon particles and is set down in equation A9.1.

Estimates of the mass-size distributions of carbon particles are made starting with the coal feed segment and proceeding to the periphery of the cell. This is because the mass-size distribution of the coal which is fed into the coal feed segment is known. Based on this, the mass of each monosize in the coal feed segment is generated by applying the relationship A9.4. This relationship defines the mass of a monosize x_r over that incremental time required to effect a reduction in particle size from one monosize to the next. In equation A9.4 the mass M_r of the monosize x_r during any incremental time is expressed as the sum of the mass of the monosize x_{r-1} in the segment during the previous incremental time and now reduced to size x_r by the reduction factor $(1 - \gamma_r)$ because of combustion and abrasion, together with the mass m_r^f of the monosize x_r in the feed during the present incremental time. Using the mass of particles of each monosize generated from this relationship, it is possible to express the mass of each monosize as a fraction of the total mass of all monosizes, and then relate this mass-size

distribution to the background carbon in the segment in question to arrive at the combustion inertia of the carbon particles in each monosize given in expression A9.6.

A comparison is made in Figure 5.1 between the above estimate of initial values of background carbon over six and seven segments and the final values obtained from the model after iterative convergence. The maximum misalignment is no more than 25%.

Figure 5.2 shows a comparison between the estimate of initial values of mass-size distributions of carbon particles in a cell of seven segments and the final values obtained from the model after iterative convergence.

5.3 Program of the Model in the Steady-State Mode

A flow chart of the essential stages of the steady-state mode of the model is shown in Figure 5.3 with a list of the equations used in the computations. The program may be subdivided into three steps.

In the first step represented by the first two blocks, a number of preliminary factors are calculated to set the computation in its context. Among these are the fraction of volatiles and fines in the feed, the subdivision of the remainder of the feed carbon into monosizes, the number of segments in the cell, and the initial background carbon in segments.

In the next step represented by the second two blocks in Figure 5.3, the mass reduction factors for combustion and abrasion are calculated. This is done by initially assuming

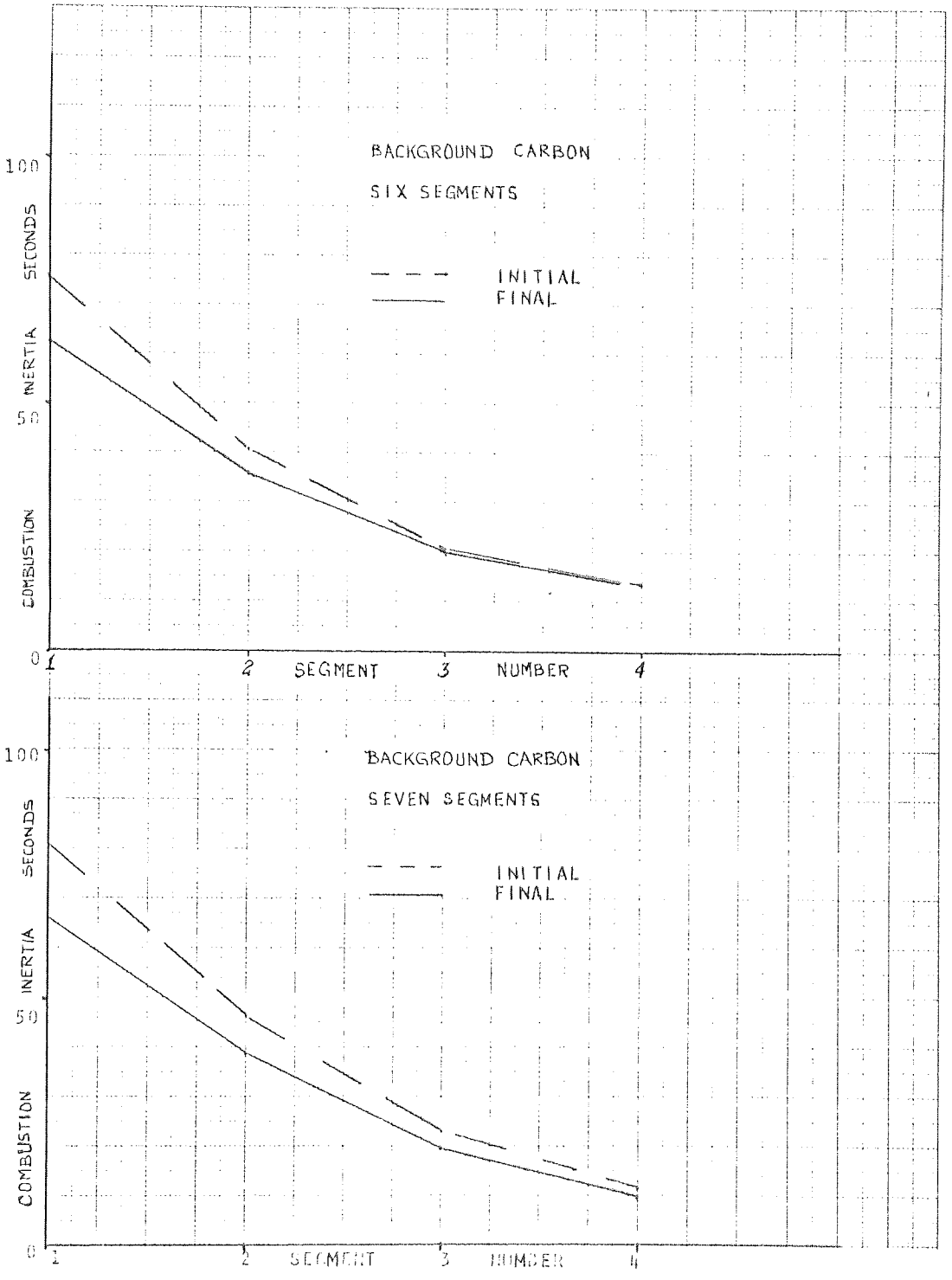

FIG. 5.1 BACKGROUND CARBON IN SEGMENTS OF COAL FEED CELL SHOWING PROXIMITY OF INITIAL VALUES TO FINAL.

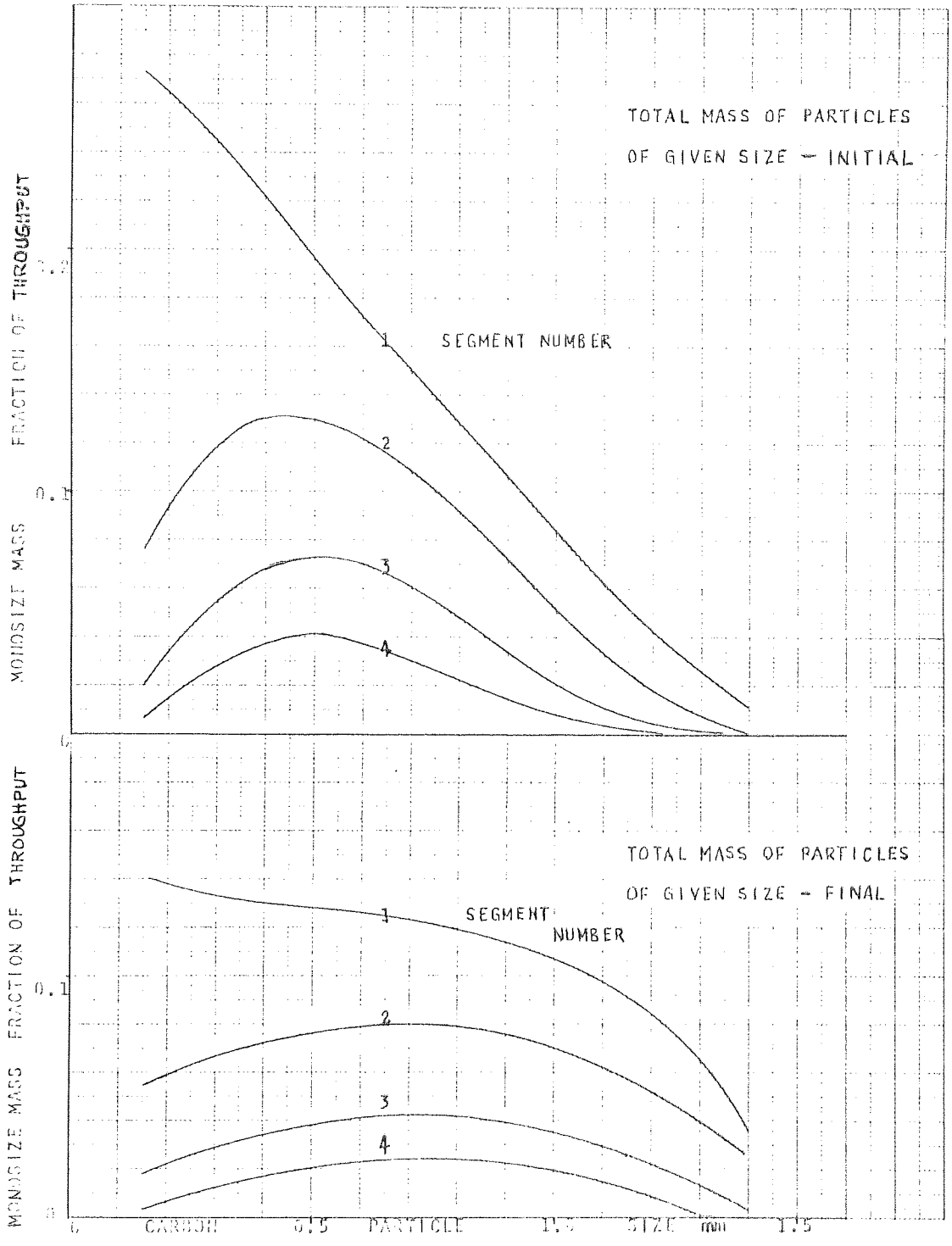

FIG. 5.2 MASS-SIZE DISTRIBUTION OF CARBON IN CELL OF SEVEN SEGMENTS SHOWING PROXIMITY OF INITIAL TO FINAL VALUES.

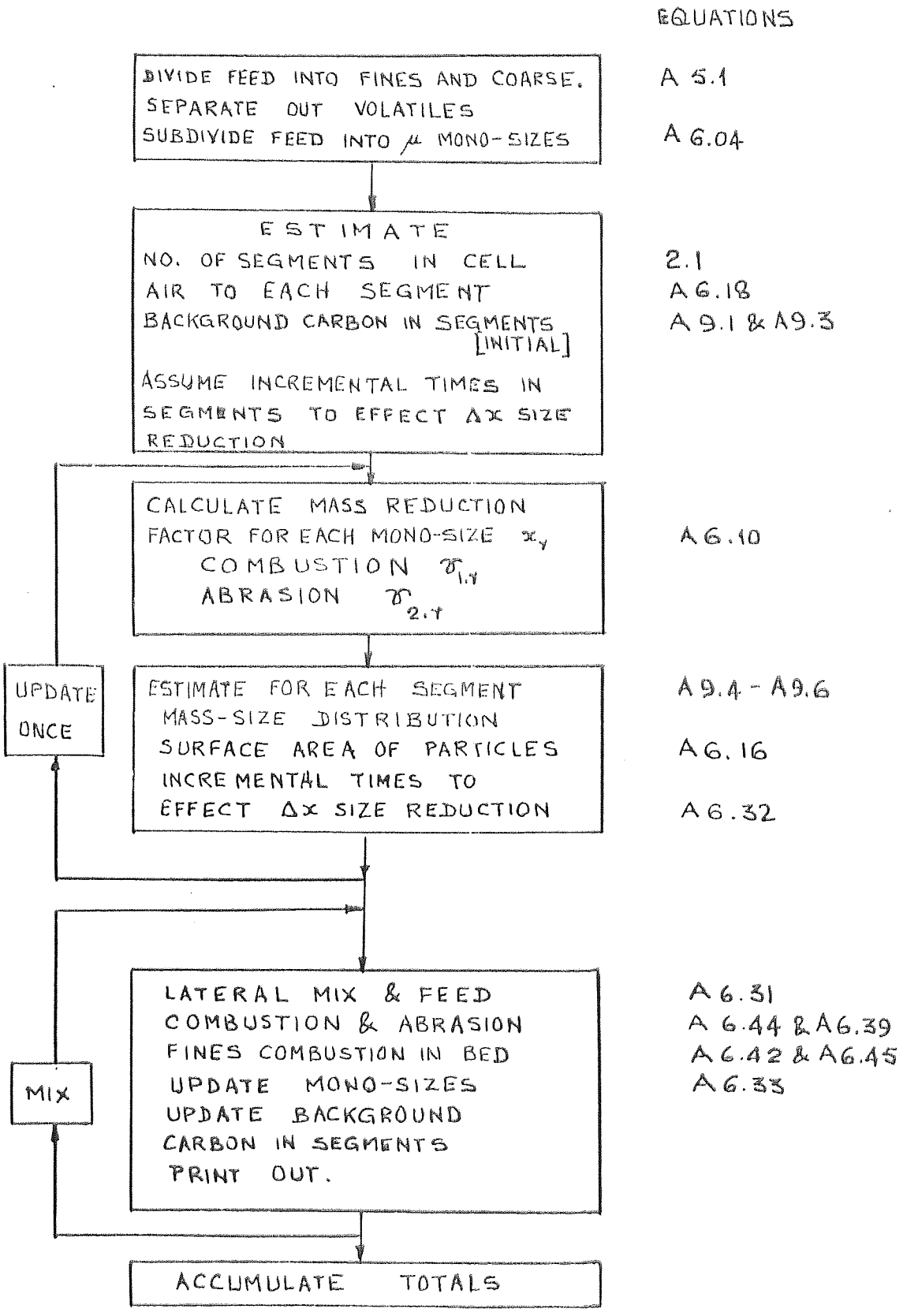

FIGURE 5.3 FLOW CHART OF ESSENTIAL STAGES OF FLUMX THE STEADY-STATE MODE

values for the ratio between segments of the incremental times to effect a particle size reduction Δx. From these, mass reduction factors for combustion and abrasion of carbon particles in the segments are derived and used with the estimates of initial mass-size distributions of carbon to define the combustion mass loss in the segments. A re-estimate is made of the ratio between segments of the incremental times to effect a particle size reduction Δx, and of the mass reduction factors for combustion and abrasion of carbon particles in the segments.

In the third step represented by the last block of Figure 5.3, the steady-state operation of feed, lateral mixing, mass loss due to combustion and elutriation, and fines burning is put into effect by a loop labelled MIX. Thus, the combustion and abrasion are based on a mechanistic size reduction of the mass-size distribution of carbon particles in each segment.

The program FLUMX of the steady-state mode of the model is given in Listing A10.1. The detailed flow chart is given in Figure A10.1, while a typical print-out is in Table A10.1. The names used in the program are related to the symbols used in the model synthesis in the nomenclature to Appendix 6. For identification, the first four lines of the print-out list the data used in the computation. By way of illustration the data for the computation in Table A10.1 shows the critical elutriation size of carbon particles x_c = 125.6 μm, the coal fired has a volatile content V = 11%, due to abrasion the particle size reduction per second is KA1 = 0.1 μ/s, while that for combustion KC1 = 1.7 μ/s and finally the lateral flow parameter B = 0.1

(fraction of surface layer in lateral flow per second). The data format to operate FLUMX is given in Table A10.2.

The main body of the print-out is arranged in columns and rows. The columns relate to the segments of the coal feed cell. The left-hand column relates to the coal feed segment, while the extreme right-hand column relates to the periphery segment of the coal feed cell. The rows of the print-out are in blocks of several lines each. The first three blocks of rows correspond in the program FLUMX, to the step of updating initially assumed values discussed above. Of these the first two blocks are based on the assumed values, while the third represents an updating of these values. Thereafter the rows are arranged in blocks of five lines, with each block of print-out representing a complete cycle of operations that corresponds to an excursion around the MIX loop of Figure 5.3 referred to above.

The factors of interest are C the background carbon, SCOMB the mass loss due to combustion of carbon, FB the fines burnt and FE + CFF the fines elutriated from the segments. The print-out of Table A10.1 is for N = 7 segments; hence, there are four columns from the central to periphery segments inclusive.

At the bottom of the print-out are totals of various mass losses, each labelled. Both the initial and final mass-size distributions of carbon particles in the segments are shown as a printout in Table A10.3.

5.4 Program of the Model in the Transient Mode

A flow chart of the essential features of the transient

mode of the model is shown in Figure 5.4 with a list of the equations, derived from the Appendices, that are used in the computations. The program may be divided conveniently into two steps.

In the first step represented by the first block in Figure 5.4, the values of background carbon, combustion and elutriation from the segments of the coal feed cell are taken from the print out of FLUMX. The background carbon is subdivided between the layers of segments, and expressed in terms of the post-transient steady-state throughput.

The second step is represented by the five blocks within the loop of Figure 5.4. These blocks represent the operation of the fluidised bed combustor with mass loss of carbon due to combustion for a step increase in coal and air throughput. The essential stages consist of adding coal throughput to the coal feed segment, vertically mixing between layers of all segments, laterally mixing between surface layers of adjacent segments, calculating the mass loss due to combustion in the transient mode, and removing all carbon burnt and fines elutriated from the segments.

The program FLUTRA of the transient mode of the model is given in Listing All.1, with a detailed flow chart in Figure All.1. Table All.1 is a typical print out from FLUTRA. It is set out in six columns, each with a heading. The entries under these columns define various constituents of the carbon losses (fraction of throughput) for the entire coal feed cell for the duration of the transient. Time is indicated by COUNT, and progresses

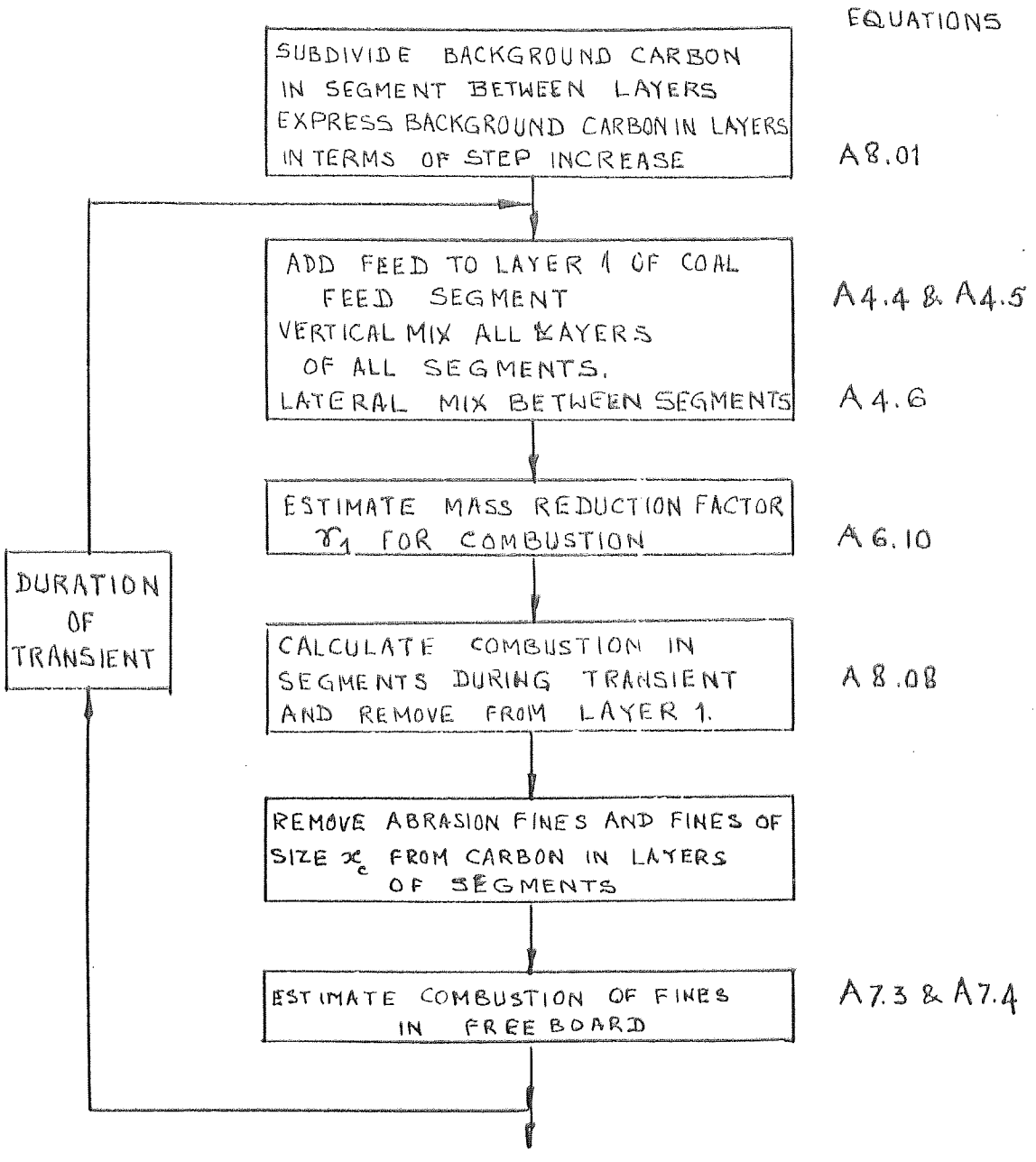

FIGURE 5.4 FLOW CHART OF THE ESSENTIAL STAGES OF FLUTRA THE TRANSIENT MODE

geometrically in binary steps of a second to cover a transient span of 17 min. in ten steps. The print out also identifies SEGKOL, the background carbon expressed as a combustion inertia (seconds) for each segment.

The main factors of interest are the changes during the transient of the combustion in the bed, and the build up of background carbon in the segments of the cell. The results shown in Table All.1 are for a cell of N = 7 segments, hence there are four values of SEGKOL the background carbon for segments number 1 to 4.

The data format required to execute FLUTRA is given in Table All.2.

Inadvertently, the print out from FLUMX used as data in FLUTRA, groups together abrasion and feed fines, and these require to be resolved. A short program XLATE in Listing All.2 translates the print out from FLUMX into a form suitable for FLUTRA. The input and output formats for XLATE are given in Table All.3.

C H A P T E R 6

PARAMETERS OF THE COMBUSTION MODEL

PARAMETERS OF THE COMBUSTION MODEL

6.1 General

The results of simulations carried out on the model depend on the values of the parameters and constants used. In Section 7 dealing with Combustion and Elutriation, arguments are advanced showing that considerable care must be taken in extrapolating from results of an experimental investigation on a pilot model to represent the operation of a full-scale plant. In particular, the confines of a plant model do not allow a realistic representation of successive sections from the coal feed area to the periphery of a coal feed cell. Near the coal feed, in a large fluidised bed, the level of background carbon is far higher than that which supports combustion in a smaller pilot model, given that both plants are operated at the same stoichiometric coal and air throughput. To build up background carbon in a pilot model to an unrealistic level by excess coal feed in an attempt to study the combustion conditions near the coal feeder in a large plant, raises questions as to the validity of the exercise, especially if the excess coal feed is maintained in the steady-state. Steady-state implies carbon loss in equilibrium with carbon feed. The air throughput can only remove part of the coal throughput which is in excess. Hence, the remainder must be lost by some other mechanism such as abrasion which comes into prominence under these conditions of excessive carbon residence time. This excess of abrasion fines, which is more reactive than the carbon particles, may result in some incomplete combustion. In fact, these very phenomena are evident in the experimental results on the

pilot plant at negative stoichiometric air throughput as shown in Figures 4.1a, b and c. In this study, extrapolation from the experimental results is avoided in an attempt to avoid problems of scale-up. The only values of parameters used in the model are implicitly deduced from experimental results. It is thus necessary to ensure the acceptability of the values of the parameters used in the absence of explicit results from experimental investigations, by subjecting them to cross-checks.

Table 6.1 contains a list of the parameters used in the model, the symbol by which each is identified and the name given to it in the program. Values are set against these parameters, and it is these that must be tested for acceptability in the absence of an experimental model fitting procedure. Broadly, this list of parameters falls into two categories. There is a number of parameters of primary significance to the functioning of the model so that it simulates reasonable conditions. These are size of coal feed cell (a function of the volatile content of the coal), lateral solids flow, and rates of size reduction of carbon particles. The second category of parameters, e.g. fractional combustion of fines in the bed and in the freeboard are of secondary importance to the simulation. Nevertheless, the importance of this second set of parameters is not to be underrated, since they have an important bearing on combustion efficiency etc. Parameters in this second category are given fixed values throughout as shown in Table 6.1.

For the steady-state mode there are three parameters of primary significance, the volatile content V of the coal, the

TABLE 6.1 Parameters of the Model and Their Estimated Values

P r i n c i p l e P a r a m e t e r s

SYMBOL	PROGRAM NAME	NOMINAL VALUE	DESCRIPTION
B	B	0.1	Lateral flow parameter (inter-segment) fraction of solids layer
e	E	0.12	Utilisation (fraction) of step increase in air during transient
f	F	0.2	Vertical flow parameter (between layers) fraction of solids layer.
k_1	KCl	1.7 μ/s	Rate of size reduction of carbon particles by combustion
V	V	11-45%	Volatile content of coal (dry ash-free basis)

N.B. The range of volatile content 11-45% corresponds to N = 7 to 2 segments in the coal feed cell. Values of V are chosen to give integer values of N from Figure 2.5.

/Table 6.1 cont....

TABLE 6.1 (cont.)

Secondary Parameters

SYMBOL	PROGRAM NAME	NOMINAL VALUE	DESCRIPTION
a_b	BY	0.01	Air by-pass (fraction of throughput)
a_x	AX	0.1	Excess air " "
a	PA	0.012	} Rosin-Rammler constants defining carbon particle size distribution
b	PB	0.5997	
k_2	KA1	0.1 μ/s	Rate of carbon particle size reduc-tion by abrasion
n	NOL	10	Number of layers in segment for solids flow
T	T	12 s	Incremental time intervals at which the computation carries out a sim-ulation
T_c	TC1	10 s	Average conbustion time of carbon particles
x_c	XC	0.125 mm	Critical particle size for elutria-tion from the bed
x_e	XE	0.1 mm	Particle size airborne in freeboard
x_o	XO	1.4 mm	Largest particle size of coal feed
Δx	DX	21.6 μm	Difference between one mono-size and the next
ϕ_o	COMB(0)	0.2	Fraction of feed fines burning in the bed
ϕ_1	COMB(1)	0.2	Fraction of abrasion fines burning in the bed
ϕ_2	COMB(2)	0.2	Fraction of fines of size x_c burning in the bed
ϕ_3	COMB(3)	0.2	Fraction of fines of size $x < x_e$ burning in the freeboard
μ	MU	59	Number of mono-size fractions the coal feed is subdivided into

lateral solids flow, parameter B, and the rate k_1 of decrease in size of carbon particles due to combustion.

In addition to the three parameters mentioned above for the steady-state mode, there are two further parameters of significance in the transient mode. These are f, the vertical solids transport parameter, and e the efficiency of utilization of the excess air during the transient.

At best, the values chosen for these important parameters are close estimates and are nominal values derived indirectly from experimental observations. It thus becomes necessary to make comparisons of the significance of variations in the nominal values of these parameters. The simulation produced by the model using this set of nominal parameter values may be said to define a nominal operating point in a multi-dimensional plane, the co-ordinates of which are defined by the individual parameters. By altering these parameters one at a time about their nominal values, while keeping the others at their nominal values, it is possible to make excursions in the multidimensional plane about the operating point along one vector at a time. In this study the simulations by the model in both the steady-state and transient modes are made so as to study the effect of altering the values of these parameters one at a time.

6.2 Nominal Values of Parameters

The nominal values for the five most significant parameters are as follows:

a. Volatile Content of Coal Fired

If it is assumed that only the volatiles and part of the feed fines burn in the coal feed segment, then the primary effect of an increase in the volatile content of the coal feed is to leave less carbon for lateral flow and subsequent combustion in the remainder of the segments of the cell. The number N of the segments that comprise the coal feed cell is thus directly dependent on the volatile content of the coal fired. The number N of segments comprising the cell defined by equation A6.20, in which it is assumed that 0.2 of the feed fines burns in the bed, is plotted in Figure 2.5.

From this graph values of volatile content of coal fired are chosen which lead to integral numbers of segments ranging from 2 to 7 in the coal feed cell in this study. This variation provides a reasonable range for interpolation using most coals. A coal feed cell of three segments is adopted as nominal in this investigation.

Normal coals used for power generation in Britain have a volatile content of 36-38%. On a dry ash-free basis the volatile content is approximately 45-47% for an ash content of say 15%. From Figure 2.5, such a coal is likely to be effective over a cell of no more than two segments to give a coal feed spacing of about 1.5 - 1.75 m using linear feeders. This is confirmed by an independent study on plant design carried out at the Coal Research Establishment, Stoke Orchard.

b. Lateral Solids Flow Parameter B

The lateral solids flow parameter is the fraction of the surface layer that undergoes solids exchange with an adjacent segment per incremental time T. The nominal value adopted in this study is a fraction 0.1 per second. A lateral diffusional flow of 0.01 would result in the same total solids exchange between all ten layers of adjacent segments per second. This value is not far removed from the value of 0.04 for the diffusion coefficient determined experimentally at CRE, Stoke Orchard, in a cold model of 1.5 m diameter using radioactive carbon injected at a point in the centre. Unfortunately, no attempt was made in the experimental program to confirm the reported[10] effect that lateral transfer is largely confined to a surface exchange between segments. Steam tubes immersed in the bed will tend to prevent lateral mixing in the lower reaches of the bed, but should not interfere with the surface spreading of solids as bubbles shed their burden there.

c. The Rate k_c of Decrease in Size of Carbon Particle Due to Combustion

With a value of $k_c = 1.7$ μ/s, the number of size fractions calculated, assuming a size reduction every second, is prohibitively large. It becomes expedient to work on an enlarged computational time basis T of about 12s for this number to be reasonable. Thus Δx, the difference in size between mono-sizes, is:

$$\Delta x = (k_c + k_a)T \qquad 6.1$$

where the particle suffers size reduction due to the rates of both combustion k_c and abrasion k_a for a time T.

The mean size of particles may now be estimated using the average combustion time T_c of particles before they reduce to elutriation size x_c as:

$$x_c + \Delta x \quad T_c \qquad 6.2$$

where Δx is the difference in size between adjacent mono-sizes from equation 6.1.

This simple estimate gives a mean particle size of 0.34 mm using the values of the variables k_c, k_a, T_c and x_c listed in Table 6.1.

This is only just on the low side for a feed size range up to 1.4 mm, but it indicates that the rate k_c of size reduction of 1.7 μ/s is reasonable. This value is used in the investigation as nominal, with values of 2.3 μ/s and 1.1 μ/s to show the significance of variations in the value of k_c.

d. Vertical Solids Transport Parameter f

In general, it is considered that vertical solids transport in fluidised beds is rapid at any rate, much faster than the lateral flow of solids. Unfortunately, controlled experiments to measure the vertical mixing had low priority in the experimental programmes. Moreover, any measurement of this parameter depends quite critically on such factors as the presence of steam tubes and their packing density. It must be remembered that the parameter f represents the bubble shedding

factor. As f approaches unity, the shedding is large while the vertical transport is small. On the other hand, as f approaches zero, the bubble shedding is small resulting in increased vertical transport of solids. A nominal value of f = 0.2 is taken in this study as being consistent with fairly rapid vertical solids transport. Because of the uncertainty attached to the value of this parameter, large fluctuations on either side of the nominal are considered, i.e. 0.1 to 0.4.

e. Efficiency of Air Uptake During the Transient Mode

From Figure 4.1b, it may be seen that the elutriated carbon fines (fraction of throughput) falls about 2% from 15% to 13% when the excess air is increased from 0 to 20%. This corresponds to an improvement of about 12% in the combustion. During the transient mode in this study, the step change in air throughput is 20%. It is reasonable to assume a similar 12% improvement in combustion. The carbon combustion is balanced by air uptake, hence the efficiency of utilisation of the excess air in the periphery segment is taken as e = 0.12.

Again, Figure 4.1b shows that this efficiency of utilisation of the step increase in air during a transient is unlikely to alter by amounts larger than 15-20%. In this study the value of e is varied by 20%.

6.3 Range of Parameter Variations

For the steady-state mode three sets of parameter variations are made in this study by varying one at a time each of

three parameters about their nominal values (N = 3 segments, B = 0.1, k_c = 1.7 μ/s). On each occasion the other two parameters are kept at nominal values. The parameter variations for investigations in the steady-state mode are shown in Table 6.2

TABLE 6.2 Three Sets of Parameter Variations for the Steady-State Mode

N	B	k_c
2 to 7	0.1	1.7
3	0.05 0.2 }	1.7
3	0.1	1.1 2.3 }

For each of these three sets of parameter variations in the steady-state mode a graphical study is presented of the background carbon in the segments (Figures 7.01-7.04), the fines elutriated from the segments (Figures 7.05-7.07), and the mass size distribution of the carbon particles (Figures 7.08-7.10) in the segments of the cell.

For the transient mode five sets of parameter variations are made by varying one at a time each of five parameters about their nominal values (N = 3 segments, B = 0.1, k_c = 1.7 μ/s, f = 0.2 and c = 0.12). On each occasion the other four parameters are kept at nominal values. The sets of parameter variations for

the transient mode are shown in Table 6.3.

TABLE 6.3. Five Sets of Parameter Variations for the Transient Mode

N	B	k_c	f	e
2 to 7	0.1	1.7	0.2	0.12
3	0.05 0.2 }	1.7	0.2	0.12
3	0.1	1.1 2.3 }	0.2	0.12
3	0.1	1.7	0.1 0.4 }	0.12
3	0.1	1.7	0.2	0.1

For each of these five sets of parameter variations in the transient mode a graphical study is made of the response to a step change in coal and air throughput of the transient of mass loss of carbon corresponding to heat evolution in the cell (Figures 7.11 - 7.15) and the build up of background carbon in the segments of the cell (Figures 7.16 - 7.19).

CHAPTER 7

DISCUSSION OF RESULTS OF THE COMBUSTION MODEL

DISCUSSION OF RESULTS OF THE COMBUSTION MODEL

The results of the simulations carried out of both the steady-state and transient modes are presented graphically to show the effect of each of the sets of parameter variations outlined above in Tables 6.2 and 6.3. From a study of the effects produced by varying these parameters, their significance in the model may be deduced.

7.1 The Steady-State Mode

The effect of the three sets of parameter variations of Table 6.2 on three factors is studied in the steady-state mode. These factors are the background carbon in the segments of the cell, the fines elutriated from the segments and the mass size distribution of carbon particles in the segments of the cell.

7.1.1 The Background Carbon in the Segments of the Cell and the Coal Feed Spacing

Values for the background carbon in the segments of the cell are shown in Figures 7.01 - 7.04 in which the straight lines merely serve to join points corresponding to values of combustion inertia in the segments.

Figure 7.01 shows the background carbon in the segments as the number N of segments in the cell is altered from 2 to 7. The background carbon is expressed as a combustion inertia in seconds of throughput, and indicates the integral of the cell throughput accumulated, or the time for which the carbon in the segment will support combustion. When expressed in units of throughput relative to the size of the cell, the

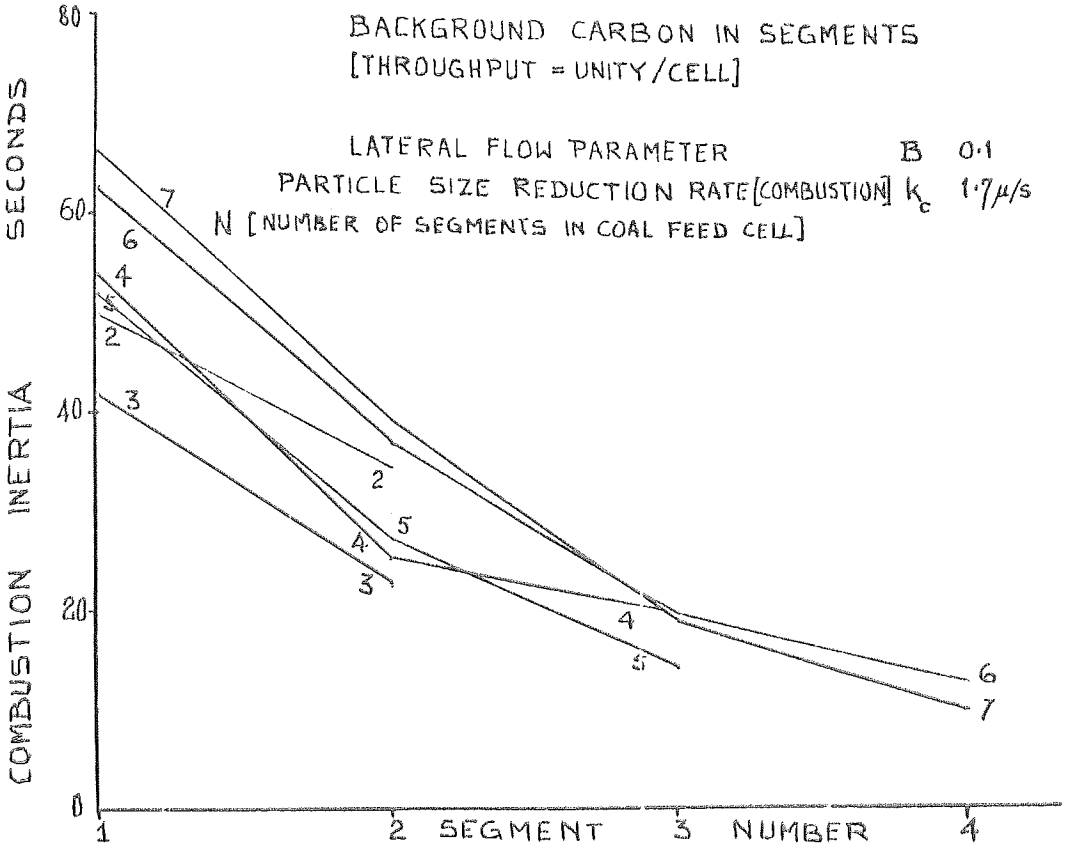

FIGURE 7.01 CARBON CONTENT OF SEGMENTS OF COAL FEED CELLS OF VARYING SIZE

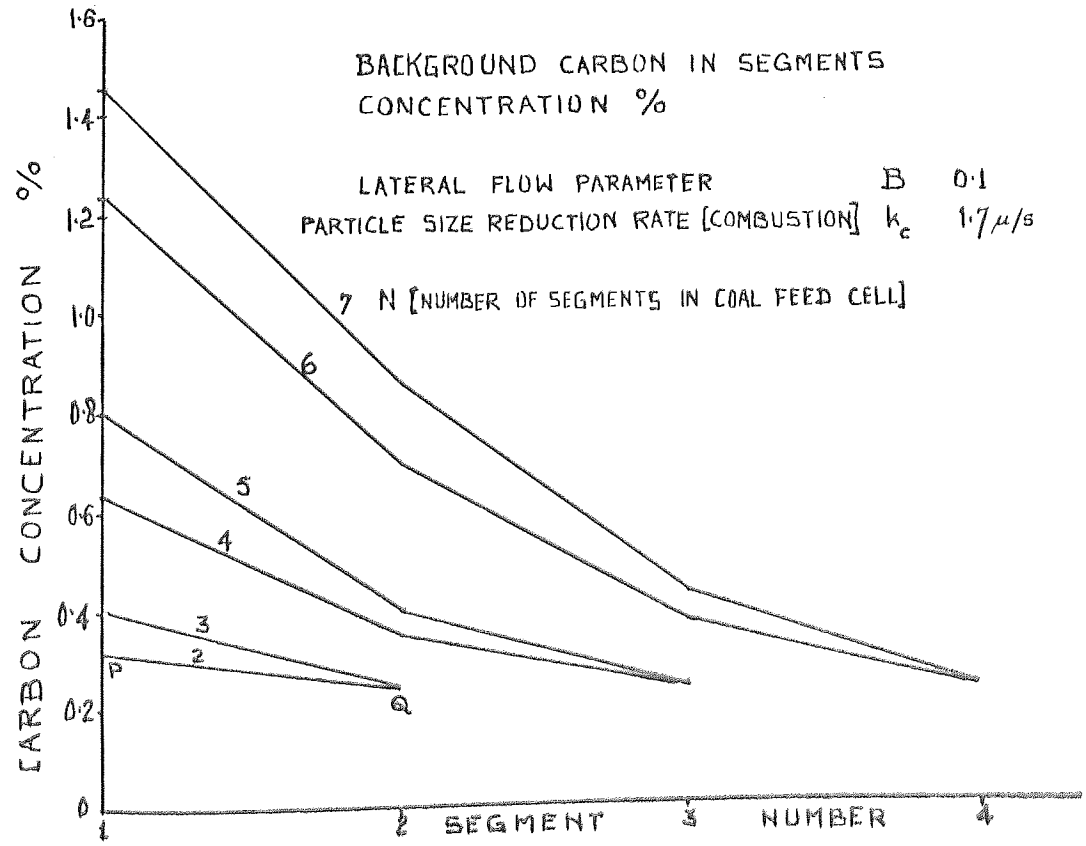

FIGURE 7.02 CARBON CONCENTRATION IN SEGMENTS OF COAL FEED CELL OF VARYING SIZE

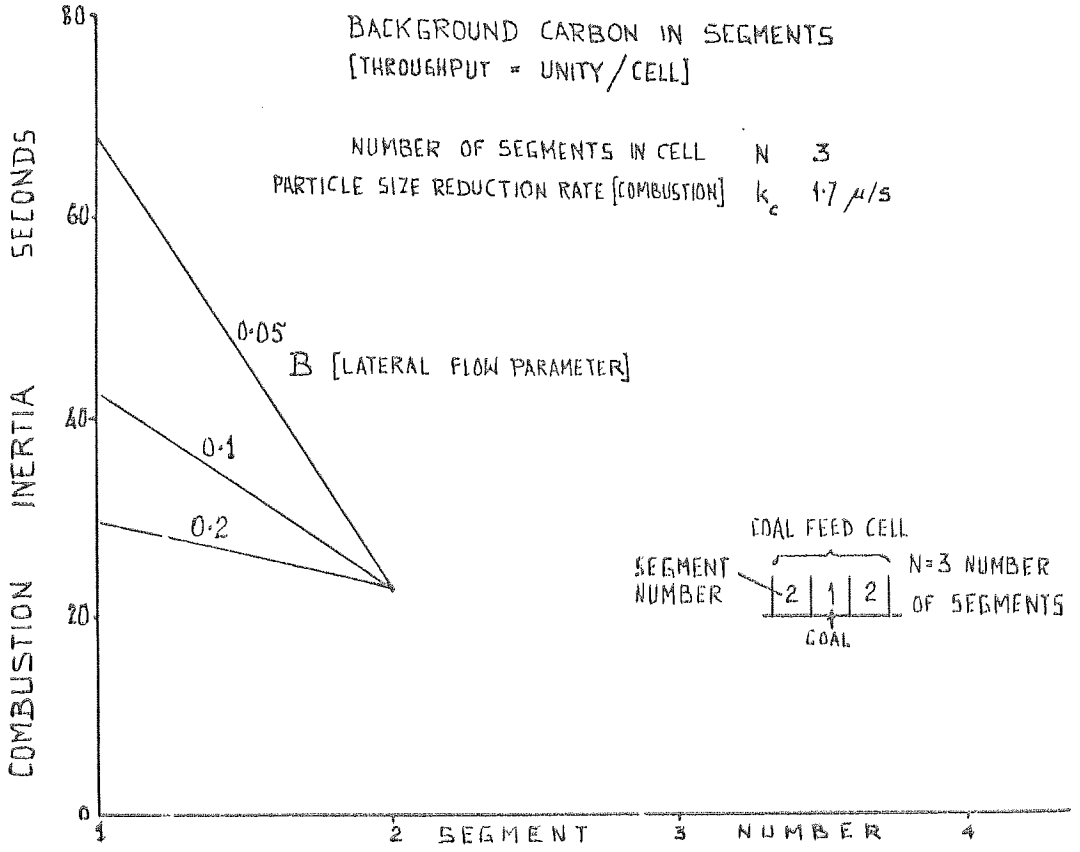

FIGURE 7.03 CARBON CONTENT OF SEGMENTS OF COAL FEED CELL SHOWING EFFECT OF VARIATION OF LATERAL FLOW PARAMETER B

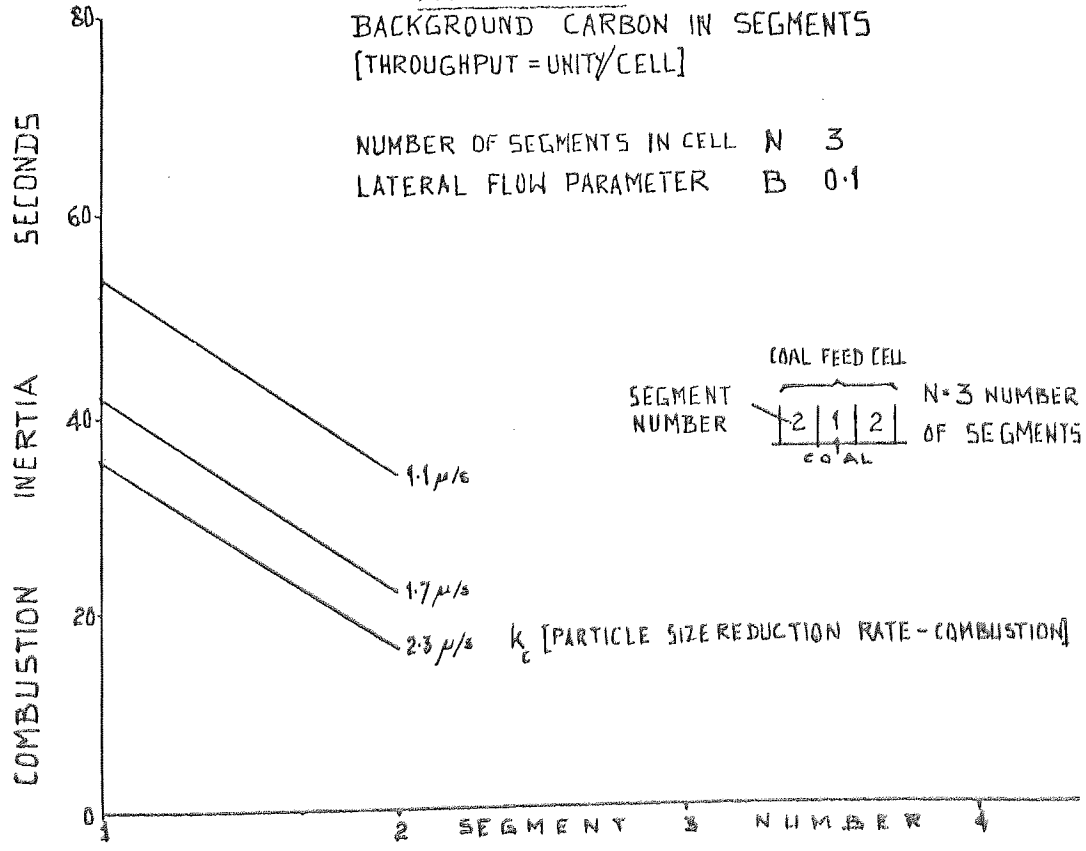

FIGURE 7.04 CARBON CONTENT OF SEGMENTS OF COAL FEED CELL SHOWING EFFECT OF VARIATION OF COMBUSTION RATE K_C

profiles indicate that the background carbon is substantially constant with segment number.

The background carbon profiles of Figure 7.01 expressed as % concentrations are plotted in Figure 7.02, and reveal the familiar profiles based on absolute units.

Normal coals used for power generation in Britain have 36-38% volatile matter. On a dry ash-free basis the volatile content is 45-47% for an ash content of, say, 15%. From Figure 2.5 such a coal is likely to spread over a cell of no more than two segments. Figure 7.02 indicates that the concentrations are 0.32% at P and 0.24% at Q in the coal feed and outer segments respectively. These values are somewhat higher than the 0.1% carbon concentration at stoichiometric throughput from Figure 4.1a obtained experimentally from the pilot plant. However, the model predictions are over two segments each of approximately 0.75 to 0.9 m width, and served by a single coal feeder, and may be expected to indicate a higher carbon concentration than that over a distance of 0.9 m in the pilot plant.

The spacing in between coal feeders is the width of the coal feed cell, since the cell is defined as being fed by a single feeder. For coals of 36-38% volatile content, the feeder spacing is of the order of 1.5 - 1.75 m. Half the segments covering the bed area would be served directly by the

coal feeder, while the remainder would depend on the lateral flow of carbon. From Figure 7.01 the background carbon accumulated in the coal feed segment is 50 seconds of cell throughput, while that in the intermediate segment between coal feed segments is 35 seconds of cell throughput. The cell as well as the entire unit of Figure 2a contains carbon equivalent to a combustion inertia of 85 seconds.

If the volatile content of the coal fired changes from that for which the coal feed spacing is designed, a loss in combustion efficiency is likely to arise. An increase in volatile content of the coal fired will lead to a lean combustion mixture (excess air) at the periphery of the cell. Decreasing the fluidising air somewhat tends to restore the combustion mixture at the periphery of the cell, but is likely to result in unburnt volatiles in the coal feed segment. Certainly, the total combustion in the cell will decrease. On the other hand, a decrease in the volatile content of the coal fired will result in the combustion of sufficient carbon in the coal feed segment to compensate for the decrease in volatiles, with the result that there will be no substantial change in the quality of combustion over the cell.

Figure 7.03 shows the effect of a variation in B, the lateral solids flow parameter. As this is decreased, a steeper background carbon profile between segments is necessary to maintain the lateral flow of carbon. On the other hand, maintaining the lateral solids flow parameter B constant, and altering the combustion rate k_c of particle size reduction as

in Figure 7.04, results in a constant differential in background carbon between segments since B is constant. The level of background carbon falls with increased combustion rate k_c of particle size reduction since a smaller population of carbon particles will support the same combustion loss of carbon as k_c increases.

7.1.2 Carbon Fines Elutriated from the Segments

Values for the carbon fines elutriated from the segments of the cell are shown in Figures 7.05 - 7.07. The straight lines have no significance and merely serve to join points corresponding to carbon losses for the various segments. The carbon loss is expressed as a fraction of the coal throughput.

Figure 7.05 shows the carbon fines elutriated from the segments as the number N of segments in the cell is altered from 2 to 7. The carbon loss from the coal feed segment is from three to ten times greater than the loss from any other segment. This is due to the fines in the feed which are confined to the coal feed segment. In the other segments of the cell the fines are generated by the size reduction of carbon particles due to combustion and abrasion.

For a coal of 36-38% volatiles, the cell is composed of two segments. Figure 7.05 indicates 0.105 of the throughput is elutriated from the coal feed segment, mainly feed fines. From the outer segment, 0.038 of the throughput is elutriated. The total fraction 0.143 of the throughput is in good agreement with the 12-15% obtained from experimental results (Figure 4.1b)

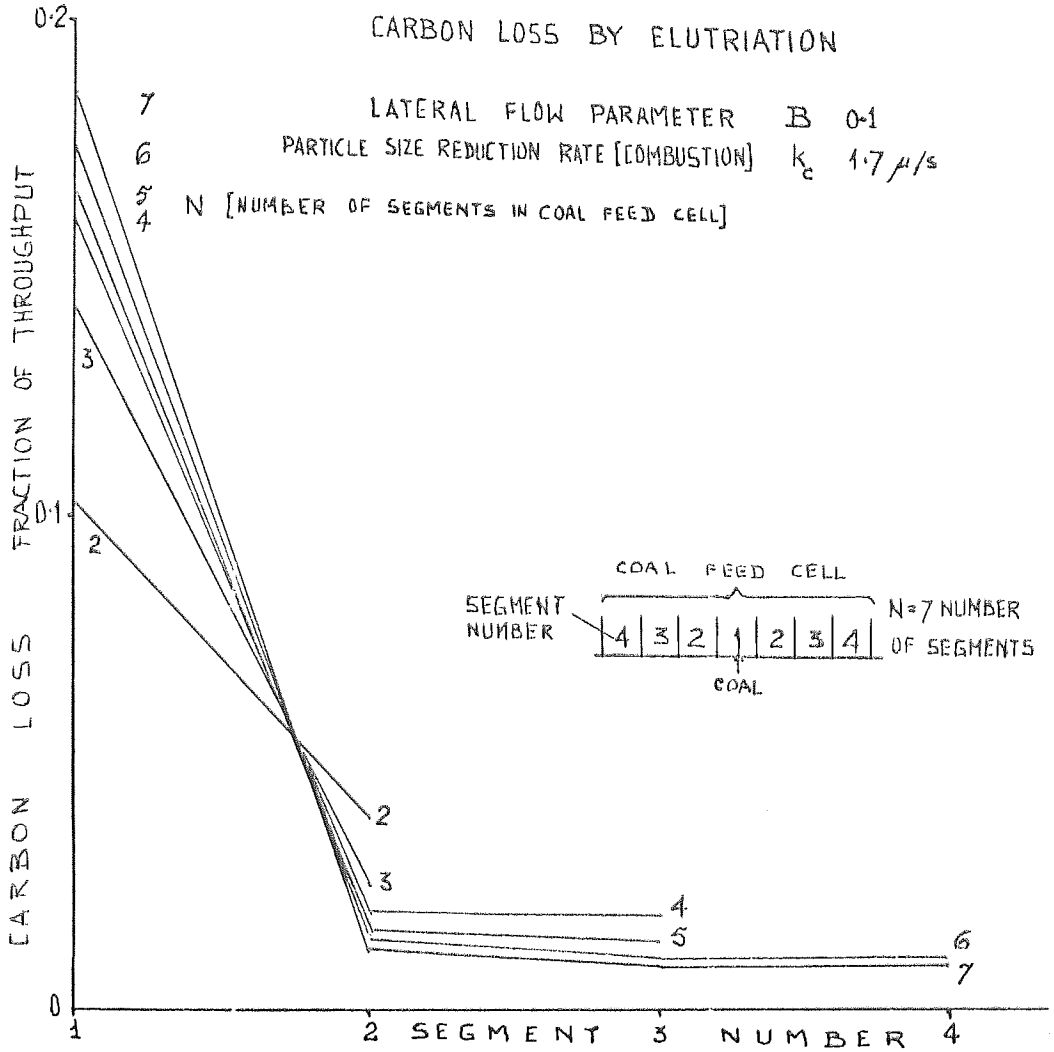

FIGURE 7.05 CARBON FINES ELUTRIATED FROM SEGMENTS OF COAL FEED CELLS OF VARYING SIZE

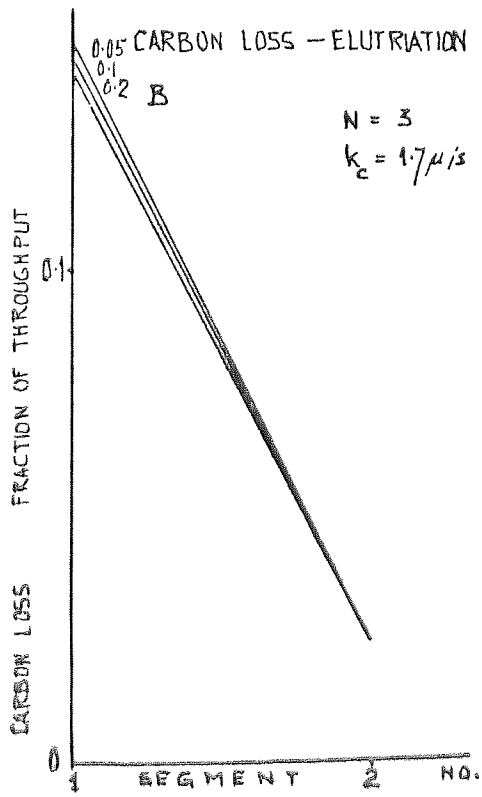

FIGURE 7.06 CARBON FINES ELUTRIATED FROM SEGMENTS. EFFECT OF VARIATION OF LATERAL

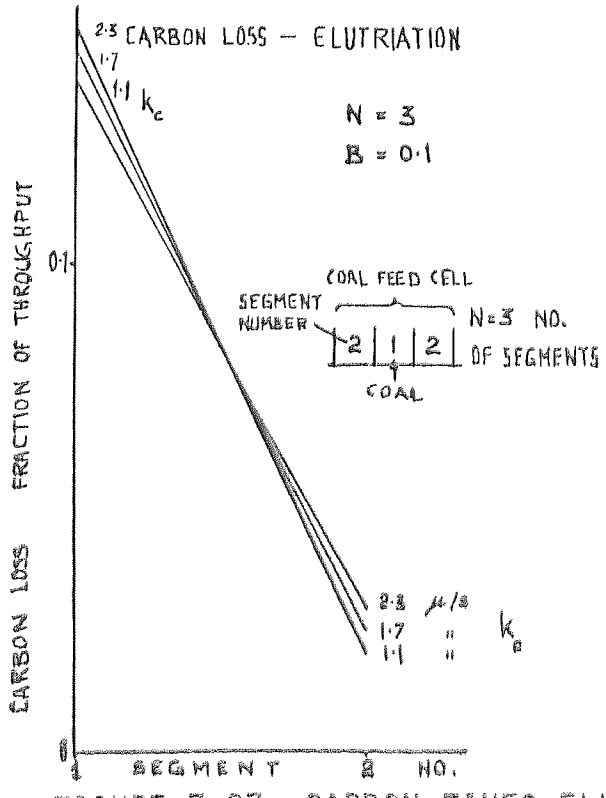

FIGURE 7.07 CARBON FINES ELUTRIATED FROM SEGMENTS. EFFECT OF VARIATION OF COMBUSTION RATE k_c

on the pilot plant operated at stoichiometric throughput.

There is no significant change in elutriated carbon loss by varying either the lateral solids flow parameter B (Figure 7.06) or the combustion rate k_c of carbon particle size reduction (Figure 7.07). It is interesting to note from Figure 7.06 that the carbon loss in the coal feed segment increases slightly as B decreases. From Figure 7.03 the background carbon in the coal feed segment must increase to provide a steeper carbon profile necessary to maintain the lateral flow of carbon as B the lateral solids flow parameter decreases. Now this increased background carbon in the coal feed segment, subjected to abrasion, results in an increase of carbon fines elutriated as B decreases (Figure 7.06).

Figure 7.07 also indicates an interesting effect. The elutriation loss of carbon from the periphery segment decreases, while the loss from the coal feed segment increases with an increase in the combustion rate k_c of size reduction of carbon particles. The explanation for the decrease of elutriation loss in the periphery segment lies in the decrease in background carbon (Figure 7.04) as k_c increases. A decreased background carbon will result in reduced elutriation loss as k_c increases.

In the coal feed segment, the elutriated carbon fines generated within the segment by abrasion and size reduction also decrease with an increase in k_c, since the background carbon decreases (Figure 7.04). However, this effect is overshadowed by the elutriated feed fines which increase slightly as k_c increases. This slight increase in feed fines

is due to rounding errors in making the number of mono-sizes integral by adjusting x_c, the critical elutriation size.

7.1.3 The Mass-Size Distribution of Carbon Particles in the Segments

The effects of the three sets of parameter variations of Table 6.2 on the mass size distributions of carbon particles in the segments of the cells are shown in Figures 7.08 - 7.10.

Figures 7.08a and b, show the mass size distribution of the background carbon in the segments as the number N of segments in the cell is varied from 2 to 7. There are two indications in this set of results. Firstly, there are more smaller particles in the inner segments of the cell than in the outer. This is due to the increased background carbon having a longer residence time. The rate of size reduction of carbon particles decreases with an increase in background carbon, resulting in an increase in smaller particles.

The second inference is that, as the number N of segments in the cell increases from 2 to 7, the smaller sized particles decrease proportionately in the outer segment. This is due to the decreased residence time of the carbon and the accompanying increase in the rate of particle size reduction. There is also a hint that there is a decrease in the number of the largest particles in the periphery segments.

As the lateral mass flow parameter B decreases, there is a significant increase of smaller carbon particles in the background carbon in the coal feed segment as shown in Figure 7.09. This is due to the high level of background carbon (Figure 7.03)

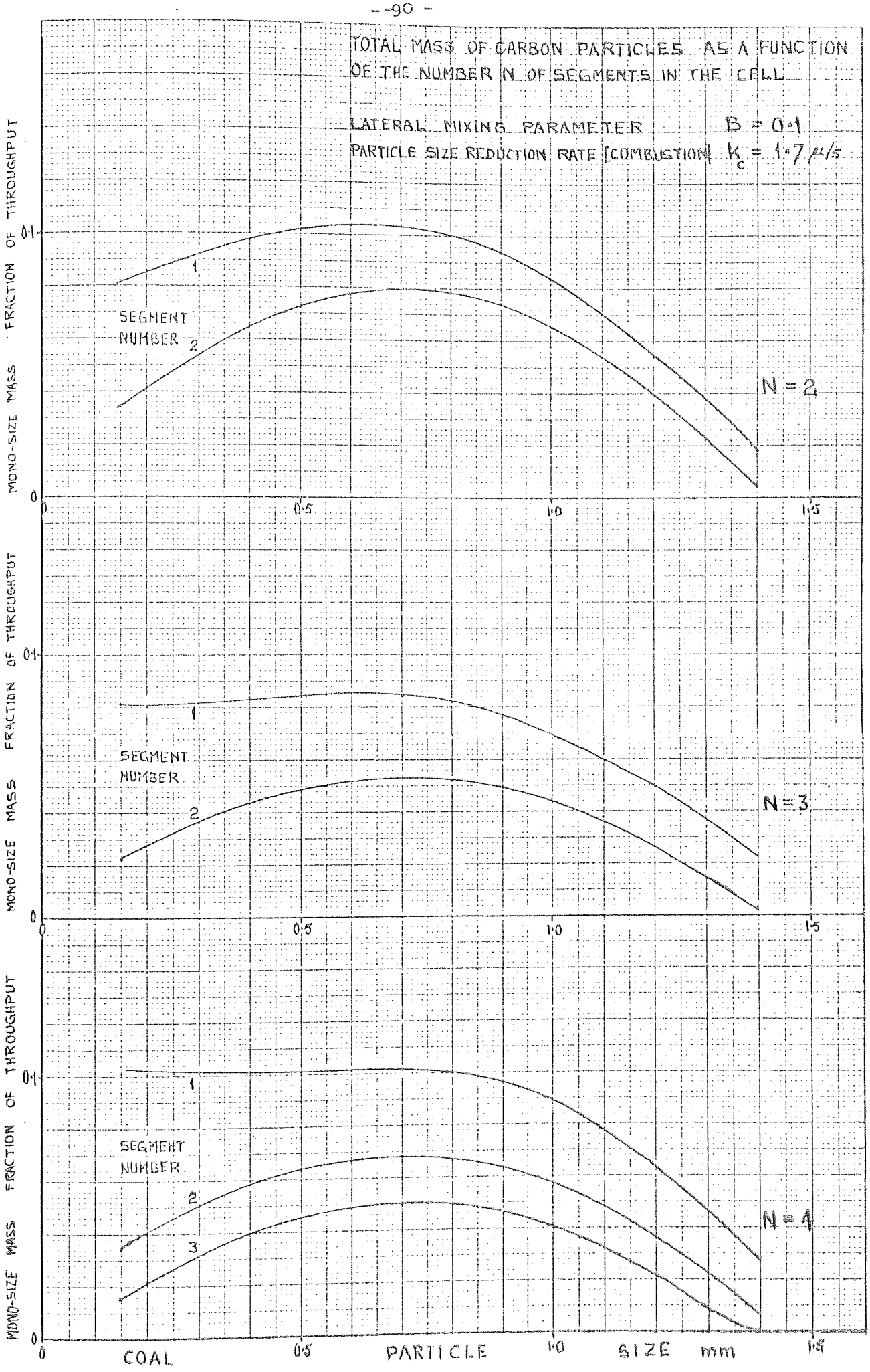

FIGURE 7.08A, MASS SIZE DISTRIBUTION OF CARBON PARTICLES IN COAL FEED CELLS OF VARYING SIZE

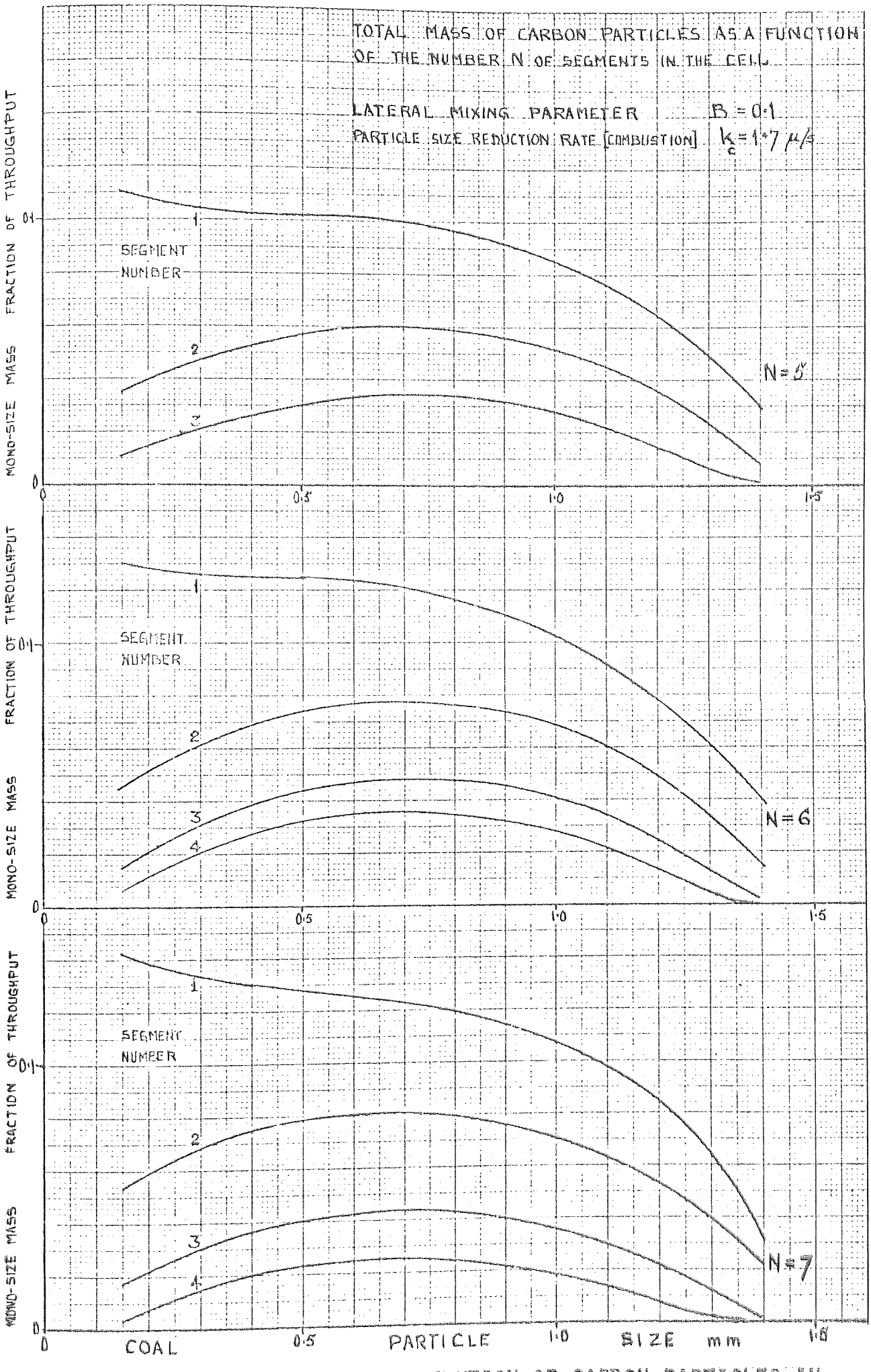

FIGURE 7.08B. MASS SIZE DISTRIBUTION OF CARBON PARTICLES IN COAL FEED CELLS OF VARYING SIZE

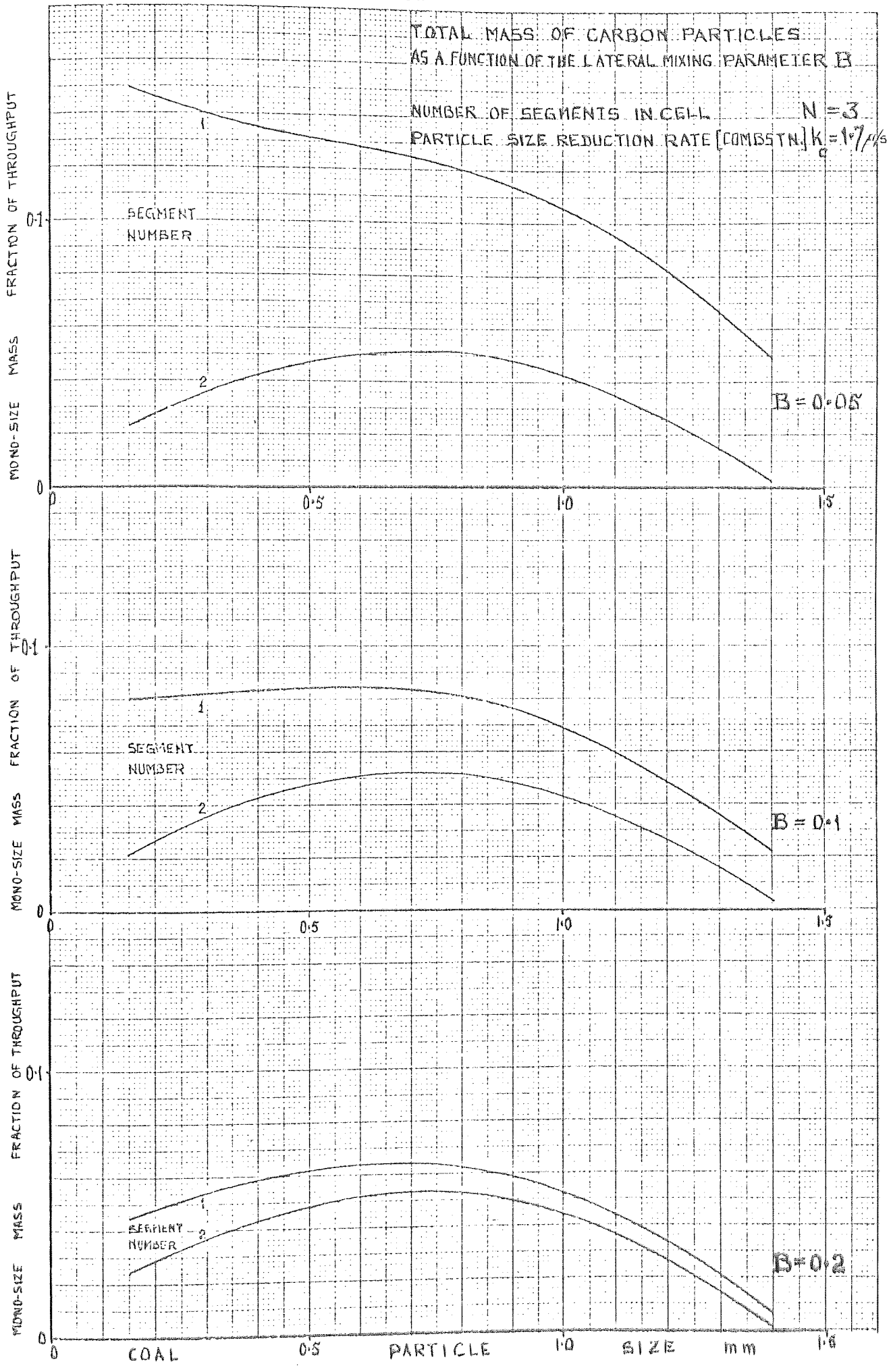

FIGURE 7.09. MASS SIZE DISTRIBUTION OF CARBON PARTICLES SHOWING EFFECT OF VARIATION OF LATERAL FLOW PARAMETER D

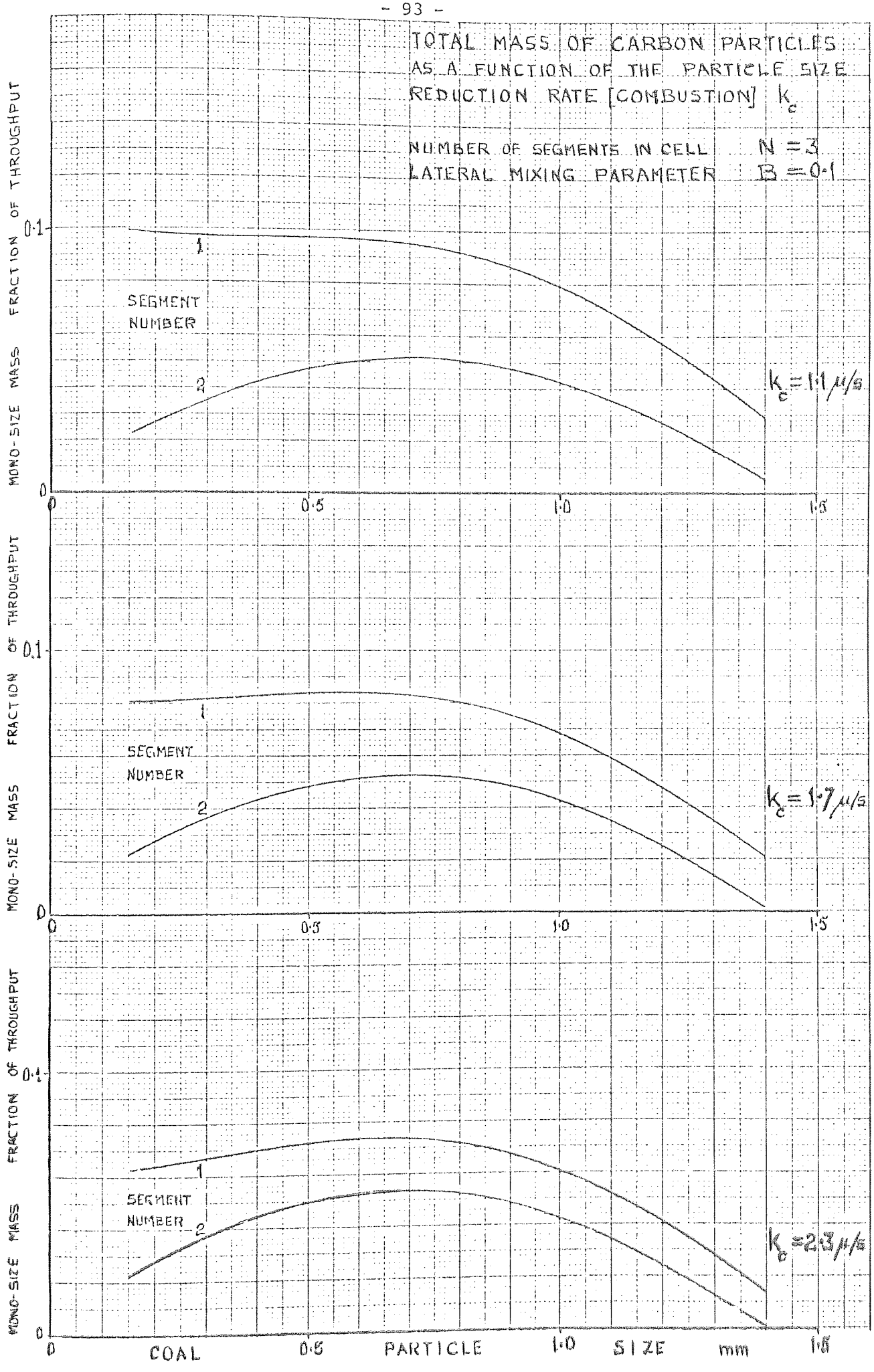

FIGURE 7.10. MASS SIZE DISTRIBUTION OF CARBON PARTICLES SHOWING EFFECT OF VARIATION OF COMBUSTION RATE PARAMETER k_c

for low values of B. An increase in the carbon population undergoing abrasion at the rate k_a results in an increase in small particles in the coal feed segment.

Figure 7.10 shows the effect of altering the rate k_c of carbon particle size reduction due to combustion. There is an increase in the content of small carbon particles in the background carbon in the coal feed segment with a decrease in k_c. Again, this is due to the high level of background carbon (Figure 7.04) for low values of k_c. An increase in the number of carbon particles at a constant rate k_a of particle size reduction due to abrasion results in an increase in small particles in the background carbon.

7.2 The Transient Mode

The effect of the five sets of parameter variations of Table 6.3 on the heat evolution within the entire cell, and the build-up of background carbon in the segments is studied in the transient mode. A uniform step increase in coal and air throughput initiates the transient mode.

7.2.1 The Transient Response of Heat Evolution

The mass loss of carbon due to combustion is used as a direct measure of the heat evolution in this study. This transient response of heat evolution is characteristic of the dynamic constituent of the first of the two terms in cascade that constitute the term b_{13} in the heat flow transfer matrix of Figure 2.1b. The first of the two terms relates the

dynamics of heat evolution in the combustion zone within a cell to the coal and air feeds. The second term relates the dynamics of the heat evolved in flowing from the combustion zone to the steam tubes. This latter is dealt with in Section 8. The effect of the five sets of parameter variations of Table 6.3 on the transient of heat evolution within the cell is shown in Figures 7.11 - 7.15. At the commencement of the step change in coal and air throughput, the increase in air is immediately effective in all segments, while the increased carbon flow to the periphery segments is established slowly as the background carbon builds up in the segments. The characteristic of heat evolution must show an instantaneous increase in carbon mass loss as the step increase in air depletes the background carbon in the segments. Now, as the background carbon in the segments is depleted the carbon mass loss due to combustion falls. Eventually the lateral flow of carbon overcomes the depletion and the background carbon builds up. This results in an increase in mass loss due to combustion. The dynamic characteristic now goes to a steady-state corresponding to the level of background carbon established. The transient of heat evolution in a coal feed cell for a 20% step change in coal and air feed rates is shown in Figures 7.11 - 7.15. These transients commence at 0.833 (= 100/120) of the final steady-state value in each case. Since the coal feed is defined in terms of the coal feed cell, this value is not absolute, and only some of the initial starting points of the transients are shown to give an indication. These transients are composed of

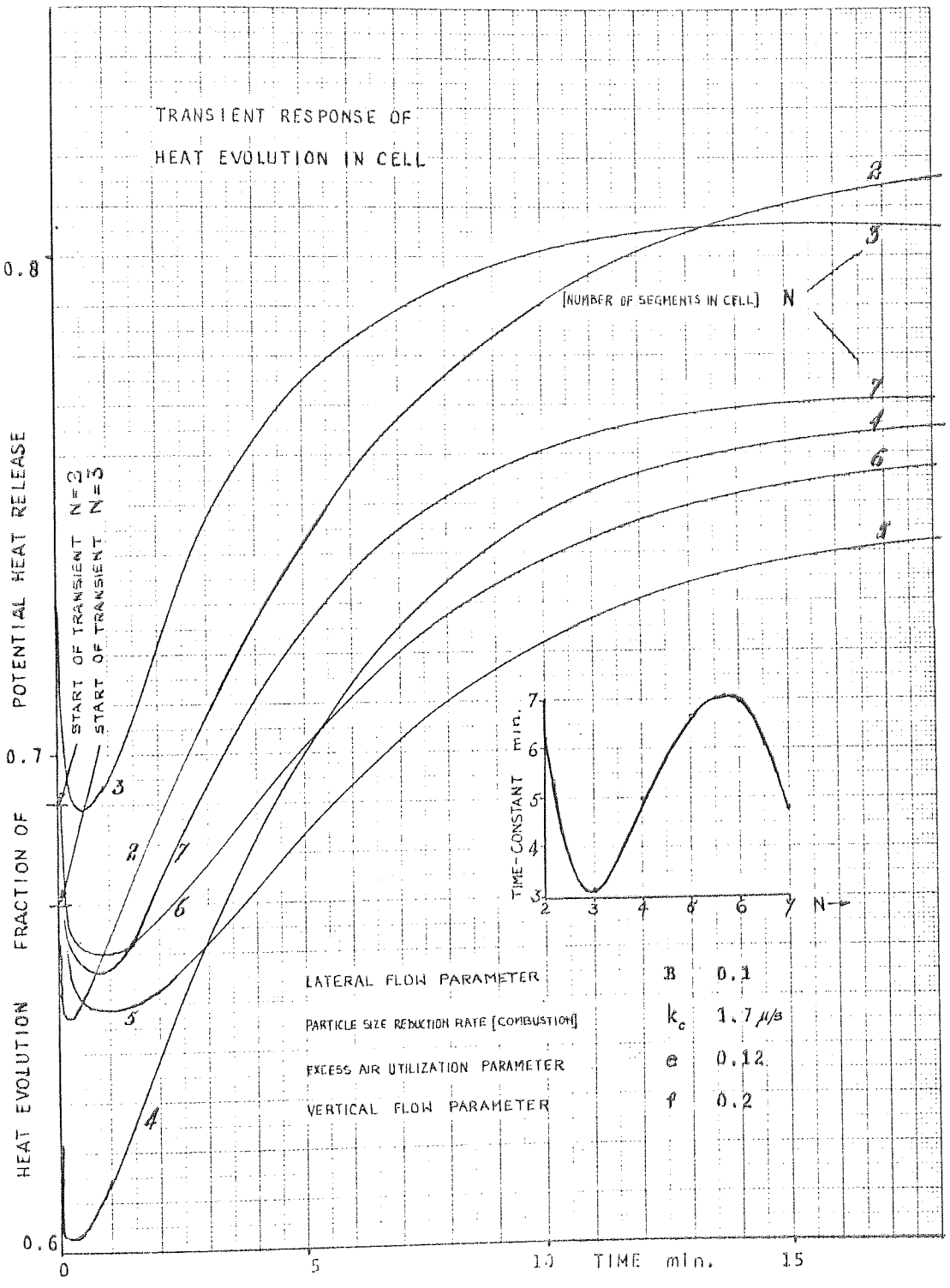

FIG. 7.11 TRANSIENT RESPONSE OF HEAT EVOLUTION IN COAL FEED CELLS OF VARYING SIZE. (N=NUMBER OF SEGMENTS IN CELL).

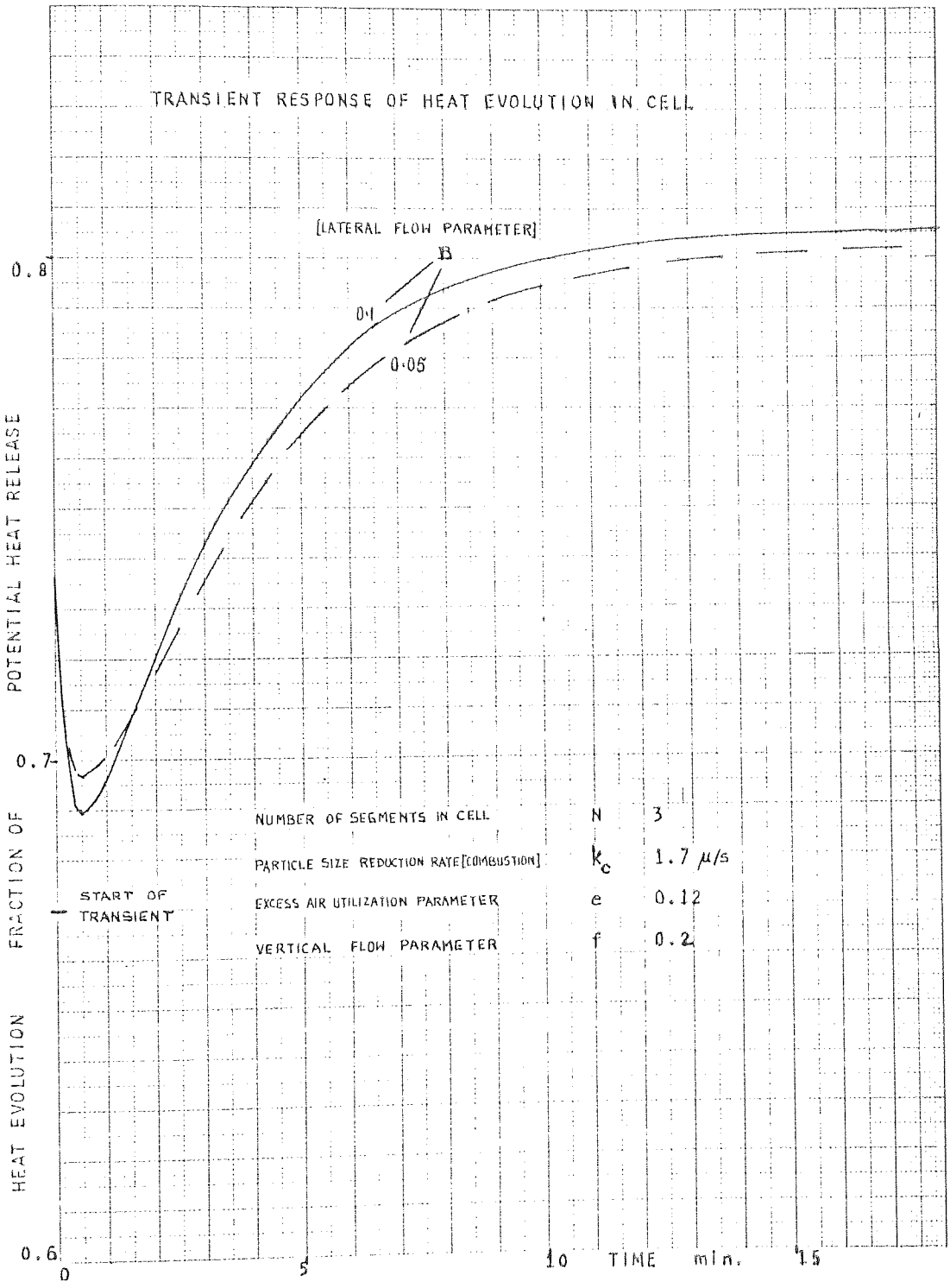

FIG. 7.12 TRANSIENT RESPONSE OF HEAT EVOLUTION IN COAL FEED CELL SHOWING EFFECT OF VARIATION OF LATERAL FLOW PARAMETER B.

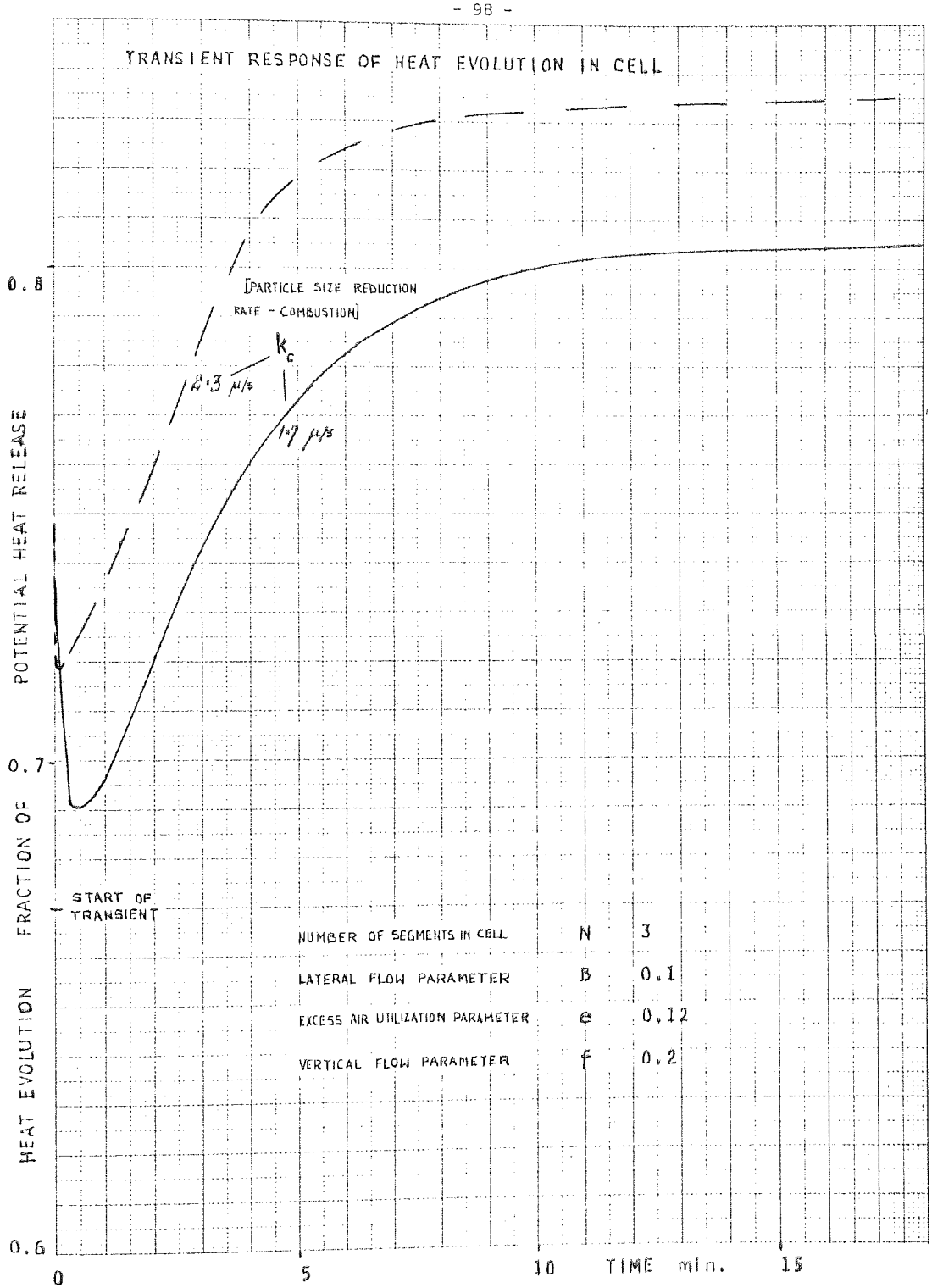

FIG. 7.13 TRANSIENT RESPONSE OF HEAT EVOLUTION IN COAL FEED CELL SHOWING EFFECT OF VARIATION OF COMBUSTION RATE k_c.

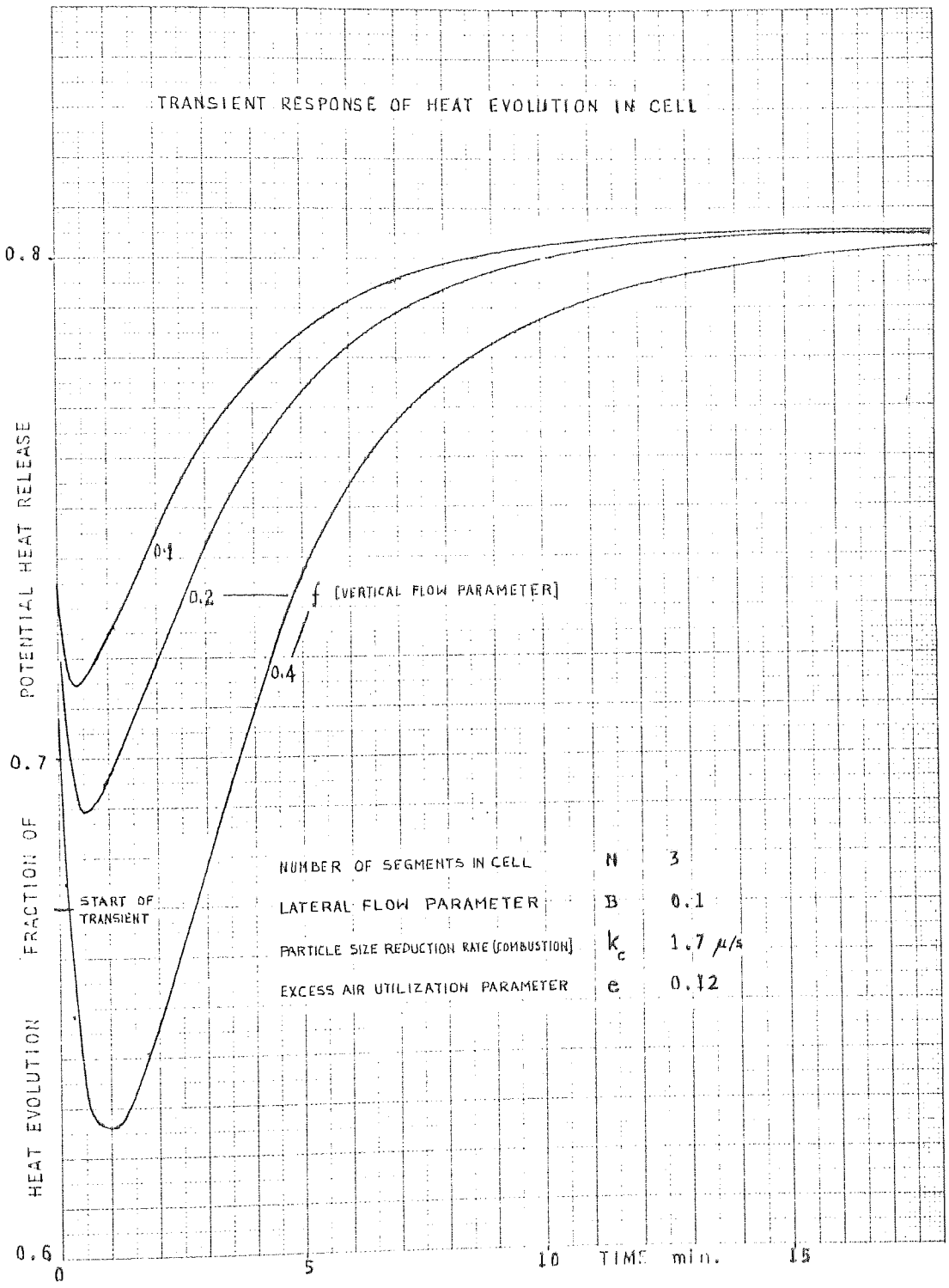

FIG. 7.14 TRANSIENT RESPONSE OF HEAT EVOLUTION IN COAL FEED CELL SHOWING EFFECT OF VARIATION OF VERTICAL FLOW PARAMETER f.

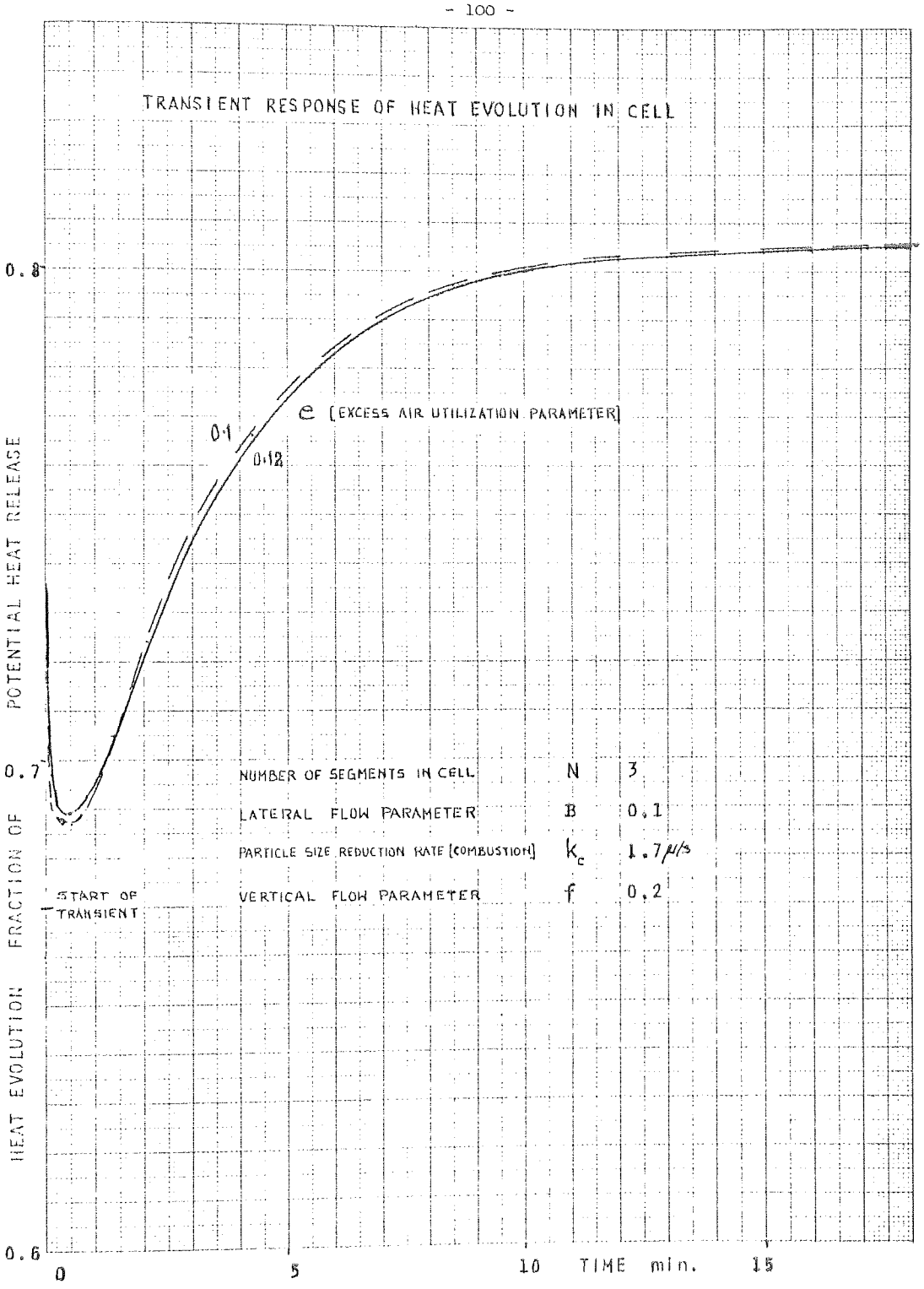

FIG. 7.15 TRANSIENT RESPONSE OF HEAT EVOLUTION IN COAL FEED CELL SHOWING EFFECT OF VARIATION OF EXCESS AIR UTILISATION e.

two constituents (Figure 9.1). The first is an instantaneous rise coupled with a decay of short time-constant (6 sec) as the step increase in air burns with the background carbon gradually depleting it. This is followed by an exponential increase in heat evolution of longer time-constant as the step increase in coal feed builds up the background carbon to a new steady-state. The dominant time-constant is between 3.5 and 6 minutes, depending on the type of coal fired (30% to 11% volatiles correspond respectively to N = 3 to 7 segments in the cell). The variation of this time-constant with the number of segments is somewhat irregular, and there appears to be a mechanism that compensates for an increase in N, the number of segments in the cell, by keeping the time-constant substantially independent of cell size. Part of the explanation may lie in the following reasoning.

Coal may be thought of as being composed of volatiles of fast throughput, and carbon of slow throughput. The background carbon is made up of this latter component only. Now the main time-constant may be approximated by:

$$\text{time-constant} = \frac{\text{total background carbon}}{\text{throughput (slow component)}}$$

As N increases, the denominator on the right of this expression increases from a small value to one that is proportional to N in the limit. On the other hand, the total background carbon in the cell from Figure 4a also increases (slower than the denominator). The time-constant alters

little and remains substantially independent of N. However, for N = 2 the dominant time-constant of 6 minutes is large because of the much diminished value of the denominator on the right in the above relationship for the time-constant, the numerator being decreased less significantly.

Figure 7.12 shows that a two to one variation in B the lateral solids flow parameter has little effect on the transient of heat release, although it does effect the rate of build up of carbon in the segments significantly as pointed out below.

The effect of an increase in the rate k_c of size reduction due to combustion on the dynamics of heat evolution is shown in Figure 7.13. Not only are the levels changed, but the nature of the transient response tends to change from that of an exponential characteristic. As k_c increases the background carbon decreases so that the carbon feed is burnt with less mixing en route, and exhibits less of the familiar characteristics of an exponential.

Figure 7.14 shows the vertical mixing as having more importance than is thought at first sight. As f increases and the vertical mixing becomes slower, it is necessary for the background carbon to increase (Figure 7.19) so as both to replenish a given rate of carbon removal from the combustion zone as well as sustain the required lateral transfer. This confirms a widely held view bearing on the design and operation of large scale plant. A dense tube packing to limit capital costs will certainly cause the vertical mixing to be the poorer. This will result in high background carbon and excessive build

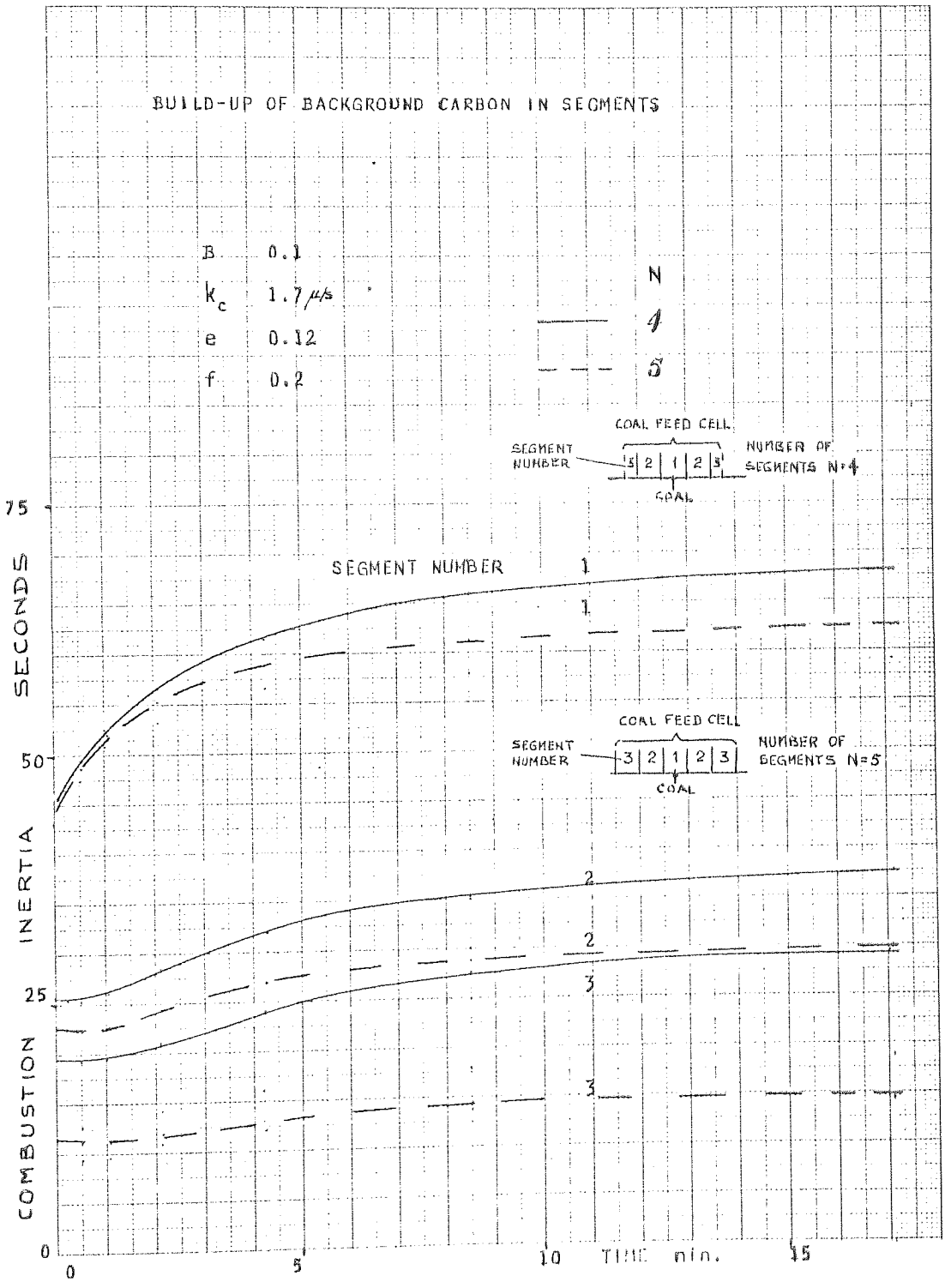

FIG.7.6a BUILD-UP OF BACKGROUND CARBON IN SEGMENTS OF CELL DURING TRANSIENT SHOWING EFFECT OF VARIATION OF CELL SIZE. (N=NO. OF SEGMENTS)

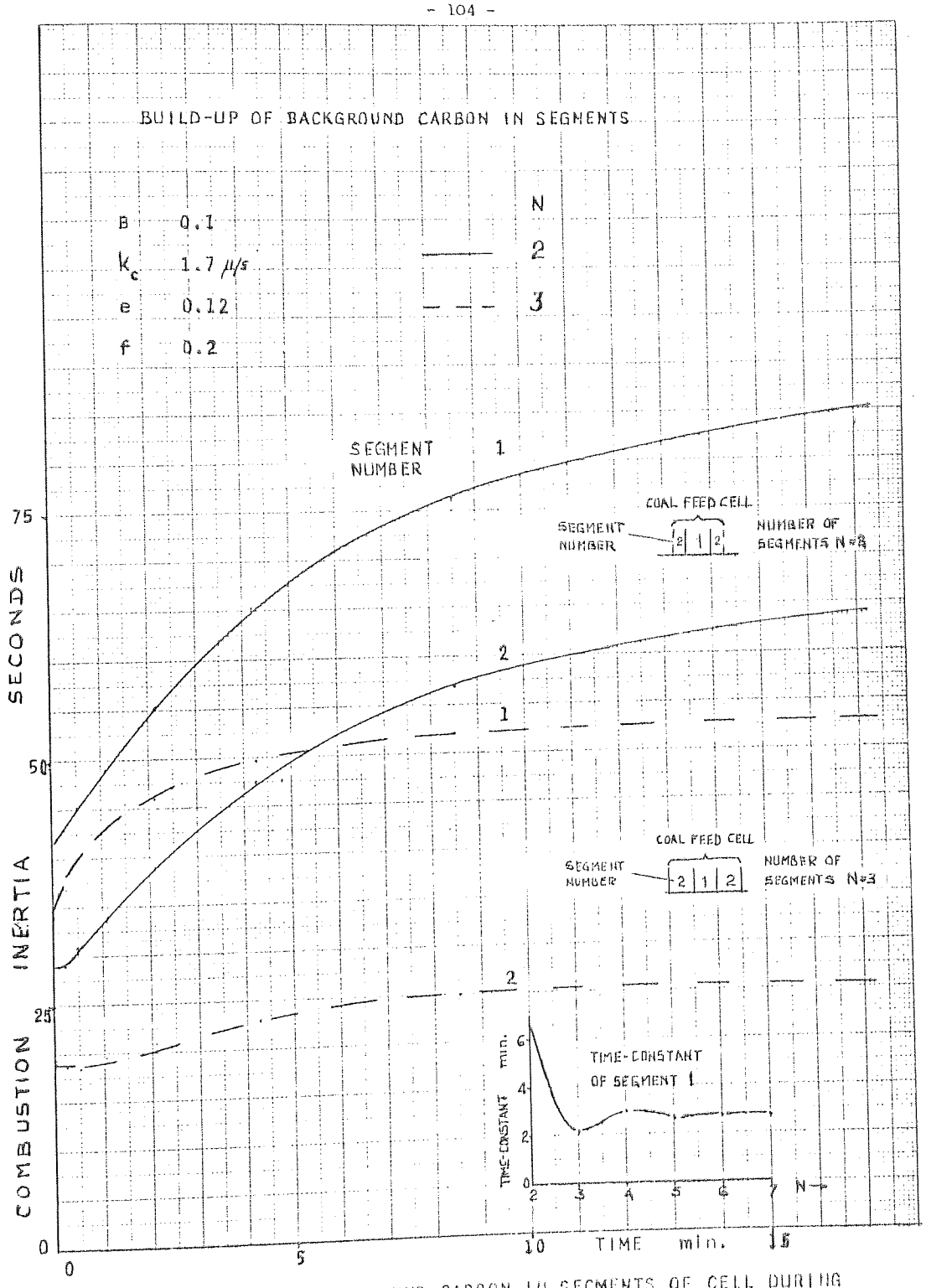

FIG. 7.16b BUILD-UP OF BACKGROUND CARBON IN SEGMENTS OF CELL DURING TRANSIENT SHOWING EFFECT OF VARIATION OF CELL SIZE. (N=NO. OF SEGMENTS)

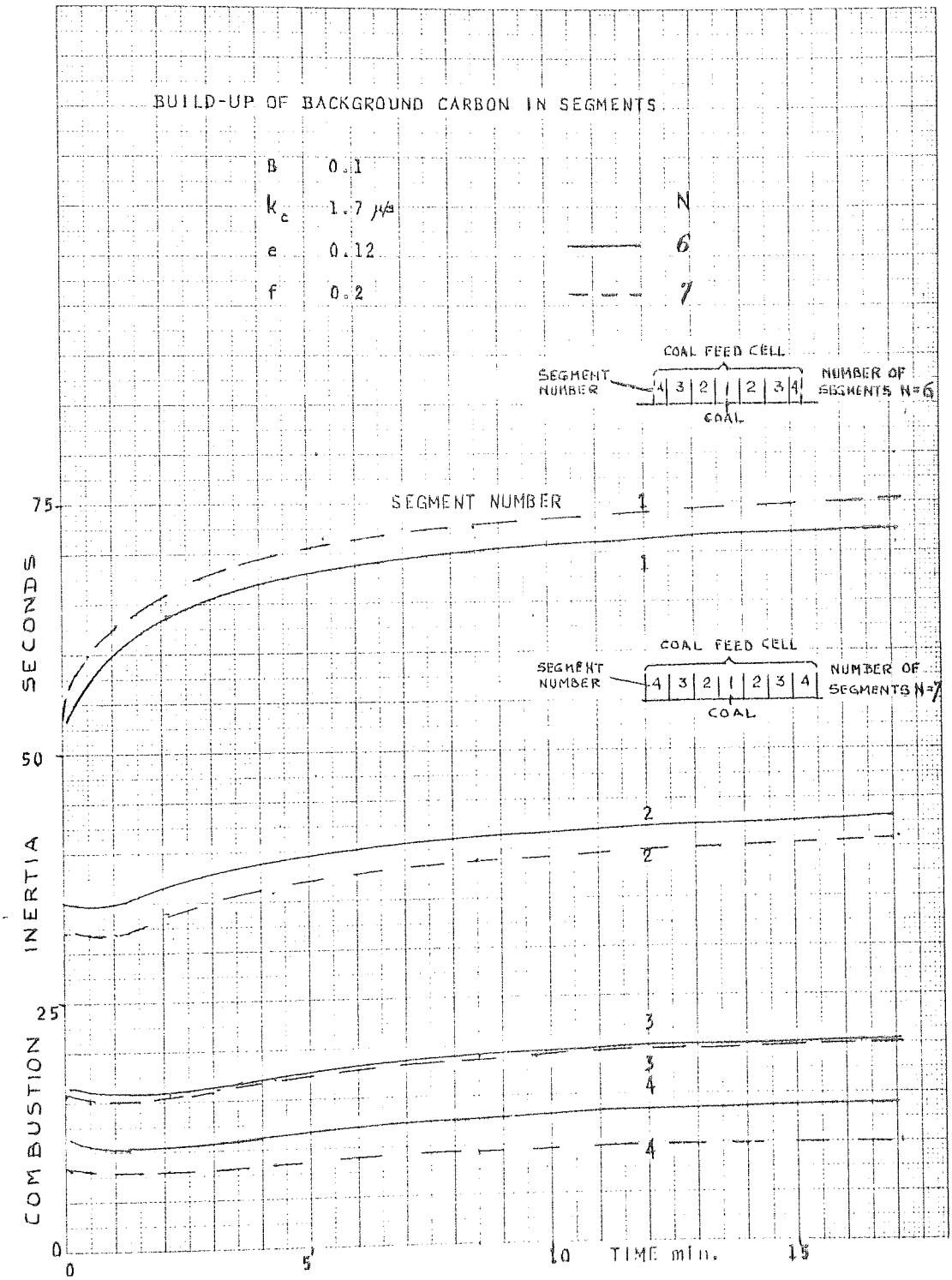

FIG.7.16c BUILD-UP OF BACKGROUND CARBON IN SEGMENTS OF CELL DURING TRANSIENT SHOWING EFFECT OF VARIATION IN CELL SIZE. (N=NO. OF SEGMENTS)

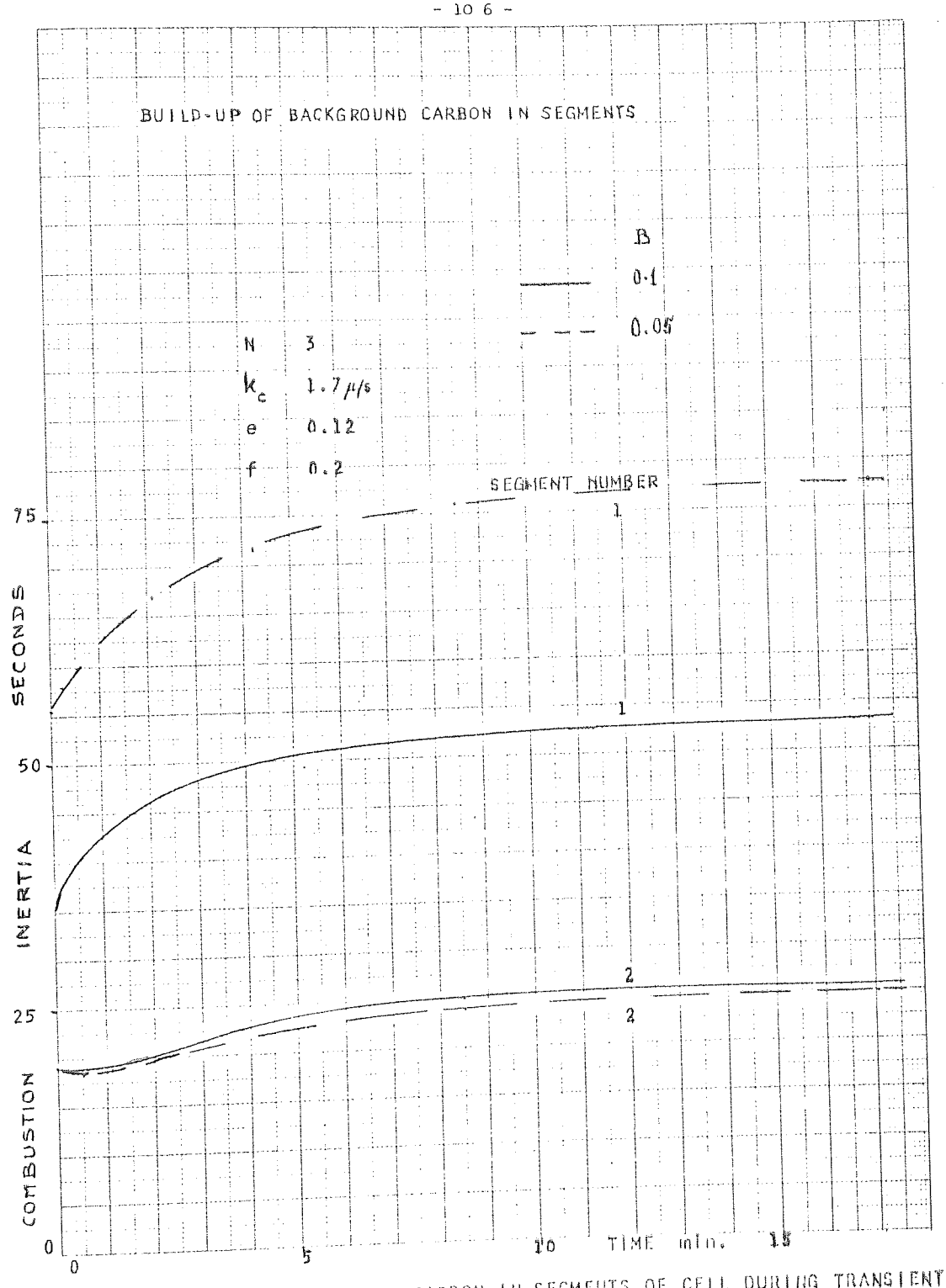

FIG. 7.17 BUILD-UP OF BACKGROUND CARBON IN SEGMENTS OF CELL DURING TRANSIENT SHOWING EFFECT OF VARIATION OF LATERAL FLOW PARAMETER B.

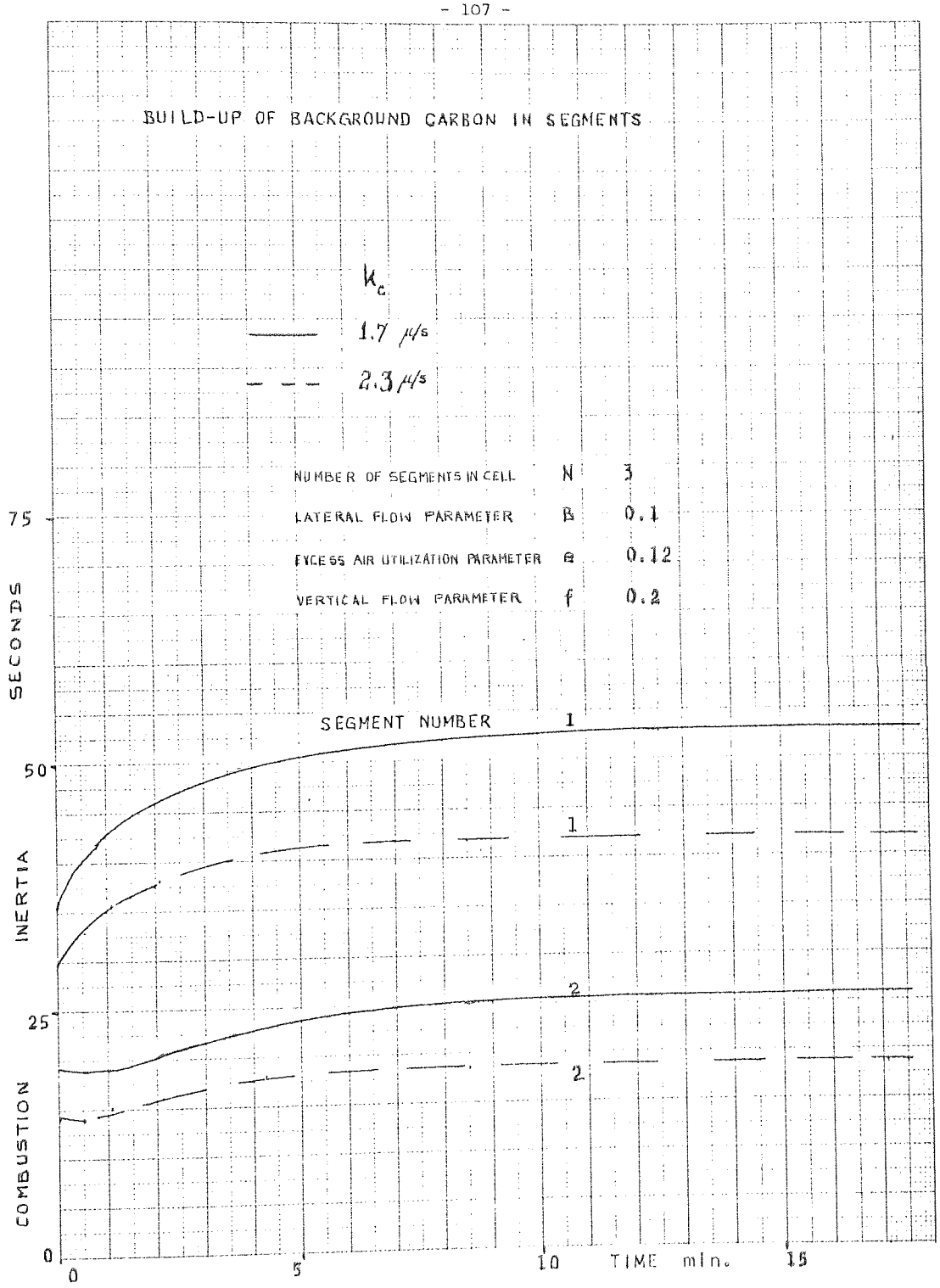

FIG. 7.18 BUILD-UP OF BACKGROUND CARBON IN SEGMENTS OF CELL DURING TRANSIENT SHOWING EFFECT OF VARIATION OF K_c.

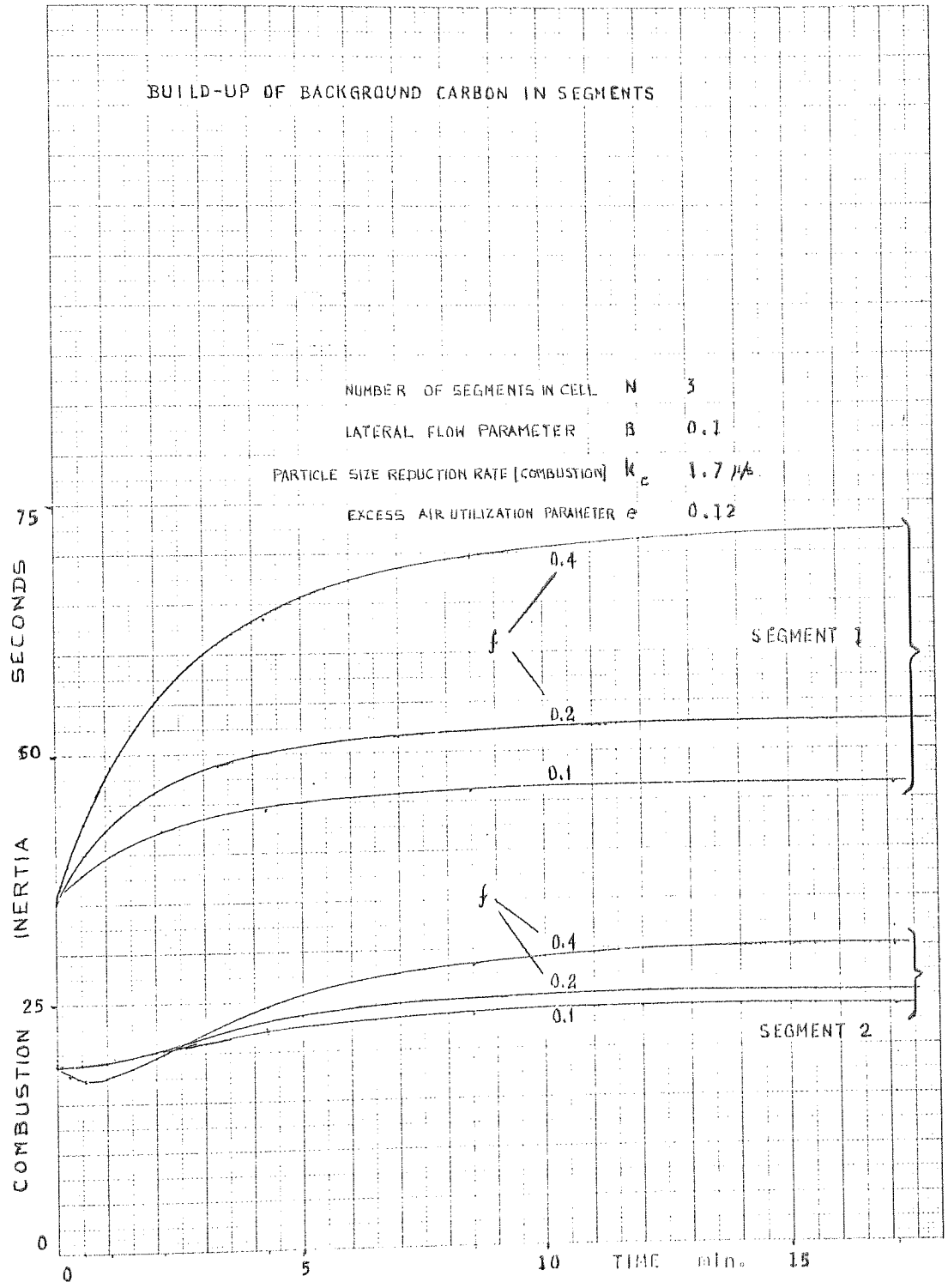

FIG. 7.19 BUILD-UP OF BACKGROUND CARBON IN SEGMENTS OF CELL DURING TRANSIENT SHOWING EFFECT OF VARIATION OF VERTICAL FLOW PARAMETER f.

up of heat in the lower reaches of the bed with the possibility of clinkering the ash, and a relatively cool upper region of the bed containing the heat transfer tubes. Both the heat flow from the combustion zone to the steam tubes, as well as the lateral flow of the carbon, are likely to decrease.

Figure 7.15 shows that the parameter e, introduced to account for a decrease in the efficiency of utilization of the instantaneous excess air during the transient, has negligible effect with a 20% variation.

7.2.2 The Build Up of Background Carbon in the Segments of the Cell During a Transient

The effect of the five sets of parameter variations of Table 6.3 on the build up of background carbon in the segments of the cell during a transient is shown in Figures 7.16 - 7.19. All these results exhibit a characteristic build up of background carbon in the coal feed segment (segment 1). In the outer segments there is an initial drop as the background carbon is initially depleted during the transient by the step increase of air which is effective immediately. Subsequently the lateral flow overcomes this depletion, and the background carbon rises to a steady-state value.

Figures 7.16a, b and c shows that the rate of build up of background carbon in the coal feed segment during a transient is reasonably constant as N the number of segments in the coal feed cell increases (inset Figure 7.16a). This result is consistent with that for the transient of heat evolution within the bed, and a similar reasoning may be followed. From

Figure 7.01 the background carbon in the coal feed segment increases only slightly as N increases. On the other hand, the carbon throughput (slow throughput components of the feed) increases in proportion to N. The time-constant of the build up of background carbon in the coal feed segment (background carbon in coal feed segment/carbon throughput) is fairly constant with respect to N.

For N = 2, the coal feed cell seems to operate so as to exhibit a characteristic closer to a homogeneous cell. Here the coal feed segment is flanked by half segments on either side and these, by reason of their diminished size, have their characteristics overshadowed.

In Figure 7.16c the periphery segment (segment 4) is shown to suffer most depletion by the step increase in air during the transient, and to recover more slowly than inner segments 2 and 3.

The change in background carbon over the transient is more marked in the coal feed segment, and decreases progressively to the periphery segment. This is because steeper potential gradients are necessary for increased lateral flow of carbon from segment to segment.

Figure 7.17 shows the effect of a two to one variation in the lateral mass flow parameter B. As B decreases, the time-constant of the build up of background carbon in segment 1 increases. This result is consistent with the increase in background carbon (Figure 7.03) in segment 1. Again, since time-constant = carbon in segment/cell throughput, and only

the numerator increases as B decreases, the time-constant must increase. In the peripheral segment, however, the effect of decreasing B delays the build up of background carbon since the rate of lateral flow is decreased.

The effect of an increase in the combustion rate k_c of particle size reduction is shown in Figure 7.18 to result in a decrease in the time-constant for build up of the background carbon in segment 1. This is consistent with a decrease in the background carbon (Figure 7.04). In the periphery segment the build up of background carbon overtakes the depletion due to the excess air during the transient earlier as k_c increases.

Figure 7.19 shows the effect of a variation in the vertical solids flow parameter f on the build up of background carbon in the segments. There is a very significant increase in the level of background carbon as f increases. An increase in f corresponds to poor vertical mixing such as might result from closely-packed steam tubes. It is necessary for the background carbon to increase so as both to replenish a given rate of carbon removal from the combustion zone as well as sustain the required lateral transfer. The time-constant of the build up of background carbon in segment 1 does not alter significantly. In the periphery segment, as f increases the depletion is more marked and the recovery of the background carbon is slower.

The effect of a variation in e, the efficiency of utilization of the instantaneous excess air during the transient on the build up of background carbon, is barely discernible and is not shown.

C H A P T E R 8

HEAT FLOW FROM COMBUSTION ZONE TO STEAM TUBES

HEAT FLOW FROM COMBUSTION ZONE TO STEAM TUBES

8.1 General

The dynamic constituents of the term b_{13} in the heat transfer matrix of Figure 2.1b is composed of a cascade of two terms shown in Figure 9.1. The first of these two terms relates the heat evolution to the coal and air throughput and is treated in sub-section 7.2.1. This heat evolution occurs in the combustion zone at the base of the fluidised bed where the oxygen uptake occurs, and is liberated in the hot ash plasma in the combustion zone, i.e. the bottom layer of each segment as indicated in Figure 1.2c. The second term of the cascade of Figure 9.1 is the characteristic of heat flow by mass transport of the hot ash plasma from the combustion zone to the steam tubes in the upper layers of the bed. Fluidised beds are characterised by reasonable thermal uniformity, and only the vertical flow of the hot ash plasma by bubble transport is able to account for the flow of heat evolution from the combustion zone at the base of the bed to the steam tubes distributed through the bed height.

When compared with the vertical flow of heat, the lateral flow of heat is negligible whether by lateral flow of solids or by conduction along a thermal gradient. The lateral flow of solids is perhaps more than an order less than the vertical flow, and hence the heat transferred laterally by this mechanism is in the same ratio to that transferred vertically. For conduction to be an effective mode of lateral heat transfer a lateral thermal gradient exceeding $100^{\circ}C/cm$ would have to obtain, quite contrary to the accepted uniform thermal characteristics.

Thus, the only effective mode of transport of heat from the combustion layers at the base of the bed to the coolant tubes suspended in the bed is by vertical transport of solids. The segments of a coal feed cell may be considered thermally insular, since lateral flow of heat is negligible.

8.2 Development

The left-hand side of Figure 1.3c shows an elevation section through a single segment of a fluidised bed combustor. The bed depth is subdivided into a number of layers (here ten) and, to illustrate the principle, five rows of coolant tubes are embedded in alternate layers. The upward vertical transport of solids by bubbles, accompanied by the downward displacement movement of solids for conservation of mass flow is that defined in equation A4.4.

Since the sensible heat capacities of all layers are identical, the temperature of a layer is directly proportional to its heat content. Initially, assume all layers at the same temperature. During an incremental time T a quantity of heat is released by combustion in layer 1 at the base of the fluidised bed. This heat may be assumed to be uniformly diffused throughout layer 1, and its effect is to raise the temperature Θ_1 of layer 1 to Θ'_1.

All those layers with coolant tubes embedded in them lose heat at a rate proportional to the temperature difference $\Theta - \psi$ where ψ is the temperature of the steam in the tubes. In the steady-state, the total quantity of heat transferred in all the

layers having tubes must be the same as that released by combustion. Knowing the heat transferred in each layer, an estimate may be made of the drop $\Delta\theta_r$ in temperature from θ_r of the sensible heat in a layer with tubes to obtain a layer temperature of θ'_r.

The heat content of the several layers is now mixed for the incremental time T by the characteristic of bubble transport to yield the individual temperature θ_r of each layer for consideration during the next increment T of time.

It is now possible to repeat the cycle of operations beginning with the release of a fresh quantity of heat in the combustion layer. The essential condition for steady-state is that thermal conservation must be satisfied, i.e.

Heat absorbed by coolant = heat released by combustion

Carrying this cycle of operations of heat release, transport and absorption to the steady-state reveals the thermal gradient through the bed depth that results from the characteristic of bubble transport.

The stages in the cycle of operations of heat release, transport and absorption are set down as a set of difference equations in Appendix 12.

8.3 Predictions

The difference equations set down in Appendix 12 are programmed in Listing A12.1 and executed until a steady-state is achieved in the vertical temperature profile as tabulated in

Table A12.1. For a given steam temperature ψ = 356^{o}C at which boiling occurs, the effect of variation of the vertical mixing parameter f is shown in Figure 8.1. With poorer vertical mixing defined by f approaching unity, such as may result from the impedence to vertical mixing of close packed steam tubes or the use of excessive fluidising velocity, an exaggerated thermal gradient across the bed height may be expected.

For a given vertical mixing parameter f = 0.4, the effect on various areas of the fluidised bed of steam tubes at 300^{o}C, 356^{o}C and 500^{o}C corresponding to heating, boiling and superheating is examined and tabulated in Table A12.1. Assuming that the heat transfer coefficient 0.5678 kW/m^{2} ^{o}C (100 Btu/^{o}F ft^{2} h) is the same at these steam conditions, the temperature would have a range of 200^{o}C as shown in Figure 8.2 for tube bundles of various temperature ranges. In practice, the tube bundles are mixed to even out this effect.

The dynamic response of heat flow from the combustion zone to the steam tubes in a segment is obtained by initiating a 10% step increase in the heat of combustion released in the combustion zone. This heat is partly removed by the steam tubes extracting heat at an increased rate, while the remainder accumulates in the bed. This accumulation of heat results in an increase in bed temperature, which in turn causes increased heat extraction by the coolant. In the steady-state all of the 10% step increase is accounted for in increased heat extraction by the coolant. The bed temperature is now at thermal equilibrium. The time trajectory is plotted in Figure 8.3. Instead of the

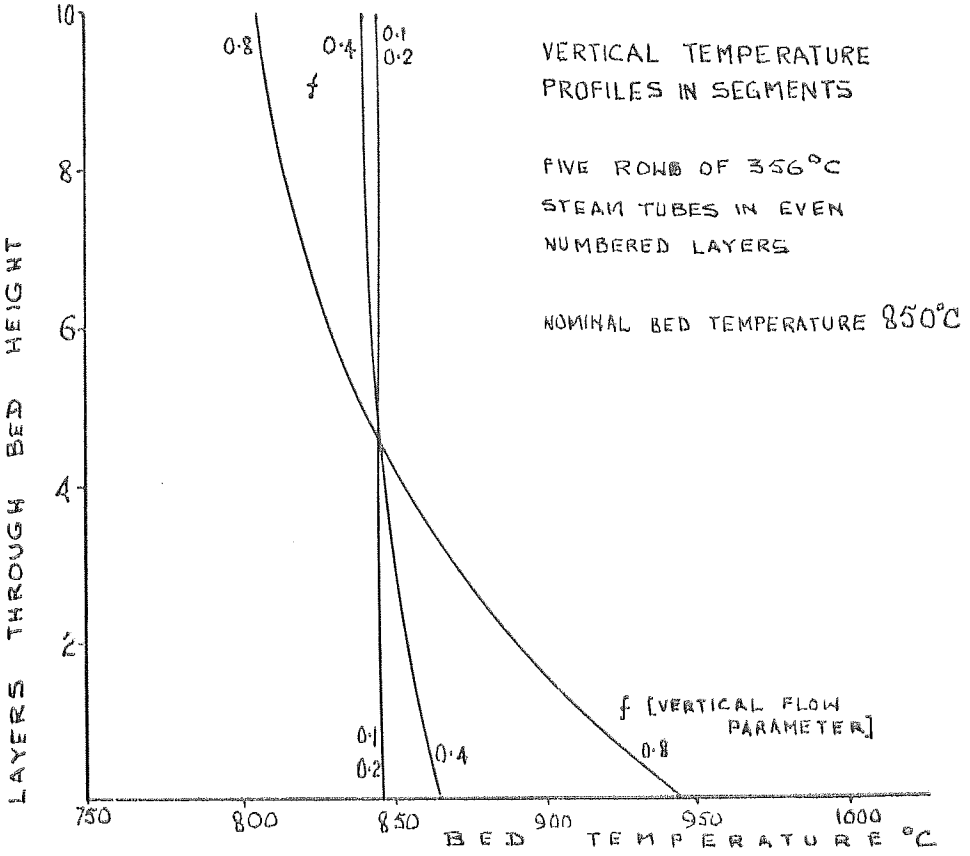

FIGURE 8.1 EFFECT OF VERTICAL FLOW PARAMETER f ON VERTICAL TEMPERATURE PROFILES IN SEGMENTS

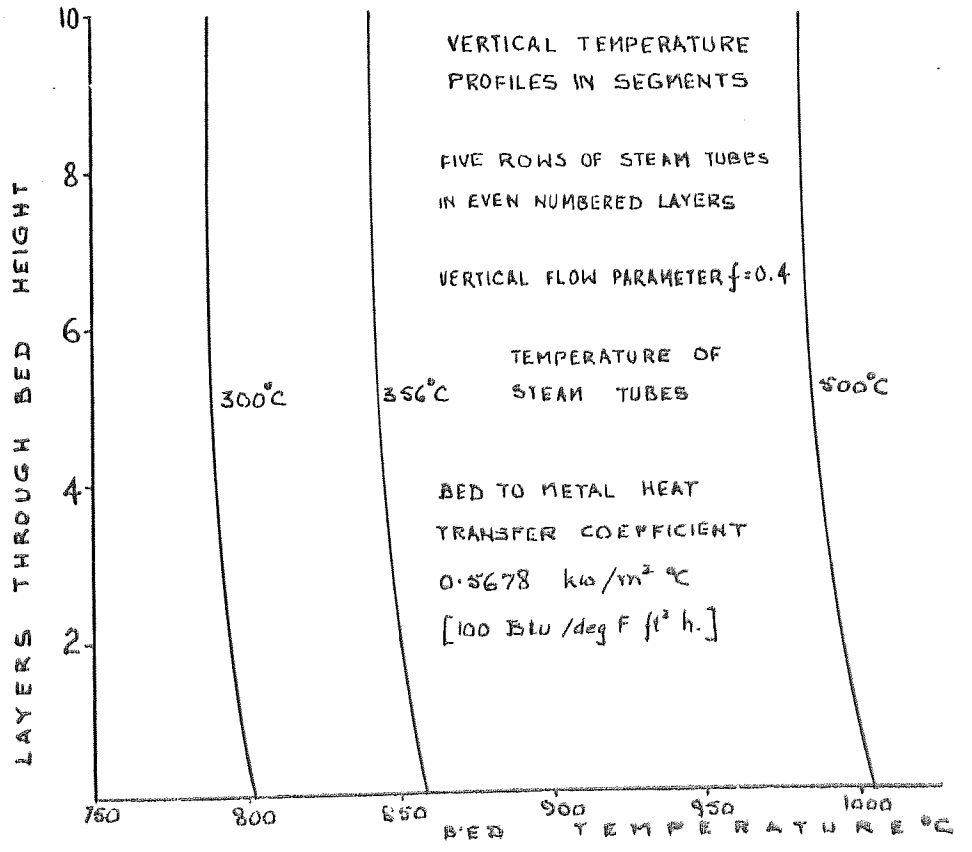

FIGURE 8.2 EFFECT OF STEAM TEMPERATURE ON BED TEMPERATURE

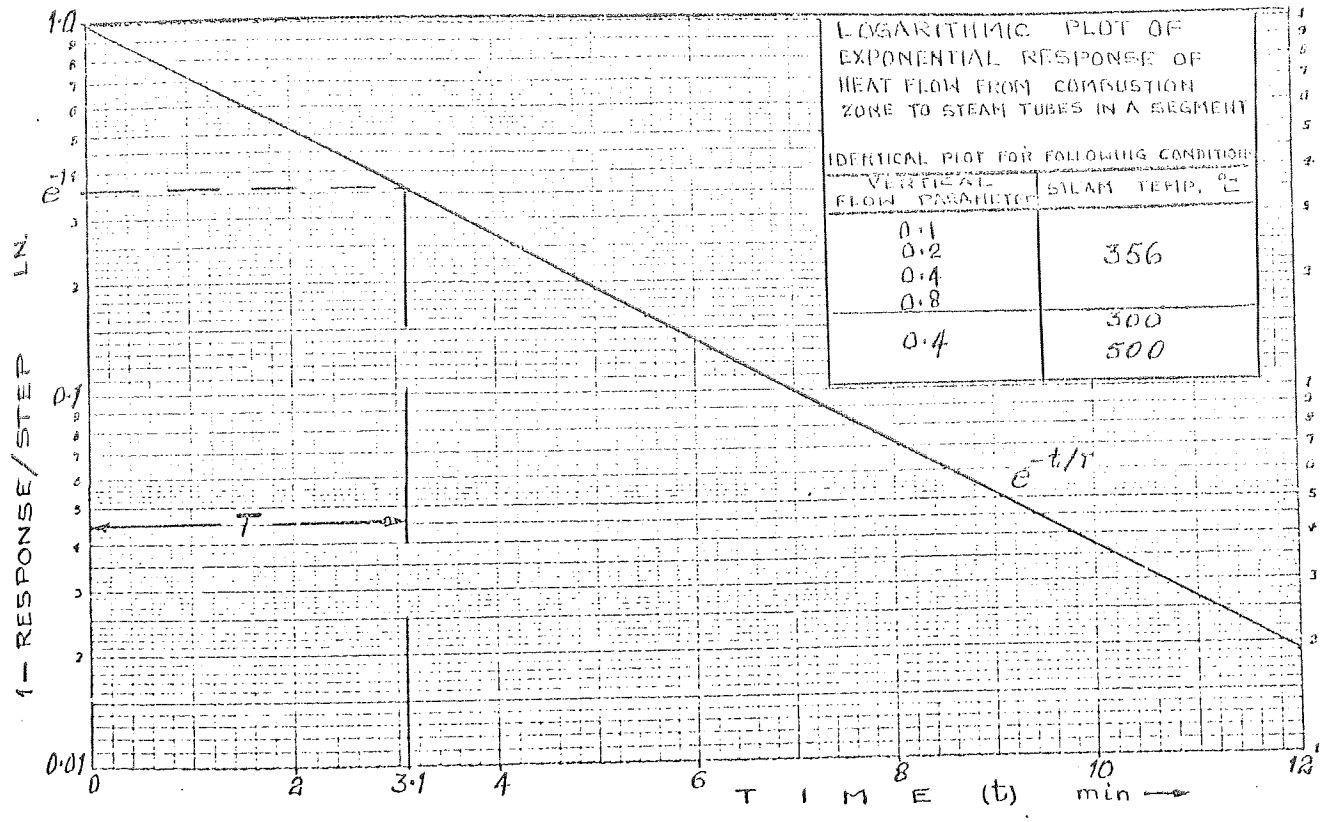

FIGURE 8.3 DYNAMIC RESPONSE OF HEAT FLOW FROM COMBUSTION ZONE TO STEAM TUBES IN A SEGMENT

ordinate being the response to the step increase, the function tabulated in Table A12.2 is

$$\ln (1 - \text{response/step})$$

For an exponential response this function is linear. The time-constant is the abscissa corresponding to an ordinate of e^{-1} and has a value from Figure 8.3 of 3.1 minutes. With such a plot a change in time-constant shows up as a line of different slope. No significant change is discernible in the time-constant over the range 0.1 to 0.8 for f, the vertical solids flow parameter, as well as a range of 300°C to 500°C in θ, the steam temperature. The transfer function of the heat flow may be expressed as a phase lag of L-transform

$$1/(1 + pT)$$

where T = 3.1 minutes. The data format and values used in the computation are given in Table A12.3.

C H A P T E R 9

THE SYSTEM DYNAMICS AND COMMENTS ON CONTROL

THE SYSTEM DYNAMICS AND COMMENTS ON CONTROL

9.1 General

Having defined the two constituents of the dynamic characteristic of the term b_{13} in the heat transfer matrix of Figure 2.1b, it is possible to represent these characteristics in cascade for analogue simulation. Then, following the procedure outlined in sub-section 2.2, the entire system of mass and heat transfer matrices may be mapped in principle. Finally, some comments are made on aspects of the control of the characteristic synthesised in this study to form a base for a systematic investigation into the problem of control and regulation.

9.2 The Dynamics of Heat Evolution and Flow

The dynamic component of the term b_{13} in the heat transfer matrix of Figure 2.1b is composed of two constituents. The first is that of heat evolution in the combustion zone as the carbon burns and is moved from layer to layer and segment to segment under the influence of the vertical and lateral solids flows. The mechanisms developed in sub-section 4.4 to represent combustion during the transient yield characteristics, as discussed in sub-section 7.2.1, that define the first constituent of the dynamic characteristic of the term b_{13}. It is composed of a phase lead term of time-constant 0.1 min to represent the anticipatory effect of the step increase in air, and a phase lag term of time-constant 5.5 min to represent the change in combustion as a result of the gradual build up of carbon through the segments of the cell. From Figure 7.11 the gain constants associated with these two time-constants

are approximately 0.2 and 0.8 respectively. The characteristics of heat evolution is shown in Figure 9.1 as the first of the two terms in cascade that represent the dynamic component of the term b_{13} in the heat transfer matrix.

The second constituent of the dynamic component b_{13} is the characteristic for heat flow from the hot ash plasma in the combustion zone to the steam tubes distributed through the bed height. This is developed in sub-section 8.2 and the characteristic defined in sub-section 8.3 is shown in Figure 9.1 as the second term in the cascade that represents the dynamics of b_{13}.

9.3 The Schematic of the Entire System

Following the reasoning developed in section 2.2, a schematic may be traced for the entire system dynamics. Such a schematic based on the system principle shown in Figure 2.2 is defined in Figure 9.2 for the mass and heat transforms. It forms the base from which a systematic investigation of the control problem for a power station based on a fluidised bed boiler may be made.

9.3.1 The Mass Transfer Matrix

In Figure 9.2 the coal fired is shown as containing 15% of ash and 85% of combustible material. Half the ash is shown as passing through the bed by elutriation, while the other half is removed from the bed over a wier. In the absence of experimental information the flows in these two streams of ash are set equal. The ash stream that flows over

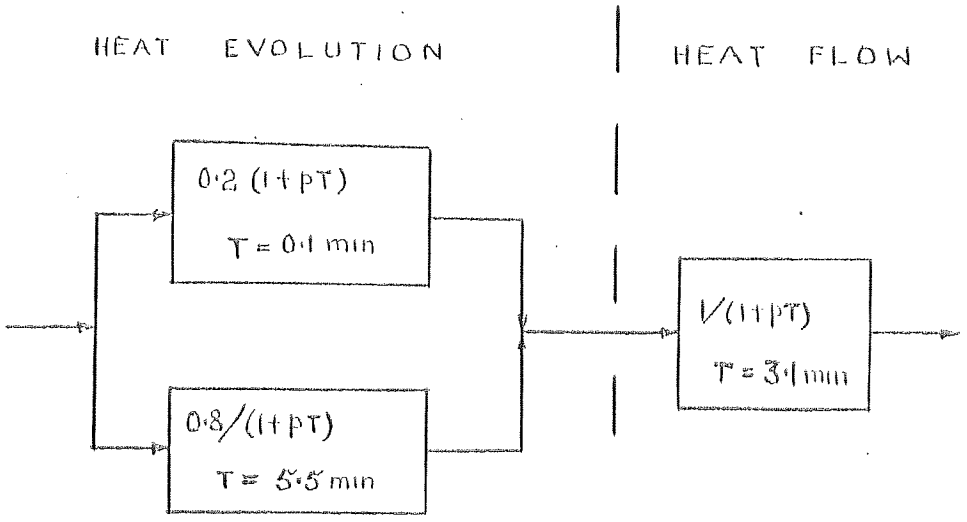

FIGURE 9.1 SIMULATION OF THE TERM b_{13} OF THE HEAT TRANSFER MATRIX. (COAL FIRED 36-38% VOLATILE MATTER)

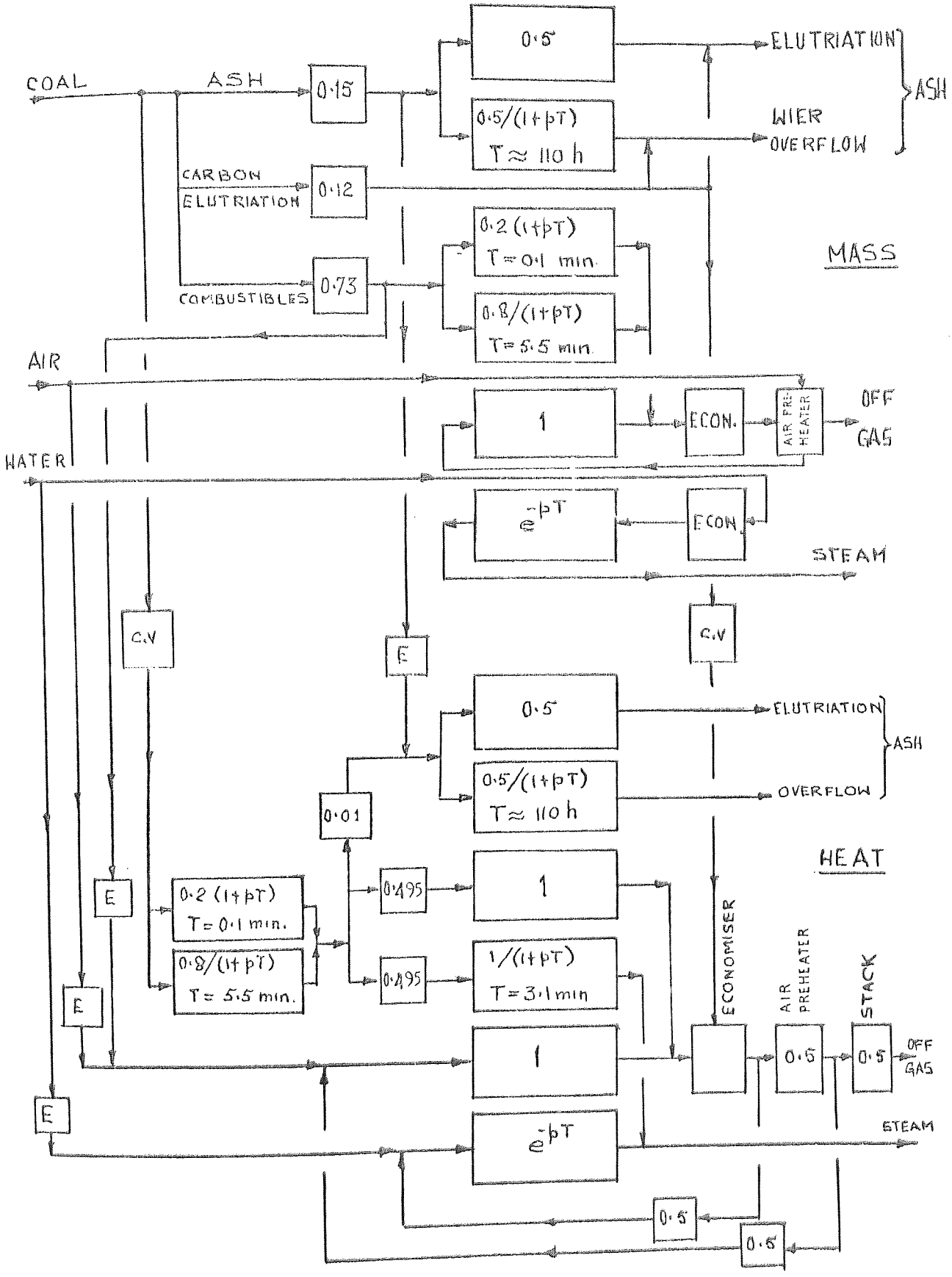

FIGURE 9.2 THE PROCESS SCHEMATIC OF A MATHEMATICAL MODEL OF A FLUIDISED COMBUSTION BOILER

the wier is subjected to a residence time in the cell which may be assumed to be an exponential of time-constant given by

time-constant = total ash in coal feed cell/half the ash stream

The total ash content of a coal feed cell composed of two segments is 1,000 kg (density of ash = 800 kg/m^3) with a coal throughput[9] to the cell of 0.032 kg/s at U = 0.75 m/s. Assuming an ash content of 15%, half the ash stream equals 0.0025 kg/s. The residence time of this ash stream in the cell gives a time-constant of 110 hours.

The combustible material which is 85% of the throughput joins the air stream after combustion. The dynamics of this term is the same as that for heat evolution as defined in Figure 9.1, since the heat evolution implies the conversion of the carbon into combustion gases. The time-constants and gain factors are identical to that of Figure 9.1.

The dynamics of air flow through the bed may be assumed instantaneous, while the steam flow in the tubes is a velocity transport time delay for a once through system. Alternatively, the characteristic for a header system may be taken from the literature[20, 21].

9.3.2 The Heat Transfer Matrix

The heat of combustion derived as the product of the coal throughput and its calorific value c.v. is liberated in the combustion zone of the bed obeying the dynamics of heat evolution shown in Figure 9.1. This heat evolution is

apportioned into three fractions as shown in Figure 9.2. In the absence of experimental knowledge derived from full-scale plant, estimates[9] of these fractions are 1% to the ash stream which leaves the bed, with the remainder of the heat evolution shared equally between the gas stream and the flow through the hot ash plasma to the steam tubes.

The dynamics for the heat loss via the ash stream by elutriation and by overflow at the wier are the same as those for the air mass flow. The heat flow to the gas stream may be assumed instantaneous, while the heat flow from the combustion zone to the steam tubes by flow of the ash plasma is the second term in the cascade shown in Figure 9.1.

The characteristics of steam flow in the tubes is as above for mass flow. It is either a transport time delay for a once through boiler or the conventional characteristic for a header system[20, 21].

The sensible heats in the incoming streams of ash, fluidising air and coolant streams are added as heat flows to the input of the boiler. The off gas passes through an economiser and a heat exchanger. Again, in the absence of experimental measurements on a full-scale plant, estimates[9] are made that the heat recovered at each stage is 50%. The heat from the economiser pre-heats the water, while that from the heat exchanger pre-heats the fluidising air. Short transport delays may be allowed for the passage of the gas through each of these two stages of economiser and heat exchanger.

9.4 Some Aspects of Control Applied to the Dynamic Characteristics revealed by this Study

The system schematic of Figure 9.2 may be used as the basis for a systematic study of the problems of control and regulation of a fluidised bed boiler. It is necessary to incorporate the boiler into the entire system[22] of hydraulic mains, evaporators, superheaters and turbines.

The only worthwhile comments that can be made here must be restricted to the primary dynamic characteristic of the term b_{13} in the heat transfer matrix as revealed by this study.

It is necessary to first define the type of input that the system may be called upon to respond to. Step changes are generally too severe in large plant. Ramp changes are usually found satisfactory both from the point of speed of response as well as stability. However, it is advantageous to get over transients as rapidly as possible and with minimum disturbance to the system.

Having determined the input type that the system is required to meet, it is useful to define an index of performance. In any system of controller and plant the error between the demand (input) and response (output) is a good indication of the quality of the overall controlled system. The design of the controller[23] may be based on minimising a performance index I which is expressed in terms of the error e(t). Thus, a minimum error squared index $I = e^2(t)dt$ will tend to force a rapid response at the expense of instability. A time weighted function such as $I = t\, e(t)dt$ will ensure correction as errors persist with time. In between these a range of choice exists to suit the

situation in question.

Furthermore, there is the question of the controller in the feed-forward or feed-back configuration; indeed, whether open loop or closed loop.

An interesting conjecture prompts itself in connection with the characteristic of heat evolution revealed by this study. In an attempt to effect a quick response with a minimum of instability, it may be advantageous to accompany a step change in coal throughput with a ramp change in fluidising air. The rate of the ramp change should extend over the dominant time-constant (5.5 min) of the phase lag in the heat evolution term in Figure 9.1. Changes in coal and air throughputs proportioned in this fashion, and operated in unison in any control or regulation loop to meet a given criterion of performance will perhaps constitute a configuration difficult to improve. The ramp increase of air ensures that the background carbon in segments is depleted at a rate not far removed from that at which it is built up by lateral flow through the segments. On the other hand, the fastest build up of the background carbon is ensured by a step increase in the coal throughput. The penalty is that over the initial stages of the transient the volatile release in the coal feed segment will have insufficient air for combustion since the step increase in coal throughput is matched by the ramp increase in air throughput only at the end of the transient time-constant.

C H A P T E R 10

SUMMARY OF CONCLUSIONS

SUMMARY OF CONCLUSIONS

The principal factors that emerge from the study are as follows:

1. Using linear coal feeders the spacing between feeders should be 1.5 - 1.75 m for coals of 36-38% volatile content.

2. The percentage of fines elutriated from the bed is likely to be 12-15% of the throughput.

3. Serious consideration should be given to feeding preheated excess air, for the combustion of the carbon fines elutriated, directly into the freeboard. There is a strong suspicion that the extra heat evolved by the increased combustion of fines within the bed does not compensate for the heat removed from the bed by the excess air itself. Moreover, the excess air results in increased fluidising velocity which in turn leads to a slight increase in critical elutriation size of particles to result in increased elutriation loss. Furthermore, with no excess fluidising air, there is a decrease in the pumping costs.

4. It may be advantageous to operate the boiler and freeboard as a two-stage process for maximum combustion efficiency. Parts of the coal feed cell near the coal feeder may be operated as a partial gasifier with the remainder of the cell operated for complete combustion. On combustion in the freeboard, the resulting CO will provide the necessary heat to raise the temperature for the further combustion of

the elutriated carbon fines. Although the cost of the convective tubing in the freeboard will increase, and it is about six times as expensive as that in the fluidised bed, there is the possibility of obviating the need for a further combustor beyond the freeboard to reduce the carbon loss to the acceptable level below 1%.

5. Altering the volatile content of the coal fired from the value for which the coal feeder spacing is an optimum, will effect the combustion efficiency of the boiler. If the volatile content of the coal fired is increased the fluidising air should be increased correspondingly to burn the volatiles liberated in the coal feed segment. Because the volatile content of the coal is increased, the carbon, which forms the remainder, decreases. This decreased carbon spreads over the remainder of the cell to give lean combustion conditions. Moreover, the increase in fluidising air to burn the extra volatiles in the coal feed segment increases further the lean combustion in the outer segments. On the other hand, a decrease in the volatile content of the coal fired will result in the combustion of sufficient carbon in the coal feed segment to compensate for the decrease in volatiles with the result that there will be no substantial change in the quality of combustion over the cell.

6. Provided the phenomenon of segmentation holds in large fluidised beds, there is likely to be 15-20% of the bed area which is relatively stagnant. If the segments correspond to

nodes or areas of high activity, these relatively stagnant areas (Figure 1.2b) correspond to anti-nodes or locations of low activity. At the design stage an allowance should be made for this effect.

7. Care should be taken in not having too close a stacking factor for the steam tube bundles. It is questionable as to whether it is desirable to break up the natural patterns of segmentation exhibited by large fluidised beds. Vertical and consequently lateral flow of solids must be affected adversely with the consequences of increased thermal gradients through the bed height as the transport of the ash plasma carrying the heat evolution to the steam tubes is decreased An excessive build-up of heat near the combustion zone will tend to cause ash clinkering, while the upper part of the bed will tend to chill and thereby decrease the heat transferred to the steam.

8. For the purpose of changes in coal and air throughput required to respond to the corrections by control or regulation loops, it may be advantageous if changes in air throughput are made via an integrator action. In this way all step changes in coal throughput will be accompanied by a ramp change in air throughput. The integrator time-constant must be that of the dominant phase lag of 5.5 min for coals of 36-38% volatile content. This ensures a minimum of depletion of the carbon inertia in the outer segments without impeding its build-up through the segments in response to changes in coal throughput.

REFERENCES

1. BADISCHE ALILIN and SODA-FOBRIK. (1957). B.P. 768,656 and B.P. 776,791.

2. COLLIS, B.A. and McLAREN, J. (1957). Coal Industry (Patents) Ltd, B.P. 871,000.

3. SKINNER, D.G. (1970). The Fluidised Combustion of Coal (book) N.C.B. London, S.W.1.

4. MARKS, W.L. and JURY, A.W. Patent Application No.44071/69. A Fluidised Bed Injector.

5. HIGHLEY, J. and MERRICK, D. (1971). The Effect of the Spacing between Solid Feed Points on the Performance of a large Fluidised Bed Reactor, A.I.Ch.E. Symposium Series 1971, 67, (116), 219-227. Fluidisation: Fundamental Studies, Solid-fluid Reactions and Applications.

6. AVEDASIAN, M. (1973). Combustion of Carbon Particles in a Fluidised Bed. Trans.Inst.Chem.Engrs. 51, (2).

7. FAN, L.T., CHEN, M.S., AHN, Y.K. and WEN, C.Y. (1969). Mixing Models with Varying Size Stage. Canadian J. Chem.E. 47, (2), 141-148.

8. WATERS, P.L., and WATTS, A. (1967). Fluidised Bed Combustion of Coal: Heat release and heat transfer studies. Fluidisation Symposium, Monash University.

9. STOCKWELL, D.H. and WILLIAMS, D.F. (1968). Private Communication.

10. WHITEHEAD, A.B. and YOUNG, A.D. (1967). Fluidisation Performance in Large Scale Equipment: Part 1. Proc.Symp. on Fluidisation, Eindhoven, p.284.

11. KOSLOV, G.I. (1958). On High Temperature Oxidation of Methane. Seventh Symposium on Combustion, Butterworth 142-149.

12. DARWIN, C. (1955). Note on Hydrodynamics. Proc.Camb.Phil. Soc., 49, Pt.2, 342.

13. REUTER, H. (1963). Mechanisms der blasen in gas-feststoff-fliesbett, Chem.Ing.Tech. 35, p.219.

14. PARTRIDGE, B.A. and ROWE, P.N. (1962). Particle Movement Caused by Bubbles in a Fluidised Bed. Proc.Symp.on Interaction between Fluids and Particles, London, Pub.Inst.Chem.Eng., 135.

15. CHENEY, A.G., HENWOOD, G.A., LYALL, E. PARTRIDGE, B.A. and ROWE, P.N. (1965). The Mechanisms of Solids Mixing in Fluidised Beds, Trans.Inst.Chem.Eng. 43, T271.

16. PARTRIDGE, B.A. and ROWE, P.N. (1965). An X-ray Study of Bubbles in Fluidised Beds, Trans.Inst.Chem.Eng.43, T157.

17. LYALL, E., PARTRIDGE, B.A. and ROWE, P.N. (1964). Cloud Formation Around Bubbles in Gas Fluidised Beds, Chem.Eng.Sci. 19, p.973.

18. PARTRIDGE, B.A. and ROWE, P.N. (1966). Analysis of Gas Flow in a Bubbling Fluidised Bed when Cloud Formation Occurs. Trans.Inst.Chem.Eng. 44, T349.

19. McLAREN, J. and WILLIAMS, D.F. (1969). Combustion Efficiency, Sulphur Retention and Heat Transfer in Pilot-plant Fluidised Bed Combustors, J.Inst.Fuel 42, 303.

20. NICHOLSON, H. (1964). Dynamic Optimization of a Boiler. Proc.IEE, 111, (8).

21. NICHOLSON, H. (1965). Dual-mode Control of a Time-varying Boiler Model with Parameter and State Estimation. Proc.IEE, 112, (2).

22. NICHOLSON, H. (1967). Integrated Control of a Non-linear Boiler Model. Proc.IEE, 114, (10).

23. KALMAN, R.E. and KOEPCKE. (1958). Optional Synthesis of Linear Sampling Control Systems Using Generalised Performance Indices. Trans.ASME, 80, (8), 1820-1826.

APPENDICES

A P P E N D I X 1

NOMENCLATURE

Symbol	Description	Units
Ash	Ash in coal	%
a_x	Air in excess of stoichiometric	%
c	Carbon in coal	%
c.v.	Calorific value of coal	k.cal/kg
H	Hydrogen in coal	%
$\dot{H}_A$	Heat flow in ash stream (loss)	k.cal/hr
$\dot{H}_a$	Heat flow in air stream (input)	k.cal/hr
$\dot{H}_c$	Heat flow in steam	k.cal/hr
$\dot{H}_{comb}$	Heat evolution rate due to combustion	k.cal/hr
$\dot{H}_{CO2}$	Heat flow in carbon dioxide } constituents of off-gas	k.cal/hr
$\dot{H}_g$	Heat flow in gas stream } constituents of off-gas	k.cal/hr
$\dot{H}_M$	Heat flow in moisture } constituents of off-gas	k.cal/hr
$\dot{H}_{N2}$	Heat flow in nitrogen } constituents of off-gas	k.cal/hr
$\dot{H}_L$	Heat loss flow	k.cal/hr
L	Latent heat of vaporisation of steam	k.cal/kg
M	Moisture in coal	%
O	Oxygen in coal	%
S_A	Specific heat of ash	
S_a	Specific heat of air	
S_{CO2}	Specific heat of carbon dioxide	
S_{N2}	Specific heat of nitrogen	
S_w	Specific heat of water	
T	Bubble plug flow time through bed height	1 second
t	Time	second
$\dot{W}_A$	Mass flow of ash	kg/h
$\dot{W}_a$	Mass flow of air	kg/h
$\dot{W}_c$	Mass flow of steam	kg/h
$\dot{W}_F$	Mass flow of coal	kg/h
$\dot{W}_g$	Mass flow of off-gas	kg/h
y	Carbon in bed ash	%
θ	Ambient temperature	^oC
θ^a	Temperature of fluidising bed	^oC
$\theta_{a.f}$	Temperature of fluidising air	^oC

A P P E N D I X 1

MASS AND HEAT FLOW TRANSFER COEFFICIENTS

A1.1 Mass Flow Coefficients

The coefficients of the mass flow matrix set down in Figure 2.1a are as follows:

a_{11}. The coefficient $\partial\dot{W}_A/\partial\dot{W}_F$ relating the ash waste $\dot{W}_A$ to the coal feed $\dot{W}_F$ is obtained from the coal analysis (Ash, %).

$$a_{11} = \partial\dot{W}_A/\partial\dot{W}_F = 0.01\ \text{Ash}/(1-0.01y) \qquad \text{(A1.1)}$$

where y is the % of carbon in the bed ash.

a_{12}. The coefficient $\partial\dot{W}_g/\partial\dot{W}_F$ relating the waste gas flow $\dot{W}_g$ to the coal feed $\dot{W}_F$ is a function of the products of combustion of coal.

$$a_{12} = \partial\dot{W}_g/\partial\dot{W}_F = 1-0.01\ \text{Ash}/(1-0.01y) \qquad \text{(A1.2)}$$

a_{22}. The coefficient $\partial\dot{W}_g/\partial\dot{W}_a$ relating the waste gas flow $\dot{W}_g$ to the air intake $\dot{W}_a$ is unity since all the air appears in the waste gas.

$$a_{22} = \partial\dot{W}_g/\partial\dot{W}_a = 1 \qquad \text{(A1.3)}$$

a_{33}. Since no alteration in mass occurs in the coolant stream,

$$a_{33} = \partial\dot{W}_c/\partial\dot{W}_c = 1 \qquad \text{(A1.4)}$$

A1.2 Heat Flow Coefficients

The coefficients of the heat flow matrix set down in Figure 2.1b are as follows:

b_{11}. The waste ash heat coefficient $\partial\dot{H}_A/\partial\dot{H}_{comb}$ is obtained by eliminating $\dot{W}_F$ from

$$\dot{H}_{comb} = \dot{W}_F \times c.v.$$

and $$\dot{H}_A = 0.01\ \dot{W}_F\ Ash \times s_A \times (\Theta - \Theta_a)$$

and is $$b_{11} = \partial\dot{H}_A/\partial\dot{H}_{comb} = 0.01\ Ash \times s_A \times (\Theta - \Theta_a)/c.v. \qquad (A1.5)$$

where s_A = specific heat of ash, c.v. = calorific value of coal and Θ and Θ_a are the temperature of the bed and the ambient temperature respectively.

b_{12}. The waste gas heat coefficient $\partial\dot{H}_g/\partial\dot{H}_{comb}$ is obtained by considering the heat flows $\dot{H}_{N_2}$, $\dot{H}_{CO_2}$ and $\dot{H}_M$ in the gas constituents, nitrogen, CO_2 and moisture.

$$\dot{H}_{N_2} = \frac{77}{23}\ 0.01\ \dot{W}_F\left[\frac{32}{12}\left(C - \frac{0.01y}{1-0.01y}\ Ash\right)\right] \times s_{N2} \times (\Theta - \Theta_a)$$

$$\dot{H}_{CO_2} = \frac{44}{12}\ 0.01\ \dot{W}_F\left[C - \frac{0.01y}{1-0.01y}\ Ash\right] \times s_{CO2} \times (\Theta - \Theta_a)$$

$$\dot{H}_M = 0.01\ \dot{W}_F\left(\frac{18}{2}\ H + M\right)\left[s_w \times (\Theta - \Theta_a) + L\right]$$

Also

$$\dot{H}_a = \frac{1}{23}\ \dot{W}_F\left[\frac{32}{12}\left(C - \frac{0.01y}{1-0.01y}\ Ash\right) + \frac{16}{2}\ H - O\right](1 + 0.01a_x)s_a \times (\Theta_{a.f.} - \Theta_a)$$

The coefficient is deduced by considering the net heat flow,

$$\dot{H}_g = \dot{H}_{N_2} + \dot{H}_{CO_2} + \dot{H}_M - \dot{H}_a$$

from the heat released by combustion into the gas stream and is

$$b_{12} = \partial\dot{H}_g/\partial\dot{H}_{comb} = \left[\dot{H}_{N2} + \dot{H}_{CO2} + \dot{H}_M - \dot{H}_a\right] / \dot{H}_{comb} \qquad (A1.6)$$

b_{13}. The heat transfer coefficient $\partial\dot{H}_c/\partial\dot{H}_{comb}$ to the coolant is obtained by considering the available heat

$$\dot{H}_c = \dot{H}_{comb} - (\dot{H}_g - \dot{H}_a) - \dot{H}_A - \dot{H}_L$$

and is

$$b_{13} = \partial\dot{H}_c/\partial\dot{H}_{comb} = \left[\dot{H}_{comb} - (\dot{H}_g - \dot{H}_a) - \dot{H}_A - \dot{H}_L\right]/\dot{H}_{comb} \qquad (A1.7)$$

$$= 1 - \partial\dot{H}_A/\partial\dot{H}_{comb} - \partial\dot{H}_g/\partial\dot{H}_{comb} - \partial\dot{H}_L/\partial\dot{H}_{comb}$$

b_{22} b_{23} Both these coefficients are unity since changes are reflected directly.

$$b_{22} = \partial\dot{H}_g/\partial\dot{H}_a = 1 \qquad (A1.8)$$

$$b_{23} = \partial\dot{H}_c/\partial\dot{H}_c = 1 \qquad (A1.9)$$

A P P E N D I X 2

NOMENCLATURE

Symbol	Listing A2.1	Description	Units
A		Plan area of segment	
A_b	AB	Bubble flow area, fraction of segment area	
A_c	AC	Cloud flow, fraction of segment area	
A_{cs}		Cloud shed, fraction of segment area	
A_p	AP	Particulate phase gas flow, fraction of segment area	
A_w	AW	Bubble wake flow, fraction of segment area	
h		Bed height, fraction of segment area	
h_g		Layer thickness of gas flow, fraction of segment area	
T		Bubble plug flow time through the bed height	1 sec.
t		Time	seconds
U	U	Fluidising velocity (empty bed)	m/s
U_b	UB	Bubble stream velocity	"
$\bar{U}_{b.r}$	UBAV	Mean velocity of bubbles over rth gas layer	"
U_o	UO	Incipient fluidising velocity	"
U_p	UP	Particulate phase gas velocity	"
U_s	US	Settling velocity of solids	"
V_b		Bubble volume	
V_c		Cloud volume	
α		U_b/U_o	
β	BETA	Wake as a fraction of the bubble volume	
ε	EPSI	Voidage in particulate phase	
ν	NOL	Number of layers for gas flow	

A P P E N D I X 2

PROFILES OF SOLIDS AND GAS STATES IN A FLUIDISED BED SEGMENT

The gross profiles of gas and solids phases within a segment may be defined as follows:

A2.1 Vertical Profiles

The various physical states of bubbles, cloud, wake and particulate phases may be considered in terms of vertical profiles through a segment. These profiles define the cross-sectional areas occupied by the several states at different bed heights. Since the gas streams are considered in horizontal layers of constant height, volumes may be treated as plan areas of cross-section effective over this height. Each of the fast moving particulate states or phases of cloud and wake, as also the slow moving particulate phase, is considered as a gas-solid entity, and expressions are deduced defining them as such. The gas constituent is defined by the voidage, while the complement of the voidage defines the solids content. In all diagrams these constituents are shown separated since they have differing velocities and do not move in unison from one interval of time to the next.

The equations defining the areas of cross-section occupied by the states in any layer are as follows.

The plan area of cross-section A of a segment may be expressed in terms of areas occupied by bubble gas A_b, cloud A_c, wake A_w and slow moving particulate phase A_p, to give:

$$A = A_b + (A_c - \Sigma\Delta A_c) + A_w + \left[A_p + (U_b/U_p)\Sigma\Delta A_c\right] \qquad (A2.01)$$

where $\Sigma\Delta A_c$ is the total cloud shed up to the layer in question.

Here $A_c/A_b = V_c/V_b = 1/(\alpha - 1)$

where $\alpha = U_b/U_o$.

It follows that the decrease in cloud area ΔA_c due to cloud shedding is

$$\Delta A_c = A_b\Delta\left[1/(\alpha - 1)\right] + \left[1/(\alpha - 1)\right]\Delta A_b \qquad (A2.02)$$

Now ΔA_c travelling at bubble velocity U_b becomes cloud shed A_{cs} travelling at particulate phase gas velocity U_p

$$\therefore \quad A_{cs} = (U_b/U_p)\,\Delta A_c \qquad (A2.03)$$

The particulate phase area A_p is increased by the addition of cloud shed with height to

$$A_p + (U_b/U_p)\,\Sigma\Delta A_c \qquad (A2.04)$$

The total gas flow is

$$AU = A_bU_b + \varepsilon\left[(A_c - \Sigma\Delta A_c)U_b + A_wU_b + \left(A_p + (U_b/U_p)\Sigma\Delta A_c\right)U_p\right] \qquad (A2.05)$$

Now,

solids flow up = solids flow down

$$A_w(1 - \varepsilon)U_b = (1 - \varepsilon)\left[A_p + (U_b/U_p)\Sigma\Delta A_c + (A_c - \Sigma\Delta A_c)\right]U_s \qquad (A2.06)$$

where the area A_w of wake flow is a fraction β of the bubble stream flow A_bU_b.

$$A_w U_b = \beta A_b U_b$$

For the particles to remain fluidised

$$U_p + U_s = U_o/\varepsilon \qquad (A2.07)$$

Equations A2.01 and A2.07 are used to eliminate A_p and U_p in A2.05 and A2.06 giving a pair of simultaneous equations the solutions to which are:

$$A_b = AU_s \Big/ \left[\beta U_b + (1 + \beta) U_s\right] \qquad (A2.08)$$

and

$$A_c - \Sigma\Delta A_c = \frac{A(U - U_o + \varepsilon U_s) - A_b\left[U_b - \beta U_o + \varepsilon\beta(U_s + U_b) - U_o + \varepsilon U_s\right]}{\varepsilon(U_b + U_c) - U_o} \qquad (A2.09)$$

Also from the above:

$$A_w = \beta A_b \qquad (A2.10)$$

and from A2.01

$$A_p + (U_b/U_p)\Sigma\Delta A_c = A - A_b(1 + \beta) - (A_c - \Sigma\Delta A_c) \qquad (A2.11)$$

Equations A2.08 to A2.11 inclusive define the vertical profiles in terms of A, U, U_o, U_b, U_s, ε and β. These profiles are shown in Figure 3.9a as a fraction of A for U = 0.9 m/s, U_o = 0.06 m/s, U_s = 0.012 m/s, ε = 0.5 and β = 0.25. Here U_b is a function of U and U_o given in equation A2.12.

A 2.2 Horizontal Layers

Horizontal gas layers facilitate the identification of the particulate phase gas. From the standpoint of computation it is most helpful if this identification, together with the

bubble transport effects, are defined at regular intervals of time.

Two differing velocities in the vertical direction require to be reconciled in this lineation, since the bubble gas travels very much faster than the particulate phase gas.

From a knowledge of the bubble gas velocity U_b over the bed depth (quoted by Whitehead and Young[4]),

$$U_b = U - U_o + 0.71\sqrt{10.8(U/U_o)^{h^{.54}}} \qquad (A2.12)$$

the bubble gas plug flow time T, over the ν gas layers of the bed is evaluated as

$$T = \sum_{r=1}^{\nu} h_{g.r} / \bar{U}_{b.r} \qquad (A2.13)$$

where $h_{g.r}$ is the height of the rth gas layer and $\bar{U}_{b.r}$ is the mean bubble velocity in that layer.

Now the bed depth h is sub-divided into ν equal gas layers* so that $h_{g.r}$ is:

$$h_{g.r} = h/\nu = TU_p \qquad (2.14)$$

Equations A2.13 and A2.14 define the horizontal lineation of Figure 3.8. Bubble gas occupies a profile section which is replaced every interval of time T. The particulate phase gas,

---

*Actually, the increase in bubble velocity with bed height itself results in an increase in the area occupied by the particulate phase. This in turn leads to a decrease in U_p, the particulate phase gas velocity, with a consequent decrease in gas layer thickness $h_{g.r}$ as r approaches ν. However, this effect is small and considerable simplification results by considering gas layers of equal thickness.

on the other hand, merely moves through a layer in each interval T. Hence, particulate phase gas which entered the bed in different time intervals may be identified. These two equations may be used in an iterative procedure to evaluate $h_{g.r.}$ the gas layer height and the time T.

Equations A2.08 to A2.11 inclusive are used to define the profiles of the various solids and gas states within the bed. For clarity, the solids and gas components of the states are shown separate in Figure 3.8a, with an indication of the velocity of each constituent. It is worth noting that the conditions of operating the fluidised bed indicated in Figure 3.8a result in no particulate phase gas entering layer 1. The cloud requirement for the first two layers is in excess of the available particulate phase gas. Subsequently, cloud shedding gives rise to slow moving particulate phase gas. Under the appropriate operating conditions (reduced fluidising velocity) the model does show slow moving particulate phase gas entering layer 1.

LISTING A2.1 FLUNDL-FRACTIONAL CROSS-SECTION AREAS OF GAS/SOLIDS PHASES

```
          DECLARE D(50) , UB(50) , UBBAR(50) , FRAC(50) ;
          DECLARE AW(50) , AC(50) , AB(50) , AP(50) ;
GETLIST(BEDHT,P,UP,EPSI,US,A ,BETA);
          UP=UB/EPSI-US;
          FR=U/UP;
          D1=.34*FR**(.33*BEDHT**.54);
          UB1=U-UP*.71*SQRT(32.2*D1);
          UB0=U-UP*.71*SQRT(32.2*.34);
          UBAV=(UB1+UB0)*.5;
          ESTN=UBAV/UP;
          MIN=ESTN-ESTN/3;
          MAX=ESTN+ESTN/3;
LP1:      DO J=1 TO MAX;
          D(J)=.34*FR**(.33*(J*BEDHT/ESTN)**.54);
          UB(J)=U-UP*.71*SQRT(32.2*D(J));
   IF J>1 THEN UBBAR(J)=(UB(J)+UB(J-1))*.5; ELSE UBBAR(J)=(UB(J)+2.34
          END LP1;
          SUM=0;
LP2:      DO J=1 TO MIN;
          FRAC(J)=1/UBBAR(J);
          SUM=SUM+FRAC(J);
          END LP2;
          TERM=ABS(1/UP-SUM);
          SUM=SUM+1/UBBAR(MIN+1);
          TERM1=ABS(1/UP-SUM);
          IF TERM1<TERM THEN GO TO ONE; ELSE NOL=MIN;
          GO TO THREE;
ONE:      I=MAX-MIN;
LP3:      DO J=2 TO I;
          FRAC(J)=1/UBBAR(MIN+J);
          SUM=SUM+FRAC(J);
          TERM2=ABS(1/UP-SUM);
          IF TERM2<TERM1 THEN GO TO TWO; ELSE NOL=MIN+J;
          GO TO THREE;
TWO:      TERM1=TERM2;
          END LP3;
THREE:    H=BEDHT*12/NOL;
          NOL=TRUNC(NOL+.5);
          PUT LIST('      GAS:  NOL = ',NOL,'  MAX = ',MAX,'  MIN = ',MI
          PUT IMAGE(H,H/(UP*12))(M1);
M1:       IMAGE;
= --.--- in      T = --.--- SEC
          SUM=0;
          PUT LIST('      UB      AW      AC      AB      AP')
LP4:      DO I=1 TO NOL;
          AB(I)=A*US/(UB(I)*BETA+US*(1+BETA));
          Z=AB(I)*(UB(I)-BETA*UP+EPSI*BETA*(US+UB(I))-UP+EPSI*US);
          AC(I)=(A*(U-UP+EPSI*US)-Z)/(EPSI*(UB(I)+US)-UP);
          AW(I)=BETA*(A*US/(UB(I)*BETA+US*(1+BETA)));
          SUM=SUM+AW(I);
          AP(I)=A-(AW(I)+AC(I)+AB(I));
          IF AP(I)<0 THEN AC(I)=AC(I)+AP(I);
          IF AP(I)<0 THEN AP(I)=0;
          END LP4;
LP5:      DO I=NOL TO 1 BY -1;
          PUT IMAGE(UB(I),AW(I),AC(I),AB(I),AP(I))(M2);
M2:       IMAGE;
---    --.---    --.---    --.---    --.---
          END LP5;
          NOL=TRUNC(1/SUM+.5);
          PUT IMAGE(NOL,BEDHT*12/NOL)(M3);
M3:       IMAGE;
NOLID:    NOL = ---      h = --- --- in
```

APPENDIX 3

NOMENCLATURE

Symbol	Description	
A	Plan area of segment	
A_B	Bubble flow area	fraction of segment area
A_c	Cloud flow area	"
A_{cs}	Cloud shed area	"
A_d	Downward displacement flow area	"
A_p	Particulate phase gas flow area	"
$\bar{A}_p$	Gross particulate phase gas ($A_p + A_{cs} + A_d$) area	"
k_2 to k_ν	Fraction of particulate phase gas displaced downwards in layers 2 to ν	
m	Incremental time number	
r	Gas layer number	
T	Bubble plug flow time through bed height	1 second
t	Time	seconds
U_b	Bubble stream velocity	m/s
$u(t)$	Unit impulse function	
ϵ	Voidage in particulate phase	
ν	Number of layers for gas flow	

A P P E N D I X 3

KINETICS OF GAS FLOW

In order to define the flows of gas in a fluidised bed the gas constituent only of the various states need be considered. This is effected by reducing the areas of states by the voidage factor as shown in Figure 3.8(b). A quantity $(A_b + \varepsilon A_c)U_b$ of cloud/bubble gas enters layer 1. It moves through the successive layers in each of which it undergoes some cloud shedding $\varepsilon\Delta A_c$. The amount of cloud/bubble gas leaving the surface after time T is $\left[A_b + \varepsilon(A_c - \Sigma\Delta A_c)\right]U_b$. The output to input relationship of this cloud/bubble flow is defined by:

$$\left[A_b + \varepsilon(A_c - \Sigma\Delta A_c)U_b\right](t) = \left[(A_b + \varepsilon A_c)U_b\right](t)\ u(t - T) \qquad (A3.1)$$

where u(t) is an impulse function.

For the particulate phase gas two additional mechanisms must be taken into account. Firstly, there is cloud shedding as the bubbles coalesce, secondly, there is the downward displacement movement of particulate phase gas. In their wake, bubbles transport solids from the base to the surface. This leaves a void which is filled by displacement from adjacent and succeeding layers above. These two phenomena result in the nature of the particulate gas flow deviating from plug flow towards perfect mixing. The amount of this deviation depends upon the magnitude of these two phenomena and in practice there results a partially mixed gas flow.

The particulate phase gas of Figure 3 (b) may be resolved

to show the effects of cloud shedding and displacement flow. This is shown in Figure 3.8(c) with an indication of the time intervals T during which the movements of the gas constituents of the several phases, displacement and cloud shedding, occur. The gas constituents in the several layers may be represented by the expressions set down in A3.2, appropriate to the end of the mth interval of time T, and expressed in terms of the cross-sectional area occupied by the constituents. These expressions define the gas phases shown in Figure 3.7(c).

LAYER

$$
\begin{aligned}
5 \quad & \left[\bar{A}_{p.5.m} + \varepsilon A_{cs.5.m}\right] \quad (1 - k_5) \\
4 \quad & \left[\bar{A}_{p.4.m} + \varepsilon A_{cs.4.m}\right] \quad (1 - k_4) + A_{d.4.m} \\
3 \quad & \left[\bar{A}_{p.3.m} + \varepsilon A_{cs.3.m}\right] \quad (1 - k_3) + A_{d.3.m} \\
2 \quad & \left[\bar{A}_{p.2.m} + \varepsilon A_{cs.2.m}\right] \quad (1 - k_2) + A_{d.2.m} \\
1 \quad & \varepsilon A_{p.1.m} + A_{d.1.m}
\end{aligned}
\qquad \text{(A3.2)}
$$

$\varepsilon A_{p.1.m}$ is constant for each interval m of time T, and represents the intake into layer 1 of particulate phase gas during time T. Now $\varepsilon A_{cs.r}$ is the amount of cloud shed gas in the rth layer and is a constant for that layer for any interval m of time. $A_{d.r.m}$ is the amount of displacement in the rth layer descending from the r + 1th layer. It is a constant proportion k_r of the content of the r + 1th layer leaving the complement $1 - k_r$ of the r + 1th layer in situ. As the particulate phase gas moves up one layer after each interval T, all that phase

consisting of particulate and displacement in the first layer during the previous time $\overline{m - 1T}$ is expressed as $\overline{A}_{p.2.m}$ in the second layer for time mT.

For the second and subsequent layers particulate phase gas, cloud shedding and displacement during $\overline{m - 1T}$ moves up from layer r - 1 to layer r and is expressed as $\overline{A}_{p.r.m}$. These terms are involved when expanded, but nevertheless indicate that the successive layers contain particulate phase gas originating further and further in the past as shown in Figure 3.7(c).

The amount of displacement gas $A_{d.r.m}$ is a function of both the particulate phase gas content and the cloud shedding in the layer above.

$$A_{d.r.m} = k_{r+1}\left[\overline{A}_{p.r+1.m} + \epsilon A_{cs.r+1.m}\right] \qquad (A3.3)$$

At the end of each period of time T the top layer of particulate phase gas leaves the fluidised bed at the surface, and the particulate phase gas content of the various layers moves up one layer. This ensures a particulate phase gas velocity U_p. The particulate phase gas content $\overline{A}_{p.r.m+1}$ of the rth layer for the $\overline{m + 1\text{th}}$ interval of time T becomes

$$\overline{A}_{p.r.m+1} = \left[\overline{A}_{p.r-1.m} + \epsilon A_{cs.r-1.m}\right](1 - k_{r-1}) + A_{d.r-1.m} \qquad (A3.4)$$

where the cloud shedding $A_{cs.r-1}$ may be taken as the average increase per layer in particulate phase gas which in turn, occurs over layers 2 to ν inclusive:

$$A_{cs} = (A_{p.\nu} - A_{p.1}) / (\nu - 1) \qquad (A3.5)$$

The value of the constant k_r for the rth layer is chosen so that the profile of the particulate phase gas approximates to A_p of equation A2.8.

In practice, this value of k_r is small enough to be negligible. Considerable simplification results since equation A3.3 reduces to insignificance, and equation A3.4 reduces to

$$\overline{A}_{p.r.m.+1} = \overline{A}_{p.r-1.m} + \varepsilon A_{cs.r-1.m} \qquad (A3.6)$$

The boundary conditions are defined by the intake of air:

$$\overline{A}_{p.1.m+1} = \varepsilon A_{p.1.m} \qquad (A3.7)$$

and the air leaving the surface of the bed during $\overline{m+1.T}$

$$\overline{A}_{p.\nu.m} + \varepsilon A_{cs.\nu.m} \qquad (A3.8)$$

Equations A3.1, A3.5 and A3.6 with the boundary conditions A3.7 and A3.8 give a gas residence time distribution shown in Figure 3.8(b) for a fluidising velocity of U = 0.9 m/s.

A P P E N D I X 4

NOMENCLATURE

Symbol	Description
$A_1 - A_5$	Carbon in layers 1 to 5 in a segment of 5 layers
A^j_n	Carbon in layer n of segment j
A	Plan area of segment (unity)
A_w	Wake area, fraction of segment area
B	Lateral solids flow parameter $0 < B < 0.5$ (fraction of surface layer exchanged between adjacent segments in time T)
f	Vertical solids transport parameter $0 < f < 1$. (bubble shedding factor in time T)
h	Bed height m
h_g	Layer thickness of gas flow m
j	Segment number
m	Incremental time number
n	Number of layers in segment relevant to solids movement
T	Bubble plug flow time through bed height 1 sec.
t	Time seconds
ν	Number of layers for gas flow

A P P E N D I X 4

THE KINETICS OF SOLIDS FLOW

The gas layer height $h_{g.r}$ of equation A2.13 has no direct relevance to the movement of solids. The synthesis of expressions defining solids mixing is facilitated by defining a layer thickness directly related to solids movement. The thickness of a layer in the segment is chosen so that a layer contains an amount of material equal to the total wake capacity of all the bubbles generated during T, the plug flow time of bubbles through the bed height. Thus the total ash/carbon content of a layer is potentially portable with each renewal of air through the bed height.

Now in a time T the wake cross-section A_w in any layer is given by equation A2.10. The total wake volume due to all the bubbles generated in the segment in a time T in all ν layers of gas, each of thickness h_g is:

$$h_g \sum_{1}^{\nu} A_w \qquad \text{(A4.1)}$$

If the thickness of the solids layer in the segment is such that the layer is of the same volume as the wake capacity of A4.1, then equating volumes

$$A\, h/n = h_g \sum_{1}^{\nu} A_w \qquad \text{(A4.2)}$$

where n is the number of layers relative to solids mixing and is

$$n = Ah/h_g \sum_{1}^{\nu} A_w \qquad \text{(A4.3)}$$

The wake transport of solids by bubbles from base to surface results in an asymmetrical pattern of vertical mixing. Upward transport by the bubbles is accompanied by an equal downward displacement. This ensures mass conservation. The algorithm that defines the composition of the rth layer containing an amount* $A_{r,m+1}$ at the end of the $(m + 1)$th interval of time T, in terms of the amounts in the layers at the end of the previous interval of time, may be deduced from the pattern of bubble transport and shedding shown in Table A4.1. The compositions A_1 to A_5 in, say, five layers at time m.T are known. The next bubble run during $\overline{m + 1}.T$ determines the compositions of the layers at the end of the $\overline{m + 1}$th time interval, in terms of A_1 to A_5.

Bubbles, having a wake carrying capacity of one solids layer, form in layer 1 during a time interval T. The entire amount of solids A_1, contained in layer 1 is picked up by the bubbles. On rising, the bubbles shed a fraction f of their wake burden (i.e. fA_1) in layer 1, and cross the boundary between layers 1 and 2 carrying an amount $(1 - f)A_1$. By displacement a quantity $(1 - f)A_2$ of the material initially in layer 2 moves down to layer 1 leaving fA_2 in layer 2. On moving into layer 2, the bubbles replenish their wake with a fraction f, i.e. fA_2. Thus, there is mass conservation in layers 1 and 2. This cycle of shedding and transport is repeated in the successive layers

---

*Only the solids content of the layers is considered; each layer contains the same amount, but its composition varies.

TABLE A4.1. PATTERN FOR VERTICAL MIXING OF SOLIDS

LAYER	Content at $m.T$	Content at $\overline{m+1}.T$			
5	A_5				$(1-f)^4A_1+f(1-f)^3A_2+f(1-f)^2A_3+f(1-f)A_4+fA_5$
4	A_4			$(1-f)^3A_1+f(1-f)^2A_2+f(1-f)A_3+fA_4$	$f(1-f)^3A_1+f^2(1-f)^2A_2+f^2(1-f)A_3+f^2A_4+(1-f)A_5$
3	A_3		$(1-f)^2A_1+f(1-f)A_2+fA_3$	$f(1-f)^2A_1+f^2(1-f)A_2+f^2A_3+(1-f)A_4$	
2	A_2	$(1-f)A_1+fA_2$	$f(1-f)A_1+f^2A_2+(1-f)A_3$		
1	A_1	$fA_1+(1-f)A_2$			

to develop the pattern shown. Finally, the entire amount transported to the surface layer is deposited there. Such a pattern is consistent with constant bubble transport and shedding, with asymmetrical mixing in a given layer extending only from one layer above, but from all the layers below the layer considered. This latter is due to the difference in velocity between the upward wake transport and the downward displacement of solids.

In order to deduce an algorithm the pattern of bubble transport may be reduced conveniently to one of bubble shedding and transport in equilibrium with bubble replenish and downward displacement.

TABLE A4.2

LAYER	Content at mT	Content at $\overline{m+1}.T$			
5	A_5				$(G_5' + T_5 + Q_5)$
4	A_4			$(G_4' + T_4 + Q_4)$	$G_4 + S_4 + D_4$
3	A_3		$(G_3' + T_3 + Q_3)$	$G_3 + S_3 + D_3$	
2	A_2	$(G_2' + T_2 + Q_2)$	$G_2 + S_2 + D_2$		
1	A_1	$G_1 + S_1 + D_1$			

During the passage of the bubble train from layer r to r + 1 there is a shedding S of solids in layer r followed by a transport T of solids into layer r + 1. This is accompanied by a displacement D of solids from r + 1 to r leaving a residue Q

in layer r + 1. The steps of this procedure are repeated from layer to layer in Table A4.2 with the addition of a further term G, the significance of which is explained below. There are two terms, one in parenthesis and the other not, for each layer during $\overline{m + 1}.T$. The term in parenthesis defines the momentary composition of the bubble stream wake during the passage of the bubble stream through the layer in question prior to shedding and moving on one layer. It is included merely for convenience. The term not in parenthesis defines the composition of the layer in question after the bubble stream has passed through it during $\overline{m + 1}.T$.

Subsequently, in the heat evolution it will be necessary to account for non-volatile combustion which occurs mainly in the first layer. It is thus necessary at this stage to identify separately that constituent of the material originating from the first layer and carried upwards and shed by bubbles. This is effected by denoting the shed material by G + S and the transported material by G' + T. Defining the pattern step by step the algorithm for the rth layer reduces to the equations of A4.4.

Thus, if

$$
\begin{aligned}
G_r &= fG'_r \\
S_r &= f(T_r + Q_r) \\
\text{and} \quad D_r &= (1 - f)A_{r+1} \\
\text{then} \quad A_r &= G_r + S_r + D_r \\
\text{and} \quad G'_{r+1} &= \frac{1 - f}{f} G_r \\
T_{r+1} &= \frac{1 - f}{f} S_r \\
Q_{r+1} &= fA_{r+1}
\end{aligned}
\qquad \text{(A4.4)}
$$

The initial conditions for layer 1 are $Q_1 = 0$, $S_1 = 0$, $T_1 = 0$, $G'_1 = A_1$.

A_n of the surface layer is evaluated from the following terms of the penultimate layer

$$A_n = G'_{r+1} + T_{r+1} + Q_{r+1} \qquad (A4.5)$$

where $r = n - 1$.

The lateral displacement of material from segment to segment occurs by an interchange along the surface affecting surface layers in the first instance. Thus, for the case of a linear feeder, from any given segment a fraction B of the material in the top layer flows laterally to each of the two adjacent segments. This mechanism is embodied in the following algorithm:

$$A^j_{n.m+1} = A^j_{n.m} + B\left[A^{j-1}_n - 2A^j_n + A^{j+1}_n\right]_m \qquad (A4.6)$$

where the notation j refers to the segment, n denotes the surface layer and mT is the mth interval T of time.

On either side of a linear coal feeder a mirror image of the segments exists, and the lateral movement of material from one half to the other is taken into account by putting

$$A^{j-1}_n = A^{j+1}_n \qquad (A4.7)$$

when $j = 1$. This ensures mass conservation in the first segment.

In addition

$$A^{j+1}_n = A^j_n \qquad (A4.8)$$

when j = periphery segment.

Boundary reflection is taken into consideration by A4.8.

It may be of interest to show that equation A4.6, which defines the lateral flow of solids from segment to segment, corresponds to diffusion. Assuming s to be the distance apart between segment centres, equation A4.6 may be re-written

$$A^{j}_{m+1} - A^{j}_{m} = s^2 B\left[\{(A^{j+1} - A^{j})/s - (A^{j} - A^{j-1})/s\}/s\right]_m$$

or $$\partial A/\partial t = s^2 B\left[\{\partial A/\partial s\big|_{j+\frac{1}{2}} - \partial A/\partial s\big|_{j-\frac{1}{2}}\}/s\right]_m$$

or $$\partial A/\partial t = s^2 B(\partial^2 A/\partial s^2) \qquad (A4.9)$$

This is the diffusion equation.

APPENDIX 5

NOMENCLATURE

Symbol	Listing A10.1	Description
a	PA	Rosin-Rammler constant
b	PB	Rosin-Rammler constant
E_f	EF	Feed fines elutriated (fraction of coal throughput in time T)
F_f	FF	Feed fines burnt within the bed (fraction of coal throughput in time T)
V	V	Volatiles in the coal fired %
x_c	XC	Critical elutriation size of carbon particles μ
ϕ_o	COMB	Fraction of feed fines burning within the bed
α_c	ax_c^b	Exponent defining the size distribution of particles

A P P E N D I X 5

FRACTIONS OF FEED FINES BURNT AND ELUTRIATED

The fraction of feed fines, per unit of coal feed, below the elutriation size x_c is given by the Rosin-Rammler relation

$$1 - e^{-ax_c^b} \qquad (A5.1)$$

where a and b are constants defining the size distribution of the coal feed.

This fraction is reduced by (1 - 0.01 V) if it is assumed that these fines lose their volatiles almost instantaneously after being fed into the bed. Furthermore, the feed fines which are subject to elutriation are also subject to combustion. The amount that burns within the bed is:

$$F_f = \phi_o (1 - 0.01V) (1 - e^{-\alpha_c}) \qquad (A5.2)$$

where ϕ_o = fraction of feed fines that burns within the bed, and $\alpha_c = ax_c^b$.

Hence, the elutriated feed fines E_f from the coal feed segment per unit of coal feed is:

$$E_f = (1 - 0.01V)\left[1 - \{\phi_o(1 - e^{-\alpha_c})\}\right] \qquad (A5.3)$$

APPENDIX 6

NOMENCLATURE

Symbol	Listing A10.1	Description
a_b	BY	Fluidising air by-passing the cell (fraction of air throughput/unit time T)
$a_b + a_e$		Air leaving the surface of the cell (fraction of air throughput/unit time T)
a_s	AO	Air leaving the freeboard (fraction of air throughput/unit time T)
a_x	AX	Excess air (fraction of air throughput/unit time T)
B	B	Lateral solids flow parameter $0 < B < 0.5$ (fraction of surface layer exchanged between adjacent segments/unit time T)
C	C	Background carbon in segment expressed as a combustion inertia (seconds)
E_f	EF	Feed fines elutriated (fraction of cell throughput/unit time T)
E_a		Abrasion fines elutriated (fraction of cell throughput/unit time T)
E_o	EO	Elutriated fines loss in stack (fraction of cell throughput/unit time T)
E_{xc}	CFE	Elutriated fines of size x_c (fraction of cell throughput/unit time T)
F	FF	Fines in the throughput (fraction of cell throughput/unit time T)
F_f	FFB	Feed fines burnt within the bed (fraction of cell throughput/unit time T)
F_a		Abrasion fines burnt within the bed (fraction of cell throughput/unit time T)
F_{xc}	CFB	Fines of size x_c burnt within the bed (fraction of cell throughput/unit time T)
j	j	Segment number
K		Carbon particle shape factor
k		$= k_1 + k_2$ total size reduction/unit time T μ/s

NOMENCLATURE (Cont'd)

Symbol	Listing A10.1	Description
k_1	KC1	Combustion size reduction/unit time T μ/s
k_2	KA1	Abrasion size reduction/unit time T μ/s
ML	SCOMB	Steady-state combustion mass loss from a segment (fraction of cell throughput/T)
m_r	M(R)	Mass of mono-size fraction of size x_r (fraction of cell throughput/T)
n_r		Number of carbon particles of mono-size x_r
N	N	Number of segments in coal feed cell
s	NOS	Periphery segment number $s = \left[2N + 3 + (-1)^N\right]/4$
S	S	Surface area of all the carbon particles in a segment
t		Time (seconds)
T	T	Bubble plug flow time though bed height = incremental time T of 1 second
T_c	TC1	Mean particle combustion time (seconds)
V	V	Volatiles in the coal fired (%)
w	W	Ratio $\dot{x}^j/\dot{x}^s$
x		Carbon particle size (μ)
x_c	XC	Critical elutriation size (μ)
x_e	XE	Particle size bouyant in freeboard (μ)
x_o	XO	Largest size of coal throughput range (μ)
Δx	DX	Difference in size between adjancent mono-sizes (μ)
$\dot{x}^j$		Rate of particle size reduction (combustion and abrasion) in segment j μ/s
$\dot{x}^s$		Rate of particle size reduction (combustion and abrasion) in segment s μ/s
$\dot{x}^j_1$	KC(J)	Rate of particle size reduction due to combustion in segment j μ/s
$\dot{x}^s_1$	KC1	Rate of particle size reduction due to combustion in segment s μ/s

NOMENCLATURE (Cont'd)

Symbol	Listing A10.1	Description
$\dot{x}_2$	KA1	Rate of particle size reduction due to abrasion
ϕ_o	COMB(0)	Fraction of feed fines burning within the bed (in time T)
ϕ_1	COMB(1)	Fraction of abrasion fines burning within the bed (in time T)
ϕ_2	COMB(2)	Fraction of fines of size x_c burning within the bed (in time T)
ϕ_3	COMB(3)	Fraction of fines of airborne size $x < x_e$ burning in freeboard (in time T)
γ	GAMMA	Mass reduction factor (combustion and abrasion) of carbon particles (in time T)
γ_1	GAMMA(1)	Mass reduction factor (combustion) of carbon particles (in time T)
γ_2	GAMMA(2)	Mass reduction factor (abrasion) of carbon particles (in time T)
μ	MU	Number of mono-size fractions in the size range x_o to x_c

A P P E N D I X 6

STEADY-STATE MASS LOSS OF CARBON FROM A SEGMENT

It is assumed that the carbon particles in a given segment undergo a zero order rate of size reduction k_1 due to combustion, and k_2 due to abrasion, such that

$$dx/dt = -k \qquad (A6.01)$$

where

$$k = k_1 + k_2$$

The given size distribution of the feed particles may be subdivided into monosize fractions, each of size Δx, such that

$$\Delta x = x_r - x_{r+1} = kT \qquad (A6.02)$$

This ensures that a particle of size x_r reduces to size x_{r+1} in the incremental time T. Integrating equation A6.01

$$x = x_{t=0} - kT \qquad (A6.03)$$

The size distribution may be subdivided into μ monosize fractions between the largest size x_o and the critical elutriation size x_c so that

$$\mu = (x_o - x_c)/\Delta x \qquad (A6.04)$$

and

$$x_r = x_o - r\Delta x \qquad (A6.05)$$

By considering a reduction Δx in a time T, as given by equation A6.02 the reduced mass m_r' of n_r particles originally of size x_r may be related to the original mass m_r of the monosize

fraction in question.

The mass m_r of a monosize fraction may be related to the particle size x_r by

$$m_r = n_r K x_r^3 \qquad (A6.06)$$

If the diameter x_r is reduced by Δx, equation A6.03 may be used to define the reduced mass m_r' as

$$m_r' = n_r K(x_r - kT)^3$$

$$= n_r K\left[x_r - (k_1 + k_2)T\right]^3$$

Expanding and using equation A6.06:

$$m_r' = m_r - Kn_r\left[l_1 x^2 - p_1 x + q_1\right] - Kn_r\left[l_2 x^2 - p_2 x + q_2\right] \qquad (A6.07)$$

where

$l_1 = 3k_1 T$; $\quad l_2 = 3k_2 T$;

$p_1 = 3k_1^2 T^2 (k_1 + 3k_2)/(k_1 + k_2)$; $\quad p_2 = 3k_2^2 T^2 (k_2 + 3k_1)/(k_1 + k_2)$

$q_1 = (k_1 + 3k_2) k_1^2 T^3$ $\quad q_2 = (k_2 + 3k_1) k_2^2 T^3$

Equation A6.07 may be written:

$$m_r' = m_r - Kn_r(lx^2 - px + q) \qquad (A6.08)$$

This is of the form:

$$m_r' = m_r - \delta m_r$$

or

$$= m_r(1 - \gamma_r) \qquad (A6.09)$$

where $\gamma_r = \delta m_r / m_r$

the fractional change in the original mass m_r and is given by:

$$\gamma_r = Kn_r(lx_r^2 - px_r + q)/m_r$$

Using equation A6.06:

$$\gamma_r = (\ell x_r^2 - px_r + q)/x_r^3 \qquad (A6.10)$$

Equation A6.09 defines the mass m_r' of the monosize fraction originally of size x_r and of mass m_r after a size reduction Δx in the incremental time T due to the combined effects of combustion and abrasion. This forms the next size fraction x_{r+1}.

By using the appropriate set of constants ℓ_1, p_1 and q_1 or ℓ_2, p_2 and q_2 in equation A6.10, the overall reduction factor γ may be expressed as the sum of the individual reduction factors γ_1 due to combustion, and γ_2 due to abrasion. Thus,

$$\gamma = \gamma_1 + \gamma_2 \qquad (A6.11)$$

This allows the net removal of carbon from a segment due to particle size reduction to be apportioned to combustion and abrasion.

In this study the coal feed cell, composed of several segments, is considered to be operated at stoichiometric coal and air feed rates. All amounts of carbon and air are expressed as fractions or multiples of the cell throughput here regarded as unity.

Because a coal feed cell may comprise several segments each with differing background carbon and carbon size distribution, the rate $\dot{x}$ of particle size reduction due to combustion varies from segment to segment. For a given segment, $\dot{m}_r$ the change in mass in the incremental time T of a monosize fraction

of size x_r undergoing size reduction at the rate $\dot{x}_r$ is obtained by differentiating equation A6.06.

$$\dot{m}_r = K' x_r^2 \dot{x}_r \qquad \text{(A6.12)}$$

where x_r^2 is proportional to the surface area of a single particle of size x_r. More generally, for all the μ monosize fractions in a segment, the total surface area S of all the carbon particles is a product of the background carbon and the surface area of the particle size distribution. Hence, the amount (fraction of cell throughput) of carbon burning in a segment in the incremental time T is

$$\sum_{r=0}^{r=\mu} \dot{m}_r = K'' S \dot{x} \qquad \text{(A6.13)}$$

Now the air supply to all segments of a coal feed cell is identical. Provided all the air is used in the combustion of carbon particles, equation A6.13 is constant for all segments. However, a different quantity (fraction of cell throughput) of fines burns in each segment, hence the net air available for combustion of carbon particles varies from segment to segment. For a given total surface area of all the carbon particles in a segment, the rate $\dot{x}$ of size reduction of carbon particles varies directly as the net air available for the combustion of carbon particles. Hence for any segment

$$\frac{S \dot{x}}{\text{net air (fraction of cell throughput) available for carbon combustion}} = \text{constant} \qquad \text{(A6.14)}$$

The surface area of the size distribution in the jth segment is:

$$(\pi/3) \sum_{r=0}^{r=\mu} n_r^j (x_o^j - \gamma\Delta x)^2 \qquad (A6.15)$$

Now S^j is the product of this expression and the background carbon C^j in segment j. Using equation A6.06, the total surface area S^j of all the carbon particles may be expressed as

$$S^j = (\pi/3K)C^j \sum_{r=0}^{r=\mu} m_r^j (x_o^j - r\Delta x) \qquad (A6.16)$$

Equation A6.14 may be used to relate the rate $\dot{x}^j$ of particle size reduction in the jth segment to the known reduction rate $\dot{x}^s$ in the periphery segment s.

$$\dot{x}^j = \dot{x}^s \left[S^s(\text{net air available for combustion of particles in segment j}) / S^j(\text{net air available for combustion of particles in segment s})\right] \qquad (A6.17)$$

In order to apply equation A6.17, it remains to define the net air (fraction of throughput air) available for combustion of carbon in the several segments of a coal feed cell.

At stoichiometric operating conditions a constant fraction $(1 - a_b)/N$ of the fluidising air for the coal feed cell is available in each segment for the combustion of both fines and carbon particles or volatiles as the case may be. In the jth segment a throughput fraction, F_b^j of the fines originating from within the segment, burns in the bed while the remainder F_e^j is elutriated from the segment. Ideally, if the elutriated fines F_e^j also burns within the bed, the combustion in the segment would match the stoichiometric air supply $(1 - a_b)/N$ to give a combustion balance between air and carbon of:

$$(1 - a_b)/N = K'' S^j x^j + F_b^j + F_e^j \qquad (A6.18)$$

For the coal feed segment designated j = 1, this balance must take account of the volatiles V, which are assumed to burn completely, to give a combustion balance of

$$(1 - a_b)/N = K'' S^1 \dot{x}^1 + F_b^1 + F_e^1 + 0.01V \qquad (A6.19)$$

A closer look at equation A6.19 reveals that F_b^1 and F_e^1 are factors overwhelmingly influenced by the fines in the feed. If it is assumed that the volatiles and the fines burnt F_b use all the available air, then the combustion balance of equation A6.19 for the coal feed segment reduces to

$$(1 - a_b)/N = F_b^1 + 0.01V \qquad (A6.20)$$

and $\dot{x}^1$ reduces to zero, there being no size reduction of carbon particles due to combustion.

Now equation A6.20 implies that all the oxygen available is taken up by the volatiles and any feed fines burnt. However, an elutriation F_e^1 of feed fines occurs from the coal feed segment, and consequently an equivalent fraction of air throughput must by-pass the bed in the remaining segments of the cell. The equivalent air by-pass in the segments is apportioned relative to the difference in background carbon between the coal feed segment and the remaining segments of the cell in turn. The air by-pass in the jth segment is a fraction designated D^j of F_e^1 the feed fines elutriated from the coal feed segment, where D^j is given by

$$D^j = \Delta C/2 \sum_{j=2}^{j=s} \Delta C^j \qquad (A6.21)$$

here

$$\Delta c^j = c^1 - c^j \qquad \text{(A6.22)}$$

The combustion balance between air and carbon in the jth segment of A6.18 reduces to:

$$(1 - a_b)/N = K'' S^j \dot{x}^j + F_b^j + F_e^j + F_e^1 D^j \qquad \text{(A6.23)}$$

This combustion balance may be used to derive an expression for the net air (fraction of air throughput) available for combustion of carbon particles in the jth segment as:

$$(1 - a_b)/N - F_b^j - F_e^j - F_e^1 D^j \qquad \text{(A6.24)}$$

By analogy from equation A6.23 the net air (fraction of air throughput) available for combustion of carbon particles in the segment s is:

$$(1 - a_b)/N - F_b^s - F_e^s - F_e^1 D^s \qquad \text{(A6.25)}$$

Expressions A6.24 and A6.25 may be used in equation A6.17 to determine the rate $\dot{x}^j$ of size reduction of carbon particles in the jth segment relative to a known rate $\dot{x}^s$ in the periphery segment s.

This change in the rate of particle size reduction from one segment to the next may be expressed by considering a fixed particle size reduction occurring over different periods of time in the individual segments. In this way the size distribution in the segments may be expressed by the same range of monosizes. If these periods of time for the same size reduction in the segments are arranged to be integers, then the same particle

size reduction Δx occurs in the segments at these respective integers of time. This allows lateral exchange between segments at increments of time T of carbon particles having the same range of mono-sizes in the segments concerned. Expressions are now deduced for the time T^j to effect a reduction Δx in particle size in segment j relative to the time T to effect the same reduction in particle size in the periphery segment s.

For abrasion the rate $\dot{x}_2$ of change in particle size x is the same for all segments, and is independent of both background carbon and particle size distribution. The rate $\dot{x}^j$ of particle size reduction due to the combined effects of combustion and abrasion in the jth segment is thus:

$$\dot{x}^j = \dot{x}^j_1 + \dot{x}_2$$

Assuming a rate of particle size reduction of k_1 due to combustion, and of k_2 due to abrasion, the total rate $\dot{x}^s$ of particle size reduction in segment s is:

$$\dot{x}^s = k_1 + k_2 \qquad \text{(A6.26)}$$

while for the jth segment

$$\dot{x}^j = k^j_1 + k_2 \qquad \text{(A6.27)}$$

Since a size reduction Δx occurs in the jth segment in a time T^j

$$\Delta x = \dot{x}^j T^j \qquad \text{(A6.28)}$$

Furthermore, since the same difference Δx between one mono-size and the next occurs in all segments, i.e. Δx = constant

$$\dot{x}^j T^j = \dot{x}^s T \qquad \text{(A6.29)}$$

Express w^j as the required ratio of the times T^j and T of particle size reduction in segments j and s respectively.

$$w^j = T^j/T = \dot{x}^s/\dot{x}^j \qquad \text{(A6.30)}$$

Substitute from equation A6.26

$$w^j = (k_1 + k_2)/(k_1^j + k_2) \qquad \text{(A6.31)a}$$

Because $k_2 << k_1$, k_1^j may be approximated to k^j when

$$w^j = (k_1 + k_2)/(k_2 + k_1/w^j) \qquad \text{(A6.31)b}$$

w^j from equation A6.32 is used in equation A6.30 to determine $\dot{x}^j$ in terms of $\dot{x}^s$. Finally, T^j the incremental time required for a size reduction Δx in the jth segment is derived from equation A6.28.

The mass interchange between surface layers of adjacent segments as expressed in equation A4.6 is applied at increments of time T to the interchange between segments of all mono-size fractions to give $m^j_{r.t+T}$ the mass of the rth mono-size in the jth segment as

$$m^j_{r.t+T} = m^j_{r.t} + B\left[m_r^{j-1} - 2m_r^j + m_r^{j+1}\right]_t \qquad \text{(A6.31)c}$$

Such lateral mass flows into segment j accumulate for w increments of time T corresponding to the incremental time T^j of segment j (equation A6.30) to give $m^j_{r.t+T^j}$

$$m^j_{r.t+T^j} = \sum_{T=T}^{T=wT} m^j_{r.t+T}$$

Following equation A6.09 this accumulated mass $m^j_{r.t+T^j}$ of the mono-size x_r is reduced by Δx due to combustion and abrasion at the next increment T^j of time to give $(m^j_{r.t+T^j})'$.

$$(m^j_{r.t+T^j})' = m^j_{r.t+T^j} (1 - \gamma^j_r) \qquad (A6.32)$$

This is now the mass of the next mono-size x_{r+1}

$$m^j_{r+1.t+T^j} = (m^j_{r.t+T^j})' \qquad (A6.33)$$

Equation A6.31 represents the lateral solids exchange between surface layers of segments. Equation A6.32 is the mass reduction that causes each monosize to decrease one size due to combustion and abrasion, while equation A6.33 represents the updating that accounts for each size reduction with the passage of incremental time T^j.

A boundary condition applies to equation A6.31 for j = 1

$$m^{j-1} = m^{j+1} \qquad (A6.34)$$

A further boundary condition applies to equation A6.31 for j = s the periphery segment of a coal feed cell, where a reflection may be said to occur.

$$m^{j+1} = m^j \quad \text{where N = odd} \qquad (A6.35)$$

$$m^{j+1} = m^{j-1} \quad \text{where N = even} \qquad (A6.36)$$

The loss of mass per incremental time T of the mono-size x_r due to the overall reduction factor γ^j_r in the jth segment may be deduced from equation A6.32 to be

$$m^j_{r.t+T^j} \ \gamma^j_r \ / \ w^j \qquad (A6.37)$$

This mass loss can be apportioned into mass loss due to combustion

$$m^j_{r.t+T^j}\ \gamma^j_{r.1}\ /w^j \qquad \text{(A6.38)}$$

by using $\gamma^j_{r.1}$ the reduction factor due to combustion, obtained by using l_1, p_1 and q_1 in equation A6.10, and to mass loss due to abrasion.

$$m^j_{r.t+T^j}\ \gamma^j_{r.2}\ /\ w^j \qquad \text{(A6.39)}$$

by using $\gamma^j_{r.2}$ the reduction factor due to abrasion obtained by using l_2, p_2 and q_2 in equation A6.10.

Fines are produced due to the reduction in size of the combined effects of combustion and abrasion of the mono-size x_{c-1} to x_c. The fines produced by this reduction in size per incremental time T is

$$(1 - \gamma^j_{\mu-1})\ m^j_{\mu-1.t+T^j}\ /w^j \qquad \text{(A6.40)}$$

Expressions A6.38 to A6.40 define the rate of removal of carbon from each mono-size in segment j. By summing over the entire range of mono-sizes the combustion and elutriation mass losses in the various segments may be defined.

From equation A6.20 the total mass loss ML^1 due to combustion of volatiles and fines in the coal feed segment per incremental time T is

$$ML^1 = 0.01V + F_b{}^1 \qquad \text{(A6.41)}$$

where the fines burnt $F_b{}^1$ is the sum of F_f the feed fines burnt from equation A5.2, together with a fraction ϕ_1 that burns of

the abrasion fines from equation A6.39, and a fraction ϕ_2 that burns of the fines of size x_c (equation A6.40) generated within the coal feed segment.

$$F_b^1 = F_f + \phi_1 \sum_{r=o}^{\mu-1} m^1_{r.t+T^1} \gamma^1_{r.2}/w^1 + \phi_2 \sum_{r=o}^{\mu-1} (1-\gamma^1_{\mu-1}) m^1_{\mu-1.t+T^1}/w^1 \quad \text{(A6.42)}$$

where the total fractional mass reduction $\gamma^1_{\mu-1}$ is identical to $\gamma^1_{\mu-1.2}$ the fractional mass reduction due to abrasion, since it is assumed no size reduction due to combustion of carbon particles occurs in the coal feed segment.

The elutriated fines E_f^1 is the sum of E_f (equation A5.3) the elutriated fraction of the feed fines, together with the remaining fraction $(1 - \phi_1)$ of abrasion fines (equation A6.39), and the remaining fraction $(1 - \phi_2)$ of the fines of size x_c (equation A6.40) generated in the coal feed segment.

$$E_f^1 = E_f + (1-\phi_1) \sum_{r=o}^{\mu-1} m^1_{r.t+T^1} \gamma^1_{r.2}/w^1 + (1-\phi_2) \sum_{r=o}^{\mu-1} (1-\gamma^1_{\mu-1})$$

$$m^1_{\mu-1.t+T^1}/w^1 \quad \text{(A6.43)}$$

From equation A6.38 the mass loss ML^j due to combustion of carbon particles of all mono-sizes per incremental time T in segment j is

$$ML^j = \sum_{r=o}^{\mu-1} m^j_{r.t+T^j} \gamma^j_{r.1}/w^j \quad \text{(A6.44)}$$

The fines burnt F_b^j is the sum of the fraction ϕ_1 of the abrasion fines (equation A6.39) that burns, together with the fraction ϕ_2 that burns of the fines of size x_c (equation A6.40) generated within segment j.

$$F_b^j = \phi_1 \sum_{r=0}^{\mu-1} m^j_{r.t+T^j} \gamma^j_{r.2}/w^j + \phi_2 \sum_{r=0}^{\mu-1} (1 - \gamma^j_{\mu-1}) m^j_{\mu-1.t+T^j}/w^j \quad \text{(A6.45)}$$

The elutriated fines E_f^j is the sum of the remaining fraction $(1 - \phi_r)$ of the abrasion fines (equation A6.39) and the remaining fraction $(1 - \phi_2)$ of the fines of size x_c (equation A6.40) generated in segment j.

$$E_f^j = (1 - \phi_1) \sum_{r=0}^{\mu-1} m^j_{r.t+T^j} \gamma^j_{r.2}/w^j + (1 - \phi_2) \sum_{r=0}^{\mu-1} (1 - \gamma^j_{\mu-1}) m^j_{\mu-1.t+T^j}/w^j \quad \text{(A6.46)}$$

In making solutions of the fines elutriated from the various segments, the constituent terms of equations A6.42, A6.43, A6.45 and A6.46 are evaluated separately so that the fines elutriated into the freeboard from all the segments of the coal feed cell may be assembled in their separate categories of feed fines, abrasion fines and fines of size x_c.

APPENDIX 7

NOMENCLATURE

Symbol	Listing A10.1	Description
a_b	BY	Fluidizing air by-passing the cell (fraction of air throughput/unit time T)
$a_b + a_e$		Air leaving the surface of the cell (fraction of air throughput/unit time T)
a_s	AO	Air leaving the freeboard (fraction of air throughput/unit time T)
a_x	AX	Excess air (fraction of air throughput/unit time T)
E_f	EF	Feed fines elutriated (fraction of cell throughput/unit time T)
E_a		Abrasion fines elutriated (fraction of cell throughput/unit time T)
E_o	EO	Elutriated fines loss in stack (fraction of cell throughput/unit time T)
E_{xc}	CFE	Elutriated fines of size x_c (fraction of cell throughput/unit time T)
E_1	FRBC1	Combustion in freeboard of elutriation size x_c to airborne size x_e (fraction of cell throughput/unit time T)
E_2	FRBC2	Combustion in freeboard of all airborne sizes below x_e (fraction of cell throughput/unit time T)
j	j	Segment number
s	s	Periphery segment number
ϕ_o	COMB(0)	Fraction of feed fines burning within the bed (in time T)
ϕ_1	COMB(1)	Fraction of abrasion fines burning within the bed (in time T)
ϕ_2	COMB(2)	Fraction of fines of size x_c burning within the bed (in time T)
ϕ_3	COMB(3)	Fraction of fines of airborne size x x_e burning in freeboard (in time T)

A P P E N D I X 7

STEADY-STATE AIR/CARBON COMBUSTION BALANCES IN THE CELL AND IN THE FREEBOARD

The quantities of air uptake and fines that burn are expressed as fractions of the cell throughput. All rates are with respect to the incremental time T.

A combustion balance between the coal and air combustion occurring within a coal feed cell may be written as:

$$1 - a_b - a_e = 1 - E_f - E^1_{xc} - 2\sum_{j=2}^{s} E^j_{xc} - E^1_a - 2\sum_{j=2}^{s} E^j_a \qquad (A7.1)$$

in which the air is expressed on the left and carbon on the right, and the terms are:

a_b	-	By-pass air of the cell
$a_b + a_e$	-	Fraction of air throughput required to burn all the fines elutriated from the surface of the bed
E_f	-	Feed fines
$E^1_{xc} + 2\sum_{j=2}^{s} E^j_{xc}$	-	Fines of size x_c elutriated from entire cell
$E^1_a + 2\sum_{j=2}^{s} E^j_a$	-	Abrasion fines elutriated from entire cell

If the excess air a_x is fed into the freeboard to increase the combustion there, the air in the freeboard is

$$a_b + a_e + a_x \qquad (A7.2)$$

Now all the fines $E^1_{xc} + 2\sum_{j=2}^{s} E^j_{xc}$ of size x_c elutriated from the surface must remain in the proximity of the surface in the freeboard until reduced to elutriation size x_e resulting in a combustion E, of

$$E_1 = (E^1_{xc} + 2\sum_{j=2}^{s} E^j_{xc}) \left[1 - (x_e/x_c)^3\right] \qquad (A7.3)$$

Of the remaining fines a fraction ϕ_3 is assumed to burn in the freeboard to give an additional freeboard combustion E_2 of

$$E_2 = (E_f + E^1_{xe} + 2\sum_{j=2}^{s} E^j_{xe} + E^1_a + 2\sum_{j=2}^{s} E^j_a)\phi_3 \qquad (A7.4)$$

Hence, the elutriation loss E_o from the freeboard is the fraction of these airborne fines that do not burn

$$E_o = (E_f + E^1_{xe} + 2\sum_{j=2}^{s} E^j_{xe} + E^1_a + 2\sum_{j=2}^{s} E^j_a)(1 - \phi_3) \qquad (A7.5)$$

Equations A7.3 to A7.5 give the carbon part in a combustion balance with air of $a_b + a_e$. Here

$$a_b + a_e - a_s = E_1 + E_2 \qquad (A7.6)$$

where a_s is the unburnt air in the stack.

The air/carbon balance of the unburnt carbon and air is

$$a_s = E_o \qquad (A7.7)$$

The air in the stack is thus

$$a_s + a_x \qquad (A7.8)$$

A P P E N D I X 8

NOMENCLATURE

Symbol	Listing All.1	Description
C^j	A	Background carbin in segment j (cell throughput pre-transient/unit time T)
C_r^j	A(J)/NOL	Carbon in layer r of segment j (cell throughput post-transient/unit time T)
$C_r^{j,}$		Carbon in layer r of segment j (cell throughput pre-transient/unit time T)
e^j	E	Efficiency of utilization of instantaneous excess air during the transient $o < e^j < 1$.
K_1	K1	Ratio of step increase of coal (post-/pre-transient throughput)
K_2	K2	Ratio of step increase of air (post-/pre-transient throughput)
ML^j	SCOMB	Combustion mass loss of carbon in segment j (pre-transient throughput/unit time T)
ML^j_t	COMB(J)	Combustion mass loss of carbon in segment j during the transient (post-transient throughput/unit time T)
n	NOL	Number of layers in segment for solids flow
S^j	S(J)	Surface area of all carbon particles in segment j

A P P E N D I X 8

TRANSIENT MASS LOSS OF CARBON FROM A SEGMENT

(All mass losses are rates expressed as fractions of throughput per unit of incremental time T)

A step increase in coal and fluidising air rates to a coal feed cell results in imbalances between the rates of coal and air feeds to segments during the transient. The increase in air is effective immediately, while the new level of coal flow can only be established after the build-up of a new background carbon gradient from segment to segment. Indeed, the step increase in air initially depletes the background carbon in the periphery segments. Now, the efficiency of utilization of air decreases with excess air. This effect is taken into account by a parameter e of value $o < e < 1$ which governs the efficiency of utilization of the instantaneous excess air during the transient. The significance of varying e is included in the study.

Prior to the step increase in coal and air the cell is operating at pre-transient stoichiometric throughput, while in the steady-state after the step increase the cell is again operating at a post-transient stoichiometric throughput. During the transition the segments of the cell are operated at varying conditions of imbalance between coal and air throughput to the segments. The transition from the pre- to post-transient conditions is effected by the following steps in this model.

a) Define the step increase or decrease as a ratio of the

post-transient to pre-transient coal and air throughput as

K_1 = post-/pre-transient throughput of coal, and

K_2 = post-/pre-transient throughput of air

b. Convert the background carbon in layer r of segment j from $C_r'^j$ expressed in pre-transient units of throughput to C_r^j expressed in post-transient throughput by dividing by K_1.

$$C_r^j = C_r'^j/K_1 \qquad (A8.01)$$

c. Finally, the combustion mass loss in segment j during the transient may be determined as follows:

Prior to the step change the combustion mass loss ML^j of carbon in segment j from equation A6.44 may be expressed as the product of the background carbon in the combustion layer and a mean reduction factor $\bar{\gamma}^j$

$$ML^j = \bar{\gamma}^j \ (C^j/n) \qquad (A8.02)$$

whence

$$\gamma^{-j} = ML^j/(C^j/n) \qquad (A8.03)$$

Provided the transient does not introduce large relative changes in background carbon in the segments, this value $\bar{\gamma}^j$ of mean reduction factor may be assumed to apply over the entire transient.

The combustion mass loss in the final steady-state is ML^j expressed in post-transient units of throughput.

$$ML^j \ K_2/K_1 \qquad (A8.04)$$

Both before and after the transient the mean reduction factor

$\bar{\gamma}^j$ gives rise to mass losses which are in combustion balance with the fluidising air. During the transient, as the background carbon builds up, it provides an instantaneous mass loss which increases in value from that before to that at the end of the transient, and is given by

$$C_1^j \ \bar{\gamma}^j \qquad \text{(A8.05)}$$

Now this instantaneous mass loss of carbon is in combustion balance with only part of the fluidising air in segment j. The remainder of the air may be said to be in instantaneous excess. As the transient progresses the instantaneous combustion increases with increase in background carbon, while the instantaneous excess air decreases.

The difference between the instantaneous mass loss of carbon of expression A8.05 and the mass loss in the final steady-state of expression A8.04 represents a potential of combustion in balance with the instantaneous excess air during the transient. Since the efficiency of utilization of the instantaneous excess air during the transient is a fraction e^j of value $o < e^j < 1$, the actual mass loss in combustion balance with the instantaneous excess air may be expressed as

$$e^j(ML^j \ K_2/K_1 - C_1^j \ \bar{\gamma}^j) \qquad \text{(A8.06)}$$

Since combustion is assumed to occur at the surface of carbon particles, and since e is a function of part of the air uptake for combustion, the parameter e^j is directly proportional to S^j the surface area of all the carbon particles in segment j.

Hence

$$e^j/S^j = \text{constant} \qquad \text{(A8.07)}$$

Equation A8.07 may be used to relate the values of e^j for the successive segments of the cell.

The sum of expression A8.05 and A8.06 defines the combustion loss ML_t^j during the transient from layer 1 of segment j as

$$ML_t^j = C_1^j \bar{\gamma}^j + e^j (ML^j K_2/K_1 - C_1^j \bar{\gamma}^j) \qquad \text{(A8.08)}$$

In the event that the step change sets the air throughput $K_2 < K_1$ the coal throughput, equation A8.08 reduces to

$$ML_t^j = ML^j K_2/K_1 \qquad \text{(A8.09)}$$

since the combustion is limited by the air supply.

During the transient the fines burnt are assumed to increase in direct proportion to the ratio of the mass loss ML_t^j during the transient, to the mass loss ML^j of equation A6.44 prior to the transient. The proportionality factor is thus

$$ML_t^j/ML^j \qquad \text{(A8.10)}$$

APPENDIX 9

NOMENCLATURE

Symbol	Listing A10.1	Description
$a_b + a_e$		Air leaving the surface of the cell (fraction of air throughput/unit time T)
B	B	Lateral solids flow parameter $0 < B < 0.5$ (fraction of surface layer exchanged between adjacent segments/unit time T)
$C^{'j}$	C (J)	Background carbon in segment j (cell throughput/unit time T)
C^s	C(NOS)	Background carbon in segment s (cell throughput/unit time T)
M_r		Mass of mono-size x_r in a segment (cell throughput/unit time T)
M_r^j		Mass of mono-size x_r in segment j (cell throughput/unit time T)
m_r^f		Mass of mono-size x_r in coal feed (fraction of cell throughput/unit time T)
m_r^j		Mass of mono-size x_r in mass-size distribution in segment j (fraction of cell throughput/unit time T)
N	N	Number of segments in coal feed cell
n	NOL	Number of layers for solids flow in a segment
T_c	TC1	Mean particle combustion time (seconds)
T^1		Incremental time (segment 1) to effect a carbon particle size reduction Δx.
T^2		Incremental time (segment 2) to effect a carbon particle size reduction Δx.
x_r		Size of rth mono-size of carbon particles

A P P E N D I X 9

INITIAL VALUES OF COMBUSTION INERTIA AND MASS-SIZE DISTRIBUTION IN SEGMENTS

In order to ensure rapid iterative convergence during computation, initial values are deduced for both the background carbon content as well as the mass size distribution of carbon particles in the segments.

(a) Initial Background Carbon Content in Segments

A cell operated at stoichiometric conditions of feed may be said to have unity coal and air throughput. An initial value of the background carbon content in the periphery segment of a cell operated at these conditions may be estimated by considering the rate of removal of carbon by combustion, the rate of mixing within the segment, and the average time of combustion of carbon particles.

The rate of removal of carbon by combustion from a segment may approximately be equated to the rate of supply of air to each segment. A coal feed cell composed of N segments has an air throughput of 1/N per segment. Thus the rate of removal of carbon is approximately 1/N of the throughput.

A segment composed of n layers may be considered to mix vertically so as to expose a fresh layer of carbon to combustion each second. If the mean combustion time of carbon particles is one second, the background carbon content in seconds is n/N.

For a mean particle combustion time of T_c seconds the background carbon content C^s in segment s reduces to

$$C^s = T_c \, n/N \qquad (A9.01)$$

Equation A9.01 may be refined somewhat by considering elutriation. Although the coal and air feed rates balance under stoichiometric conditions, a considerable fraction of the coal feed is lost from the bed as elutriated fines. In the steady-state a fraction of air throughput equivalent to these elutriated fines must pass through the bed without burning. Thus, instead of an air throughput of 1/N being available for combustion of carbon in a coal feed cell as in equation A9.01, the quantity is

$$(1 - a_b - a_e)/N \qquad \text{(A9.02)}$$

where $a_b + a_e$ is the fraction of air throughput required to burn all the fines elutriated from the bed as in equation A7.01.

Having estimated the background carbon content C in the segment on the periphery of the coal feed cell, that in the other segments of the cell may be deduced from lateral flow considerations since the difference in background carbon between successive segments gives rise to the lateral flow between segments. Thus

$$(C^j - C^{j+1})B/n = z(1 - a_b - a_e)/N \qquad \text{(A9.03)}$$

where z is defined below.

Here the lateral exchange between segments is a fraction B of the difference between the background carbon C^j/n and C^{j+1}/n in the surface layers of adjacent segments. Where the net lateral flow is into the periphery segment, this difference must be sufficient to supply the combustion in that segment as given by expression A9.02. Here z takes on the value unity.

Proceeding towards the centre of the coal feed cell the lateral flow must supply the combustion requirements of all segments towards the periphery and

$$z = 1, 2, 3, 4 \ldots \quad \text{for N = odd}$$

$$\text{or} \quad z = .5, 1.5, 2.5 \ldots \quad \text{for N = even}$$

Figure 5.1 shows the proximity of this estimate of the initial value of the background carbon content to the final values for N = 6 and 7.

(b) Initial Mass-Size Distribution of Carbon Particles in Segments of a Cell

The mass of each mono-size in the successive segments of a cell is generated commencing with the coal feed segment, since the coal feed size distribution is known. The mass-size distribution for each segment is obtained by expressing the mass of each mono-size as a proportion of the total mass of all mono-sizes in the segment in question.

In the coal feed segment (segment 1) all carbon particles undergo a mono-size reduction due to abrasion over consecutive increments of time T^1 which is a function of the rate of particle size reduction in that segment. Of the largest size x_o the coal feed cell can only contain a mass which is fed during the incremental time T^1. For the next size x_1 the mass is the sum of that of size x_1 from the feed during the present time T^1, together with the now reduced mass of particles originally of size x_o from the feed of the previous time T^1 and now reduced to size x_1.

For any general size x_r the mass M_r of the mono-size x_r during the incremental time T^1 may be expressed as the sum of the mass of the mono-size x_{r-1} during the previous incremental time T^1 and now reduced by $(1 - \gamma_r)$ because of combustion and abrasion, together with the mass m_r^f of the mono-size x_r in the feed during the present time T^1.

$$M_r = M_{r-1}(1 - \gamma_r) + m_r^f \qquad \text{(A9.04)}$$

Using equation A9.04 the mass M_r of each mono-size is built up for the entire size range of particles within the coal feed segment.

This mass M_r is used as the feed m_r^f to generate the mass of particles of each mono-size in the next segment (segment 2), in which carbon particles undergo a reduction in size over consecutive increments of time T^2, and so on through the successive segments of the cell.

The particle mass-size distribution m_r^j in segment j is deduced from the mass M_r^j of particles of each mono-size as generated above. This is accomplished by expressing the mass M_r^j of each mono-size as a proportion of the total mass of all mono-sizes.

$$m_r^j = M_r^j \Big/ \sum_{r=1}^{\mu-1} M_r^j \qquad \text{(A9.05)}$$

Finally, the mass-size distribution m_r^j may be used to deduce the combustion inertia of the carbon particles in each mono-size as

$$m_r^j C^j \qquad \text{(A9.06)}$$

where C^j is the combustion inertia of the background carbon in segment j.

Figure 5.2 shows the proximity of this estimate of the initial mass to the final mass of the background carbon in each mono-size for a coal feed cell of seven segments.

A P P E N D I X 1 0

THE STEADY-STATE MODE PROGRAM DETAILS

In this Appendix are assembled the following details in connection with the computer program of the steady-state mode of the model.

Listing A10.1	The Program FLUMX
Figure A10.1	The Flow Chart of FLUMX
Table A10.1	A Typical Printout from FLUMX
Table A10.2	The Data Format for FLUMX
Table A10.3	The Mass-Size Distribution/Segment

LISTING A10.1 FLUMX-PROGRAM OF STEADY-STATE MODEL

```
        DCL TME CHAR(6);
        TME=TIME;
        TCONV:PROC;
        H=FLOAT(SUBSTR(TME,1,2));
        MINIT=FLOAT(SUBSTR(TME,3,2));
        SEC=FLOAT(SUBSTR(TME,5,2));
        RETURN(60*H+MINIT+SEC/60);
        END TCONV;
        T1=TCONV;
        DCL(COUNT,TIM,R,LOOP)BINARY FIXED,(KA1,KC0,KC1,LCM)DEC FLOAT
        DCL(COMB,ETA,TT,TC)(0:3) DEC FLOAT;
        DCL(C,S,FB,W,KC,SUMDIS,CFE,SCOMB,FE,DUMP3)(4)DEC FLOAT;
        DCL PR(35)INITIAL(2,3,5,7,11,13,17,19,23,29,31,37,41,43,47,5
            59,61,67,71,73,79,83,89,97,101,103,107,109,113,127,131,1
            139,149);
        DCL (Q1,Q2,Q3)(4,2),(GAMMA1,GAMMA2)(0:550,4);
        DCL (N(0:550,0:4),DIST(0:550,0:4)) DEC FLOAT;
        DCL DDT CHAR(8);
        DCL DTE CHAR(6); DTE=DATE;
        DCL DON FILE PRINT;
        DDT=SUBSTR(DTE,5,2)||'/'||SUBSTR(DTE,3,2)||'/'||SUBSTR(DTE,1,
        2);
        GET LIST(KA1,AX,B,BY,NOL,KC1,T,TC1,V,PA,PB)SKIP;
        GET LIST(XC,XE,X0,ETA,TC,TT) SKIP;
REP:    GET DATA(ZZ)SKIP;  IF ZZ<0 THEN STOP;
        V=ZZ;
        DX=(KA1+KC1)*T;
        MU=TRUNC((X0-XC)/DX+.5);
        TYME=TIME;
        XC=X0-MU*DX;
        PUT SKIP(2);
        PUT DATA(DDT,TYME)SKIP;
        PUT DATA (PA,PB,XE,XC,X0) SKIP;
        PUT DATA(NOL,AX,BY,V,MU) SKIP;
        PUT DATA(KA1,KC1,TC1,B,DX) SKIP;
L2:     DO I=0 TO 3/*0- FEED FINES IN BED, 1- ABRASION FINES IN BED*/
        /* 2- FINES SIZE XC IN BED */;
        COMB(I)=(1+AX*(I=3))*ETA(I)*TT(I)/TC(I);
        /* 3- FINES IN FREEBOARD */;
        END L2;
        PUT DATA(COMB,T) SKIP;
        FB,FE,C=0;
        FF=T*(1-.01*V)*XC**PB/X0**PB;
        COUNT=-1;
CHECK,LOOP=0;
L4:     DO R=0 TO MU-1/*  CALCS NON-VOL FEED*/;
```

LISTING A10.1 (CONT.) FLUMX

```
      M(R,0)=T*(1-.01*V)*((X0-R*DX)**PB-(X0-(R+1)*DX)**PB)/X0**PB;
      END L4;
      LCM=1;
ONE:  FFB=FF*COMB(0);
      IF COUNT<0 THEN FB(1)=FFB;
      TN=1/(.01*V+FB(1)/T)/* NUMBER OF SEGMENTS*/;
      N=TRUNC(TN+.5);
      IF N< 5 THEN N=1;
      SEGAIR=(1-BY)/N;
      DUMP=SEGAIR-.01*V;
      DUMP=DUMP*(DUMP>0);
      IF (FFB/T)>DUMP THEN FFB=T*DUMP;
      FB(1)=FFB;
      FFE=FF-FFB;
      PFF=FF/T;
      PFFB=FFB/T;
      PFFE=FFE/T;
      IF COUNT=0 THEN PUT DATA(PFF,PFFB,PFFE,TN) SKIP;
      NOS=TRUNC((N+1)*.5+.5);
      IF COUNT>=0 THEN GO TO L8;
      C(NOS)=TC1*NCL*(SEGAIR-FFE/(T*N))/*INITIAL CONCENTRATIONS*/;
      IF MOD(N,10B)=0 THEN Z=-.5;ELSE Z=0;
L6:   DO J=NOS-1 TO 1 BY -1;
      Z=Z+1;
      C(J)=Z*NOL*(SEGAIR-FFE/(T*N))/B+C(J+1);
      END L6;
      PUT SKIP;
      PUT DATA (C) SKIP;
      S=0;
      IF COUNT>=0 THEN GO TO L8;
J3:   LOOP=LOOP+1;
      DIST=0;
      SUMDIS=0;
L8:   DO J=1 TO NOS;
      IF COUNT>=0 THEN GO TO L16;
      IF J>1 THEN GO TO J4; ELSE DO;
L10:  DO R= 0 TO MU-1;
      DIST(R,0)=M(R,0);
      END L10;
      KC(1)=0;
      KC(2),KC(3),KC(4),KC(5)=KC1;
      END;
J4:   IF LOOP>1 THEN GO TO J10;
      W(NOS)=1/*INITIAL REL. COMB. TIMES*/;
      W(1)=(KA1+KC1)/KA1;
      IF NOS<4 THEN GO TO J6;
      W(3)=2;
```

LISTING A10.1 (CONT.) FLUMX

```
          W(2)=3;
          GO TO J8;
J6:       IF NOS<3 THEN GO TO J8;
          W(2)=2;
J8:       Q1(J,1)=3*KC(J)*T;
          Q1(J,2)=3*KA1*T;
          Q2(J,1)=3*KC(J)*KC(J)*T*T*(KC(J)+3*KA1)/(KC(J)+KA1);
          Q2(J,2)=3*KA1*KA1*T*T*(KA1+3*KC(J))/(KA1+KC(J));
          Q3(J,1)=(KC(J)+3*KA1)*KC(J)*KC(J)*T*T*T;
          Q3(J,2)=(KA1+3*KC(J))*KA1*KA1*T*T*T;
L12:      DO R=0 TO MU-1;
          Z1=X0-R*DX;
          GAMMA1(R,J)=(Q1(J,1)*Z1*Z1-Q2(J,1)*Z1+Q3(J,1))/(Z1*Z1*Z1);
          /* SIZE REDUCTION FACTOR FOR COMBUSTION */;
          GAMMA2(R,J)=(Q1(J,2)*Z1*Z1-Q2(J,2)*Z1+Q3(J,2))/(Z1*Z1*Z1);
          /* SIZE REDUCTION FACTOR FOR ABRASION */;
          END L12;
J10:      DIST(0,J)=M(J)*DIST(0,J-1)/*INITIAL SIZE DISTRIBUTIONS*/;
L14:      DO R=1 TO MU-1;
          DIST(R,J)=DIST(R-1,J)*(1-GAMMA1(R,J)-GAMMA2(R,J))
          +W(J)*DIST(R,J-1);
          SUMDIS(J)=SUMDIS(J)+DIST(R,J);
          END L14;
L16:      DO R=0 TO MU-1;
          IF COUNT >=0 THEN GO TO J12;
          M(R,J)=DIST(R,J)/SUMDIS(J)*C(J)/*RELATE SIZE DIST. TO CONC.
J12:        S(J)=S(J)+M(R,J)/(X0-R*DX);
          END L8;
          IF LOOP>1 THEN GO TO J14;
          PUT DATA(W) SKIP;
          PUT FILE(DON) EDIT('MU','SIZE','SIZE DISTRIBUTION / SEGMENT',
            (J DO J=1 TO NOS))(PAGE,X(4),A(2),X(4),A(4),X(34),A(27),
            SKIP,X(10),(NOS) (X(15),F(1,0)));
          DO I=1 TO MU-1;
          PUT FILE(DON) EDIT(I,X0-I*DX,(M(I,J) DO J=1 TO NOS))(SKIP,
            (2) (F(7,0)),X(2),(NOS) (E(16,4)));
          END;
J14:      DUMP1=0;
L18:      DO J=2 TO NOS;
          IF (J=NOS)&(MOD(N,2)<>1) THEN Z=1; ELSE Z=2;
          DUMP1=DUMP1+Z*(S(1)-S(J));
          END;
          IF MOD(N,2)=0 THEN Z=2;ELSE Z=1;
          DUMP2=T*SEGAIR-Z*(FB(NOS)+FE(NOS))-FFE/((N-1)*Z);
          IF DUMP2<=0 THEN DO;
          TC1=TC1/3;
          COUNT=-1;
```

LISTING A10.1 (CONT.) FLUMX

```
        LCM=1;
        CHECK=CHECK+1;
        FB,FE,C=0;
        IF CHECK>2 THEN STOP;
        GO TO ONE;END;
L20:    DO J=1 TO NOS/*UPDATE REL. COMB. TIMES*/;
        IF (J=NOS)&(MOD(N,2))<.1 THEN Z=2;ELSE Z=1;
        DELTAJ=(S(1)-S(J))/DJMP1;
        DUMP3(J)=T*SEGAIR-(FB(J)+FE(J))*Z-FFE/((N-1)*Z)
        *(J-=1)-(.01*V*(J=1));
        IF DUMP3(J)<=0 THEN GO TO J16;
        W(J)=DUMP2*S(J)/(DUMP3(J)*S(NOS));
J16:     W(J)=(KA1+KC1)/(KA1+KC(J)/W(J));
        W(J)=TRUNC(W(J)+.5);
        IF W(J)<.5 THEN W(J)=1;
        END L20;
        IF LOOP <= 2 THEN GO TO J3;
        IF COUNT=0 THEN PUT DATA (DUMP3) SKIP;
        IF COUNT=0 THEN PUT DATA (W) SKIP;
        T2=TCONV;
        IF (T2-T1) > 5 THEN STOP;
        IF NOS<3 THEN LCM=W(1);
        ELSE DO/*L.C.M. OF REL. COMB. TIMES*/;
        LCM=1;
L22:    DO I=1 TO NOS-1;
        LCM=LCM*W(I);
        END L22;
        ZM=W(1);
L24:    DO I=2 TO NOS-1;
        ZM=MAX(ZM,W(I));
        END L24;
 KP:    PROC(P,Q);
        IF P/Q=TRUNC(P/Q) THEN RETURN(1B);ELSE RETURN(0B);
        END KP;
        I=1;
 J18:    IF PR(I)>=ZM THEN GO TO J24;
        IF KP(LCM,PR(I))=1 THEN GO TO J20;
        I=I+1;
        GO TO J18;
 J20:    LCM=LCM/PR(I);
L26:    DO J=1 TO NOS-1;
        IF KP(LCM,W(J))=0 THEN GO TO J22;
        END L26;
        GO TO J18;
 J22:    LCM=LCM*PR(I);
        I=I+1;
        GO TO J18;
```

LISTING A10.1 (CONT.) FLUMX

```
        END;
 J24:   TIM=0;
        Z4=(MOD(TIM,2)=0);
 MIX:   FE,CFE,SCOMB,FB=0;
        COUNT=COUNT+1;
 L28:   DO NUM=1 TO LCM;
        FE(I)=FE(I)+FFE;
        SCOMB(I)=SCOMB(I)+.01*V*T;
        FB(I)=FB(I)+FFB;
        TIM=TIM+1;
 L30:   DO R=0 TO MU-1/*  LATERAL MIXIMG ALGOPITHM  */;
        Z1=M(R,2);
 L32:   DO J=1 TO NOS;
        IF J=1 THEN M(R,1)=M(R,1)+M(R,0)/*FEED*/;
        Z2=M(R,J);
        IF J¬=NOS THEN DO;
        M(R,J)=M(R,J)+B*T/NOL*(Z1-2*Z2+M(R,J+1));
        GO TO J25;
        END;
        M(R,J)=M(R,J)+T*B/NOL*(Z1-2*Z2+Z1*Z4+Z2*(Z4<.5));
 J25:   Z1=Z2;
        END L30;
 L34:   DO J=1 TO NOS;
        Z3=(J¬=NOS)+(J=NOS)*(1-Z4*.5);
        IF(MOD(NUM,W(J)))>.001 THEN GO TO J26;
        CFE(J)=CFE(J)+M(MU,J)*(1-COMB(2))*Z3/*FINES*/;
        FB(J)=FB(J)+M(MU,J)*COMB(2)*Z3;
        M(MU,J)=0;
 L36:   DO K=0 TO MU-1;
        FE(J)=FE(J)+M(K,J)*(1-COMB(1))*GAMMA2(K,J)*Z3/*FINES*/;
        FB(J)=FB(J)+M(K,J)*COMB(1)*GAMMA2(K,J)*Z3;
        SCOMB(J)=SCOMB(J)+M(K,J)*GAMMA1(K,J)*Z3/*COMBUSTION*/;
        M(K,J)=M(K,J)*(1-GAMMA1(K,J)-GAMMA2(K,J));
        END L36;
 L38:   DO K=MU TO 0 BY -1;
        M(K,J)=M(K-1,J)/*UPDATE SIZE*/;
        END L38;
        M(0,J)=0;
 J26:   END L34;
        END L28;
        C=0;
 L40:   DO J=1 TO NOS;
 L42:   DO R=0 TO MU-1;
        C(J)=C(J)+M(R,J)/*UPDATE CONCENTRATION*/;
        END L42;
        END L40;
        CFE=CFE/(LCM*T);
```

LISTING A10.1 (CONT.) FLUMX

```
      FE=FE/(LCM*T);
      SCOMB=SCOMB/(LCM*T);
      FB=FB/(LCM*T);
      PUT SKIP;
      PUT DATA(CFE) SKIP;
      PUT DATA (FE) SKIP;
      PUT DATA(SCOMB) SKIP;
      PUT DATA(FB) SKIP;
      CFE=CFE*T;
        SCOMB=SCOMB*T;
      FE=FE*T;
      FB=FB*T;
      PUT SKIP;
      PUT DATA(C) SKIP;
      IF COUNT=0 THEN GO TO ONE;
      IF (TIM/LCM<110B)|(COUNT<10B) THEN GO TO MIX;
      TCFE=CFE(1);
      TFE=FE(1);
      TSCOMB=SCOMB(1);
      TFB=FB(1);
      Z3=2;
L44:  DO J=2 TO NOS;
      TCFE=TCFE+CFE(J)*Z3;
      TFE=TFE+FE(J)*Z3;
      TSCOMB=TSCOMB+SCOMB(J)*Z3;
      TFB=TFB+FB(J)*Z3;
      END L44;
      TFE=TFE/T;
     TCFE=TCFE/T;
      TSCOMB=TSCOMB/T;
      TFB=TFB/T;
      FRBC1=TCFE*(1-(XE/XC)**3)/*COARSE FINES BURNING IN FREEBOARD
      FRBFE=TCFE-FRBC1;
      FRBC2=(FRBFE+TFE)*COMB(3)/* FINE FINES BURNING IN FREEBOARD
      FRBFE=FRBFE+TFE-FRBC2/* FREEBOARD FINES ELUTRIATED */;
      TOTALC=(TSCOMB+TFB+FRBC1+FRBC2);
      AO=1+AX-TOTALC;
      PUT DATA(LCM,COUNT,TIM) SKIP;
      PUT EDIT('SUM OF COMBUSTION IN BED',TSCOMB+TFB,
       'UNBURNT AIR IN STACK',AO)(R(M2));
      PUT EDIT('COARSE FINES BJRNING IN FREEBOARD',FRBC1,
      'FINE FINES BURNING IN FREEBOARD',FRBC2)(R(M2));
      PUT EDIT('FREEBOARD FINES ELUTRIATED',FRBFE)(R(M2));
      PUT EDIT('TOTAL COMBUSTION ',TOTALC,'AVERAGE CARBON LOST',
      TOTALC+FRBFE)(R(M2));
      PUT SKIP(4);
      PUT DATA(S);
```

LISTING A10.1 (CONT.) FLUMX

```
      PUT FILE(DON) EDIT('MU','SIZE','SIZE DISTRIBUTION / SEGMENT'
        (J DO J=1 TO NOS))(PAGE,X(4),A(2),X(4),A(4),X(34),A(27),
        SKIP,X(10),(NOS) (X(15),F(1,0)));
      DO I=1 TO MU-1;
      PUT FILE(DON) EDIT(I,XO-I*DX,(M(I,J) DO J=1 TO NOS))(SKIP,
        (2) (F(7,0)),X(2),(NOS) (E(16,4)));
      END;
      GO TO REP;
M2:   FORMAT(SKIP,X(6),2 (A(36),F(10,5),X(5)));
      END FLUMX4;
```

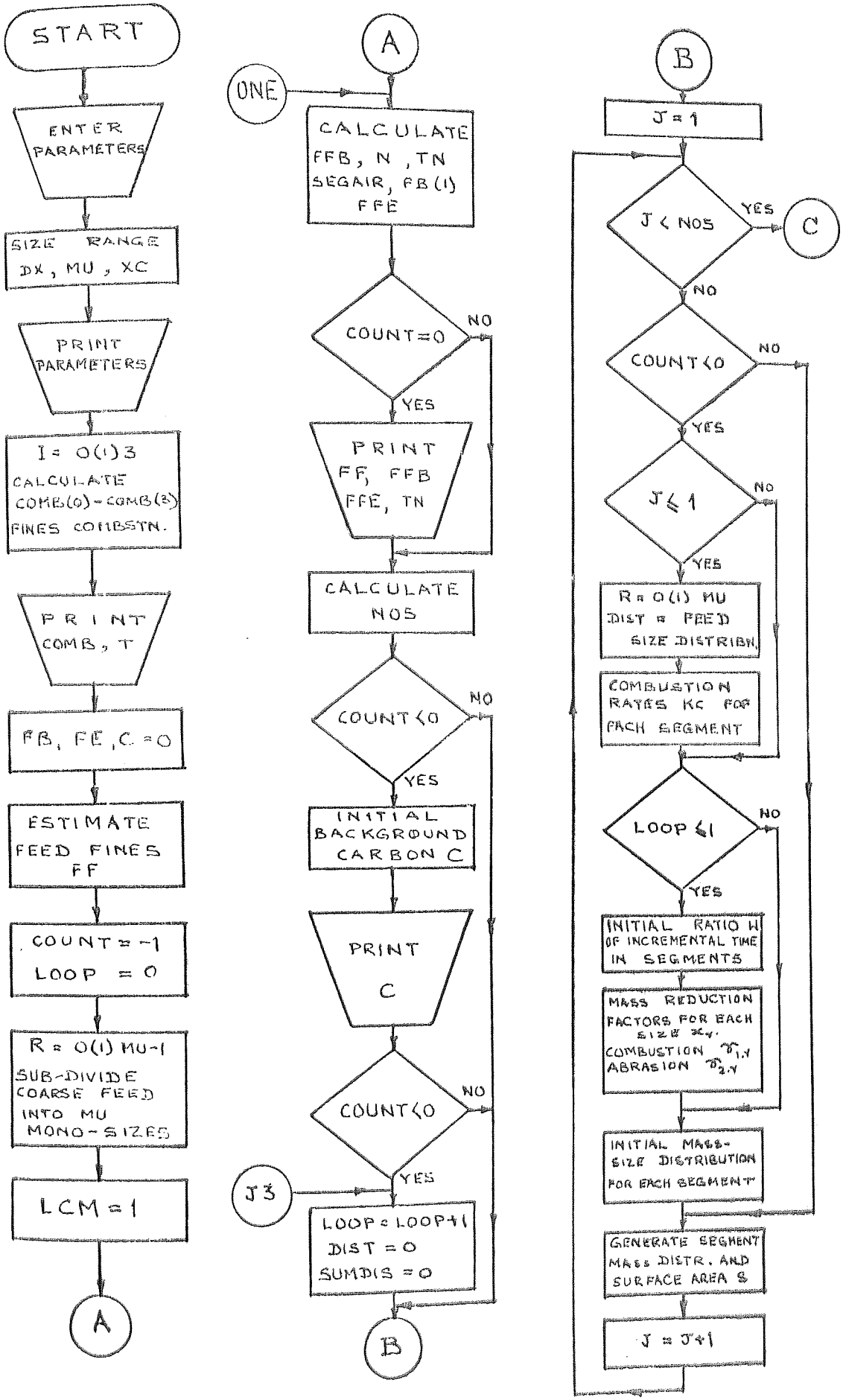

FIG. A10.1 FLOWCHART OF STEADY-STATE MODE — FLUMX

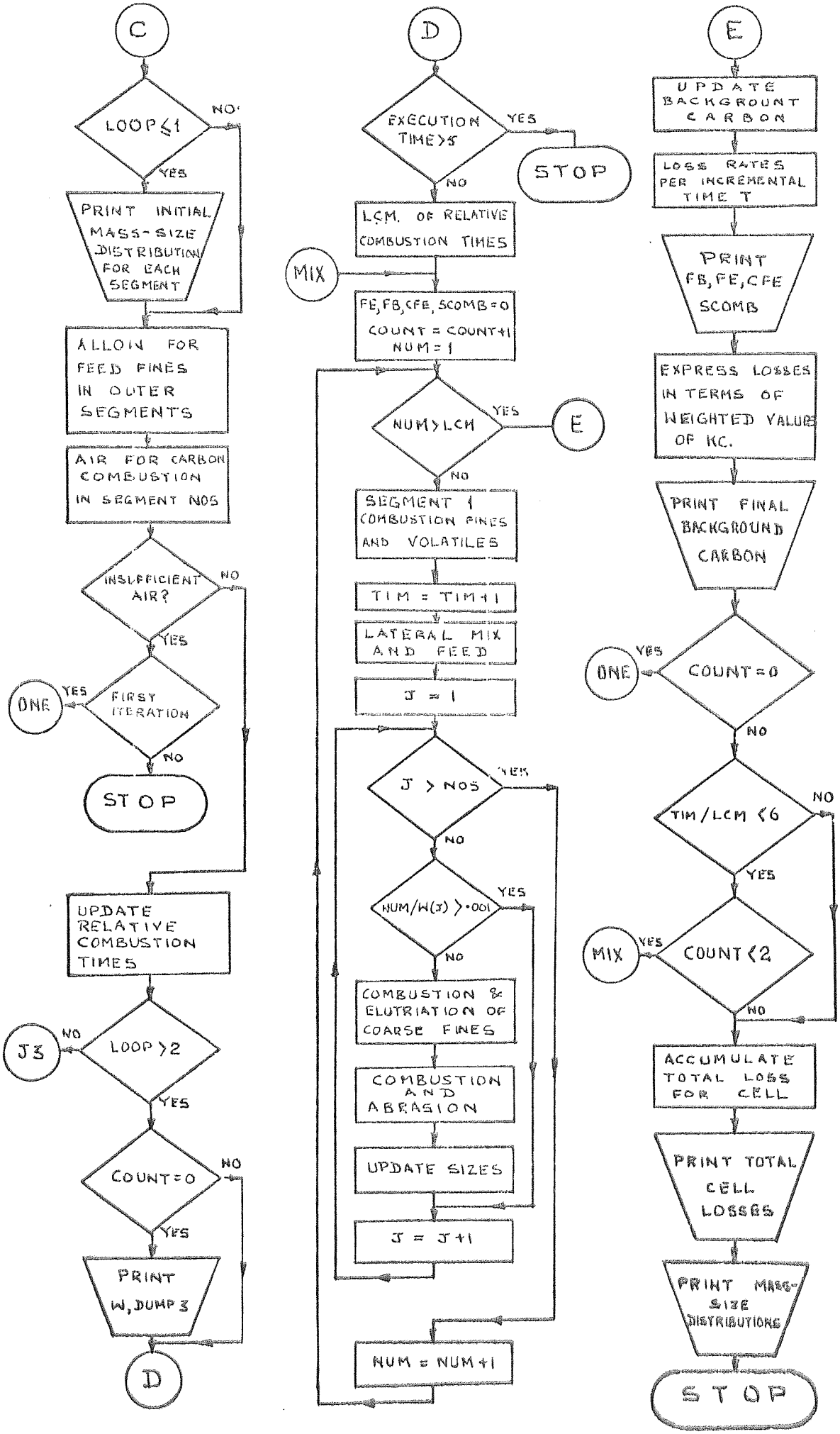

FIG. A10.1 (CONTD.) FLOWCHART OF STEADY-STATE MODE — FLUMX

TABLE A10.1 TYPICAL PRINTOUT FROM FLUMX FOR THE STEADY-STATE MODE (N = 7)

```
DT='03/11/71'          TYME= 1.32214E+08;
A= 1.19999E-02         PB= 5.99699E-01        XE= 1.00000E+02        XC= 1.25000E+02        XO= 1.40000E+03;
DL=        10          AX= 1.99999E-01        BY= 9.99999E-05        V= 1.10000E+01         MU=        59;
CA1= 9.99999E-02       KC1= 1.69999E+00       TC1= 1.00000E+01       G= 9.99999E-02         DX= 2.15999E+01
DMS(0)= 1.99999E-01    COMB(1)= 1.99999E-01   COMB(2)= 1.99999E-01   COMB(3)= 3.35999E-01   T= 1.20000E+01;

C(1)= 3.11813E+01      C(2)= 4.63803E+01      C(3)= 2.31946E+01      C(4)= 1.15973E+01;
U(1)= 1.79999E+01      U(2)= 3.00000E+00      U(3)= 2.00000E+00      U(4)= 1.00000E+00;

CFE(1)= 0.00000E+00    CFE(2)= 1.17182E-02    CFE(3)= 6.34552E-03    CFE(4)= 4.57045E-03;
FE(1)= 1.80106E-01     FE(2)= 8.15784E-03     FE(3)= 5.87414E-03     FE(4)= 5.66167E-03;
SCOMB(1)= 1.09999E-01  SCOMB(2)= 1.63254E-01  SCOMB(3)= 1.18002E-01  SCOMB(4)= 1.14028E-01;
FB(1)= 3.19999E-02     FB(2)= 4.96893E-03     FB(3)= 3.05493E-03     FB(4)= 2.55803E-03;

C(1)= 6.52104E+01      C(2)= 3.71041E+01      C(3)= 1.82147E+01      C(4)= 8.63579E+00;
F= 2.51558E+00         FFB= 3.77142E-01       FFE= 2.13823E+00       TN= 7.04678E+00;
DUMP3(1)=-3.51278E-01  DUMP3(2)= 1.17040E+00  DUMP3(3)= 1.22977E+00  DUMP3(4)= 1.23220E+00;
U(1)= 1.80000E+01      U(2)= 4.00000E+00      U(3)= 2.00000E+00      U(4)= 1.00000E+00;

CFE(1)= 5.43900E-03    CFE(2)= 8.73458E-03    CFE(3)= 5.79181E-03    CFE(4)= 3.60140E-03;
FE(1)= 1.79999E-01     FE(2)= 5.23427E-03     FE(3)= 4.79580E-03     FE(4)= 4.42663E-03;
SCOMB(1)= 1.09999E-01  SCOMB(2)= 1.04980E-01  SCOMB(3)= 8.66928E-02  SCOMB(4)= 8.95226E-02;
FB(1)= 3.32545E-02     FB(2)= 3.49208E-03     FB(3)= 2.64679E-03     FB(4)= 2.00717E-03;

U(1)= 6.47826E+01      C(2)= 3.79342E+01      C(3)= 1.87943E+01      C(4)= 9.20109E+00;

CFE(1)= 5.35145E-03    CFE(2)= 8.52533E-03    CFE(3)= 5.50983E-03    CFE(4)= 3.26744E-03;
FE(1)= 1.79991E-01     FE(2)= 5.15488E-03     FE(3)= 4.75675E-03     FE(4)= 4.48647E-03;
SCOMB(1)= 1.09999E-01  SCOMB(2)= 1.03704E-01  SCOMB(3)= 9.60026E-02  SCOMB(4)= 9.09849E-02;
FB(1)= 3.32182E-02     FB(2)= 3.42241E-03     FB(3)= 2.58662E-03     FB(4)= 1.93863E-03;

C(1)= 6.56440E+01      C(2)= 3.87156E+01      C(3)= 1.94252E+01      C(4)= 9.67947E+00;

CFE(1)= 5.32917E-03    CFE(2)= 8.48735E-03    CFE(3)= 5.47105E-03    CFE(4)= 3.23535E-03;
FE(1)= 1.79997E-01     FE(2)= 5.19385E-03     FE(3)= 4.81001E-03     FE(4)= 4.58068E-03;
SCOMB(1)= 1.09999E-01  SCOMB(2)= 1.04318E-01  SCOMB(3)= 9.71361E-02  SCOMB(4)= 9.29349E-02;
FB(1)= 3.32142E-02     FB(2)= 3.42016E-03     FB(3)= 2.57045E-03     FB(4)= 1.95418E-03;

C(1)= 6.59484E+01      C(2)= 3.89613E+01      C(3)= 1.95866E+01      C(4)= 9.78833E+00;
```

TABLE A10.1 (CONT.)

```
CFE(1)= 5.32713E-03    CFE(2)= 8.48515E-03    CFE(3)= 5.47083E-03    CFE(4)= 3.23029E-03;
FE(1)= 1.80000E-01     FE(2)= 5.20670E-03     FE(3)= 4.83020E-03     FE(4)= 4.60718E-03;
SCOMB(1)= 1.00000E-01  SCOMB(2)= 1.04582E-01  SCOMB(3)= 9.75208E-02  SCOMB(4)= 9.34740E-02;
FB(1)= 3.32143E-02     FB(2)= 3.42282E-03     FB(3)= 2.57522E-03     FB(4)= 1.96178E-03;

C(1)= 6.60121E+01      C(2)= 3.90094E+01      C(3)= 1.96271E+01      C(4)= 9.80516E+00;

CFE(1)= 5.32750E-03    CFE(2)= 8.48626E-03    CFE(3)= 5.47266E-03    CFE(4)= 3.24213E-03;

FE(1)= 1.80000E-01     FE(2)= 5.20964E-03     FE(3)= 4.83415E-03     FE(4)= 4.61187E-03;
SCOMB(1)= 1.00000E-01  SCOMB(2)= 1.04641E-01  SCOMB(3)= 9.76101E-02  SCOMB(4)= 9.35684E-02;
FB(1)= 3.32145E-02     FB(2)= 3.42383E-03     FB(3)= 2.57668E-03     FB(4)= 1.96367E-03;

C(1)= 6.60213E+01      C(2)= 3.90160E+01      C(3)= 1.96309E+01      C(4)= 9.80700E+00;

CFE(1)= 5.32772E-03    CFE(2)= 8.48672E-03    CFE(3)= 5.47324E-03    CFE(4)= 3.24281E-03;
FE(1)= 1.80001E-01     FE(2)= 5.21000E-03     FE(3)= 4.83471E-03     FE(4)= 4.61244E-03;
SCOMB(1)= 1.00000E-01  SCOMB(2)= 1.04650E-01  SCOMB(3)= 9.76211E-02  SCOMB(4)= 9.35796E-02;
FB(1)= 3.32146E-02     FB(2)= 3.42405E-03     FB(3)= 2.57696E-03     FB(4)= 1.96398E-03;

C(1)= 6.60225E+01      C(2)= 3.90166E+01      C(3)= 1.96313E+01      C(4)= 9.80714E+00;
TIM= 3.60000E+01       COUNT=      6          TIN=      216;
     SUM OF COMBUSTION IN BED                0.75085   UNBURNT AIR IN STACK                0.35240
     COARSE FINES BURNING IN FREEBOARD       0.01968   FINE FINES BURNING IN FREEBOARD     0.07707
     FREEBOARD FINES ELUTRIATED              0.15230
     TOTAL COMBUSTION                        0.84759   AVERAGE CARBON LOST                 0.99990

S(1)= 7.53185E-01      S(2)= 3.82709E-01      S(3)= 1.84374E-01      S(4)= 9.23654E-02;
```

TABLE A10.2. DATA FORMAT FOR FLUMX

KA1, AX, B, BY, NOL, KC1, T, TC1, V, PA, PB, XC, XE,

XO, ETA, TC, TT.

ZZ = Values of the parameter that the investigation is to cover

ZZ = -1.

TABLE A10.3 INITIAL MASS-SIZE DISTRIBUTION / SEGMENT

MU	SIZE	1	2	3	4
1	1378	8.4925E-02	1.0861E-02	1.0233E-03	9.1262E-05
2	1357	1.2763E-01	2.1409E-02	2.5004E-03	2.6625E-04
3	1335	1.7049E-01	3.5158E-02	4.8857E-03	6.0386E-04
4	1314	2.1351E-01	5.1992E-02	8.3498E-03	1.1733E-03
5	1292	2.5670E-01	7.1631E-02	1.3041E-02	2.0505E-03
6	1270	3.0005E-01	9.4037E-02	1.9087E-02	3.3162E-03
7	1249	3.4357E-01	1.1901E-01	2.6592E-02	5.0538E-03
8	1227	3.8727E-01	1.4639E-01	3.5642E-02	7.3472E-03
9	1206	4.3113E-01	1.7602E-01	4.6300E-02	1.0279E-02
10	1184	4.7517E-01	2.0773E-01	5.8611E-02	1.3929E-02
11	1162	5.1939E-01	2.4137E-01	7.2600E-02	1.8373E-02
12	1141	5.6380E-01	2.7677E-01	8.8271E-02	2.3678E-02
13	1119	6.0838E-01	3.1376E-01	1.0561E-01	2.9906E-02
14	1098	6.5315E-01	3.5219E-01	1.2459E-01	3.7108E-02
15	1076	6.9810E-01	3.9189E-01	1.4516E-01	4.5326E-02
16	1054	7.4325E-01	4.3270E-01	1.6724E-01	5.4589E-02
17	1033	7.8859E-01	4.7444E-01	1.9077E-01	6.4914E-02
18	1011	8.3412E-01	5.1696E-01	2.1563E-01	7.6304E-02
19	990	8.7986E-01	5.6008E-01	2.4172E-01	8.8747E-02
20	968	9.2579E-01	6.0363E-01	2.6895E-01	1.0222E-01
21	946	9.7193E-01	6.4745E-01	2.9703E-01	1.1668E-01
22	925	1.0183E+00	6.9136E-01	3.2596E-01	1.3206E-01
23	903	1.0648E+00	7.3526E-01	3.5566E-01	1.4830E-01
24	882	1.1116E+00	7.7879E-01	3.8549E-01	1.6531E-01
25	860	1.1585E+00	8.2195E-01	4.1572E-01	1.8297E-01
26	838	1.2057E+00	8.6451E-01	4.4600E-01	2.0117E-01
27	817	1.2531E+00	9.0630E-01	4.7612E-01	2.1977E-01
28	795	1.3007E+00	9.4714E-01	5.0584E-01	2.3861E-01
29	774	1.3486E+00	9.8695E-01	5.3495E-01	2.5753E-01
30	752	1.3966E+00	1.0252E+00	5.6320E-01	2.7636E-01
31	730	1.4449E+00	1.0621E+00	5.9037E-01	2.9489E-01
32	709	1.4934E+00	1.0974E+00	6.1620E-01	3.1292E-01
33	687	1.5422E+00	1.1307E+00	6.4046E-01	3.3026E-01
34	666	1.5911E+00	1.1620E+00	6.6290E-01	3.4667E-01
35	644	1.6403E+00	1.1911E+00	6.8327E-01	3.6193E-01
36	622	1.6897E+00	1.2178E+00	7.0133E-01	3.7583E-01
37	601	1.7393E+00	1.2418E+00	7.1684E-01	3.8814E-01
38	579	1.7891E+00	1.2630E+00	7.2957E-01	3.9862E-01
39	558	1.8392E+00	1.2812E+00	7.3931E-01	4.0708E-01
40	536	1.8894E+00	1.2962E+00	7.4582E-01	4.1330E-01
41	514	1.9398E+00	1.3077E+00	7.4893E-01	4.1709E-01
42	493	1.9904E+00	1.3157E+00	7.4843E-01	4.1828E-01
43	471	2.0412E+00	1.3198E+00	7.4418E-01	4.1671E-01
44	450	2.0922E+00	1.3198E+00	7.3602E-01	4.1227E-01
45	428	2.1432E+00	1.3156E+00	7.2384E-01	4.0485E-01
46	406	2.1944E+00	1.3069E+00	7.0756E-01	3.9440E-01
47	385	2.2456E+00	1.2935E+00	6.8712E-01	3.8091E-01
48	363	2.2968E+00	1.2752E+00	6.6253E-01	3.6442E-01
49	342	2.3480E+00	1.2517E+00	6.3380E-01	3.4501E-01
50	320	2.3990E+00	1.2228E+00	6.0104E-01	3.2285E-01
51	298	2.4498E+00	1.1883E+00	5.6440E-01	2.9817E-01
52	277	2.5002E+00	1.1479E+00	5.2410E-01	2.7125E-01
53	255	2.5501E+00	1.1014E+00	4.8043E-01	2.4249E-01
54	234	2.5992E+00	1.0484E+00	4.3380E-01	2.1235E-01
55	212	2.6472E+00	9.8889E-01	3.8472E-01	1.8142E-01
56	190	2.6937E+00	9.2247E-01	3.3379E-01	1.5035E-01
57	169	2.7379E+00	8.4895E-01	2.8183E-01	1.1991E-01
58	147	2.7788E+00	7.6816E-01	2.2980E-01	9.0969E-02

TABLE A10.3 (CONT.) FINAL MASS - SIZE DISTRIBUTION / SEGMENT

MU	SIZE	1	2	3	4
1	1378	3.9464E-01	1.5218E-01	2.3972E-02	1.3769E-03
2	1357	5.1394E-01	2.4433E-01	4.9642E-02	3.5572E-03
3	1335	5.9392E-01	3.0991E-01	8.6780E-02	8.7594E-03
4	1314	6.5573E-01	3.6316E-01	1.1694E-01	1.9012E-02
5	1292	7.1595E-01	4.0994E-01	1.4709E-01	3.0152E-02
6	1270	7.6418E-01	4.5660E-01	1.7421E-01	4.2049E-02
7	1249	8.0534E-01	4.8569E-01	2.0013E-01	5.5209E-02
8	1227	8.4172E-01	5.1659E-01	2.2380E-01	6.9926E-02
9	1206	8.7425E-01	5.4409E-01	2.4563E-01	8.4454E-02
10	1184	9.0366E-01	5.6885E-01	2.6574E-01	9.8783E-02
11	1162	9.2659E-01	5.9128E-01	2.8441E-01	1.1307E-01
12	1141	9.5547E-01	6.1181E-01	3.0175E-01	1.2730E-01
13	1119	9.7861E-01	6.3070E-01	3.1786E-01	1.4094E-01
14	1098	1.0002E+00	6.4810E-01	3.3281E-01	1.5392E-01
15	1076	1.0206E+00	6.6422E-01	3.4668E-01	1.6618E-01
16	1054	1.0397E+00	6.7914E-01	3.5951E-01	1.7783E-01
17	1033	1.0578E+00	6.9299E-01	3.7132E-01	1.8870E-01
18	1011	1.0750E+00	7.0593E-01	3.8216E-01	1.9857E-01
19	990	1.0913E+00	7.1771E-01	3.9211E-01	2.0764E-01
20	968	1.1068E+00	7.2870E-01	4.0119E-01	2.1601E-01
21	946	1.1214E+00	7.3861E-01	4.0941E-01	2.2354E-01
22	925	1.1354E+00	7.4809E-01	4.1681E-01	2.3027E-01
23	903	1.1486E+00	7.5657E-01	4.2341E-01	2.3627E-01
24	882	1.1612E+00	7.6424E-01	4.2922E-01	2.4156E-01
25	860	1.1731E+00	7.7114E-01	4.3425E-01	2.4609E-01
26	838	1.1844E+00	7.7729E-01	4.3852E-01	2.4989E-01
27	817	1.1951E+00	7.8269E-01	4.4204E-01	2.5299E-01
28	795	1.2052E+00	7.8737E-01	4.4481E-01	2.5539E-01
29	774	1.2149E+00	7.9133E-01	4.4685E-01	2.5708E-01
30	752	1.2239E+00	7.9457E-01	4.4817E-01	2.5809E-01
31	730	1.2325E+00	7.9712E-01	4.4877E-01	2.5843E-01
32	709	1.2406E+00	7.9898E-01	4.4866E-01	2.5811E-01
33	687	1.2483E+00	8.0018E-01	4.4786E-01	2.5713E-01
34	666	1.2556E+00	8.0066E-01	4.4637E-01	2.5550E-01
35	644	1.2625E+00	8.0049E-01	4.4420E-01	2.5325E-01
36	622	1.2691E+00	7.9967E-01	4.4136E-01	2.5039E-01
37	601	1.2752E+00	7.9816E-01	4.3785E-01	2.4693E-01
38	579	1.2812E+00	7.9601E-01	4.3368E-01	2.4288E-01
39	558	1.2868E+00	7.9314E-01	4.2886E-01	2.3827E-01
40	536	1.2923E+00	7.8966E-01	4.2337E-01	2.3309E-01
41	514	1.2975E+00	7.8546E-01	4.1723E-01	2.2737E-01
42	493	1.3026E+00	7.8056E-01	4.1044E-01	2.2112E-01
43	471	1.3076E+00	7.7496E-01	4.0298E-01	2.1434E-01
44	450	1.3125E+00	7.6861E-01	3.9486E-01	2.0706E-01
45	428	1.3175E+00	7.6149E-01	3.8606E-01	1.9929E-01
46	406	1.3224E+00	7.5356E-01	3.7657E-01	1.9102E-01
47	385	1.3275E+00	7.4477E-01	3.6637E-01	1.8230E-01
48	363	1.3329E+00	7.3506E-01	3.5544E-01	1.7312E-01
49	342	1.3386E+00	7.2439E-01	3.4379E-01	1.6352E-01
50	320	1.3446E+00	7.1253E-01	3.3133E-01	1.5349E-01
51	298	1.3512E+00	6.9948E-01	3.1805E-01	1.4307E-01
52	277	1.3585E+00	6.8502E-01	3.0389E-01	1.3228E-01
53	255	1.3667E+00	6.6894E-01	2.8879E-01	1.2114E-01
54	234	1.3761E+00	6.5097E-01	2.7266E-01	1.0969E-01
55	212	1.3869E+00	6.3069E-01	2.5541E-01	9.7970E-02
56	190	1.3998E+00	6.0762E-01	2.3652E-01	8.6034E-02
57	169	1.4152E+00	5.8102E-01	2.1702E-01	7.3952E-02
58	147	1.4341E+00	5.4987E-01	1.9551E-01	6.1817E-02

A P P E N D I X 1 1

THE TRANSIENT MODE PROGRAM DETAILS

The following is a list of the details in connection with the computer program of the transient mode of the model contained in this Appendix:

LISTING A11.1 FLUTRA-PROGRAM OF TRANSIENT MODE

```
FLUTRA:PROC OPTIONS (MAIN);
        DECLARE CHARLI FILE PRINT;
        OPEN FILE(CHARLI) LINESIZE(132);
        OPEN FILE(SYSPRINT) LINESIZE(132);
        DCL(TRAFB,TRAFE)(1) CTL;
        DCL(A,RAT,TRCFB,TRCFE,CCMB,TCT) (1,1) CTL;
       DCL (C,E,S,GAMMA,SCCMB)(1) CTL;
       DCL(AFB,AFE,CFB,CFE)(1) CTL;
       DCL DDT CHAR(8), DTE CHAR(6),K1 DECIMAL,K2 DECIMAL;
       DTE=DATE;
       DDT=SUBSTR(DTE,5,2)||'/'||SUBSTR(DTE,3,2)||'/'||
       SUBSTR(DTE,1,2);
       TYME=TIME;
       PUT EDIT(DDT,TYME) (SKIP,A(9),X(10),F(8,0));
       PUT FILE (CHARLI) EDIT(DDT,TYME) (SKIP,A(9),X(10),F(8,0));
  LPC: DO KOND=1 TO 6;
       CCUNT,TCCMB,TFB,FRDC,FRDFE,SUM=0;
       GET LIST(N) SKIP;
       PUT LIST(N)PAGE;
       NCS=TRUNC((N+1)*.5+.5) ;
       GET LIST(NCL) SKIP;
       ALLOCATE A(NCS,NCL),C(NCS),E(NCS),S(NCS),GAMMA(NCS);
       ALLOCATE SCCMB(NCS),AFB(NCS),AFE(NCS),CFE(NCS),CFE(NCS);
       ALLOCATE CCMB(NCS,NCL),RAT(NCS,NCL);
        ALLOCATE TRAFB(NCS),TRAFE(NCS);
        ALLOCATE TRCFB(NCS,NCL),TRCFE(NCS,NCL),TCT(NCS,NCL);
       A=0 ;
       C,E,S,GAMMA,SCCMB,TRAFE,TRAFB,AFE,AFE,CFE,CFE=C;
       RAT,TCT,TRCFE,TRCFB,CCME =0;
        TCCMB=0 ;
       GET LIST(E(NCS),C,S,B,PFFE,PFFB) SKIP;
        GET LIST(SCCMB,V,F,AFB) SKIP;
        GET LIST(AFE,CFB) SKIP ;
        GET LIST(CFE,XE,XC,PRCP2,T,P,REF) SKIP;
       PUT FILE(CHARLI) DATA(REF) SKIP;
       TX=T;
       PRCP1=1-(XE/XC)**3;
       E=E(NOS)*S/S(NOS);
       E=(E<1)*E+(E>1)*1;
LP20:  DO J=1 TO NCS;
       A(J,1)=C(J)/NCL;
 LP22: DO LAY=2 TO NCL;
       A(J,LAY)=A(J,1)/*INITIAL CONCENTRATIONS IN EACH LAYER*/;
       END LP20;
   GET LIST(K1,K2) SKIP;
       A=A/K1 ;
 ONE:   IF COUNT>=REF THEN GO TO LAST;
```

LISTING A11.1 (CONT.) FLUTRA

```
        DO J=1 TO NCS/*VERTICAL MIXING ALGORITHM*/;
         IF J¬=1 THEN GO TO J14;
         IF T<1.5 THEN GO TO J12;
         DO LAY=1 TO NCL/*ADD COARSE FEED TO ALL LAYERS IF T LARGE*/
         A(J,LAY)=A(J,LAY)+(1-.01*V-PFFE-PFFB)*T/NCL;
         END;
         GO TO J14;
  J12:   A(J,1)=A(J,1)+(1-.01*V-PFFE-PFFB)/*ADD COARSE FEED WHEN T=1
  J14:   ALCASH=A(J,1);
        G,R=0;
  LP3C:  DO LAY=1 TO NCL-1;
        AL=F*ALCASH;
        SB=F*(G+R);
        D=(1-F)*A(J,LAY+1);
        A(J,LAY)=AL+SB+D;
        ALDASH=(1-F)/F*AL;
        G=(1-F)/F*SB;
        R=F*A(J,LAY+1);
        END LP30;
        A(J,NCL)=ALCASH+G+R;
        END ;
        Z4=(MOD(N,2)<.1);
         IF T<1.5 THEN GO TO J16;
  LP34:  DO LAY=1 TO NCL/*LATERAL MIXING ALGORITHM ALL LAYERS*/;
         Z1=A(2,LAY);
  LP36:   DO J=1 TO NCS;
         Z2=A(J,LAY);
        IF J¬=NCS THEN DO;
        A(J,LAY)=Z2+B*T/NCL*(Z1-2*Z2+A(J+1,LAY));
        GO TO J15;
        END;
        A(J,LAY)=Z2+B*T/NCL*(Z1-2*Z2+Z1*Z4+Z2*(Z4<.5));
  J15:   Z1 =Z2;
         END LP34;
         GO TO J168;
  J16:   Z1=A(2,NCL);
  LP4C:  DO J=1 TO NCS/*LATERAL MIXING ALGORITHM*/;
        Z2=A(J,NCL);
        IF J¬=NCS THEN DO;
        A(J,NCL)=A(J,NCL)+B*(Z1-2*Z2+A(J+1,NCL));
        GO TO J17;
        END;
        A(J,NCL)=A(J,NCL)+B*(Z1-2*Z2+Z1*Z4+Z2*(Z4<.5));
  J17:  Z1=Z2;
        END LP40;
  J168: IF COUNT>.5 THEN GO TO LP50;
         DO J=1 TO NCS;
```

LISTING A11.1 (CONT.) FLUTRA

```
          IF T<1.5 THEN DO;
        GAMMA(J)=SCOMB(J)/(A(J,1)*K1);
         GO TO J165;
        END;
         GAMMA(J)=SCOMB(J)/(A(J,1)*K1)*T/NCL;
J165:    ;
         END ;
        IF GAMMA(NCS)<1 THEN GO TO J8;
         T=TRUNC(A(NCS,1)/SCOMB(NCS))*NCL;
J8:     IF (2*T*B/NCL)<1 THEN GO TO J10;
       T=NCL/(B*2);
J10:   T=TRUNC(T/NCL)*NCL;
       IF T<NCL THEN T=1;
          IF T¬=TX THEN DO;
      PUT FILE(CHARLI) SKIP DATA(T);
        PUT LIST (T);
         TX=T;
        GO TO J168;
         END;
LP50:    DO J=1 TO NCS;
        /*CALCULATE NEW COMBUSTION DURING TRANSITION PERIOD*/;
LP51:    DO LAY=1 TO NCL;
         IF J¬=1 THEN GO TO J19;
        IF (T<1.5)&(LAY>1) THEN GO TO J39;
        IF LAY¬=1 THEN GO TO J18;
         COMB(1,1)=(.01*V+PFFB)*((K2>K1)+(K2<=K1)*K2/K1)*((T>1)*T/NC
        +(T<1.5));
J18:     COMB(1,LAY)=COMB(1,1);
         GO TO J20;
J19:     IF (T<1.5)&(LAY>1) THEN GO TO J39;
       CTEST=SCOMB(J)*K2/K1*((T>1)*T/NCL+(T<1.5))-A(J,LAY)*GAMMA(J);
        IF CTEST<0 THEN CTEST=0;
        COMB(J,LAY)=A(J,LAY)*GAMMA(J)+B(J)*CTEST;
        IF COMB(J,LAY)>.8*A(J,LAY) THEN COMB(J,LAY)=.8*A(J,LAY);
        A(J,LAY)=A(J,LAY)-COMB(J,LAY);
J20:   RAT(J,LAY)=COMB(J,LAY)/SCOMB(J)*K2/K1;
          IF (J=1)|((J=NCS)&(MCC(N,2)<.01)) THEN Z=1; ELSE Z=2;
       TCOMB=TCOMB+Z/T*COMB(J,LAY);
        TRAFB(J)=AFB(J)*RAT(J,LAY)/NCL;
        TRAFE(J)=AFE(J)*RAT(J,LAY)/NCL;
        TRCFB(J,LAY)=CFB(J)*RAT(J,LAY);
        TRCFE(J,LAY)=CFE(J)*RAT(J,LAY);
        Q=1;
        TOT(J,LAY)=TRAFB(J)+TRAFE(J)+TRCFB(J,LAY)+TRCFE(J,LAY);
J30:   IF Q*TOT(J,LAY)>.8*A(J,LAY) THEN DO;
        Q=Q*.8;
        GO TO J30;
```

LISTING A11.1 (CONT.) FLUTRA

```
      END;
      A(J,LAY)=A(J,LAY)-G*(TRCFF(J,LAY)+TRCFE(J,LAY));
      TFB=TFB+G*Z/T*(TRCFB(J,LAY)+TRAFB(J)*NCL);
      TCFE=TCFE+G*Z/T*TRCFE(J,LAY);
     TAFE=TAFE+G*Z/T*TRAFE(J)*NCL;
LP52: DO LAY1=1 TO NCL;
      A(J,LAY1)=A(J,LAY1)-G*(TRAFE(J)+TRAFB(J));
     END LP52;
     END LP51;
J39:  END LP5C;
 PB=TCCMB+TFB;
      SUM=TCCMB+TFB+TCFE+TAFE+FFFE;
     FRBC=TCFE*PROP1;
     FRBFE=TCFE-FRBC;
     TAFE=TAFE+FRBFE;
     FRBC=FRBC+TAFE*PROP2;
     FRBFL=FRBFE+TAFE-FRBC+FFFE;
     CCUNT=CCUNT+1;
     IF CCUNT<1.5 THEN DO;
     PUT DATA(N)SKIP; PUT FILE(CHARLI)DATA(N)SKIP;
      PUT EDIT('COARSE COMB ',' FINES COME ',
      '  BED COME  ',' FRB COMB  ',' ELUT  ',' TOT CARBON  '
      (SKIP,(6) (X(4),A(12),X(4)));
      PUT FILE (CHARLI) EDIT('COARSE COMF ',' FINES COMB ',
      '  BED COMB  ',' FRB COMB  ',' ELUT  ',' TOT CARBON  '
      (SKIP,(6) (X(4),A(12),X(4)));
     END;
    IF (MOD(COUNT,P)<.5)|(CCUNT<1.5) THEN DO;
     PUT FILE(CHARLI) DATA(CCUNT) SKIP;
    DO J=1 TO NCS;
     SEGKCL=0;
    DO LAY=1 TO NCL;
     SEGKCL=SEGKCL+A(J,LAY);
    END;
     PUT DATA(J,SEGKCL)SKIP;
     PUT FILE (CHARLI) DATA(J,SEGKCL)SKIP;
    END;
     P=P*2 ;
    PUT EDIT(TCCMB,TFB,PB,FRBC,FRBFE,SUM)(SKIP,(6) (E(15,4),X(5)
     PUT FILE(CHARLI) EDIT(TCCMB,TFB,PB,FRBC,FRBFE,SUM)
      (SKIP,(6) (E(15,4),X(5)));
     PUT FILE(CHARLI) SKIP;
     END;
     TCCMB,SUM,TFB,FRBC,FRBFE,TCFE,TAFE=0;
     GO TO CNE;
LAST: FREE A,C,E,S,GAMMA,SCCME,AFB,AFE,CFB,CFE,CCME;
     FREE RAT,TRAFB,TRAFE,TRCFE,TRCFB,TCT;
```

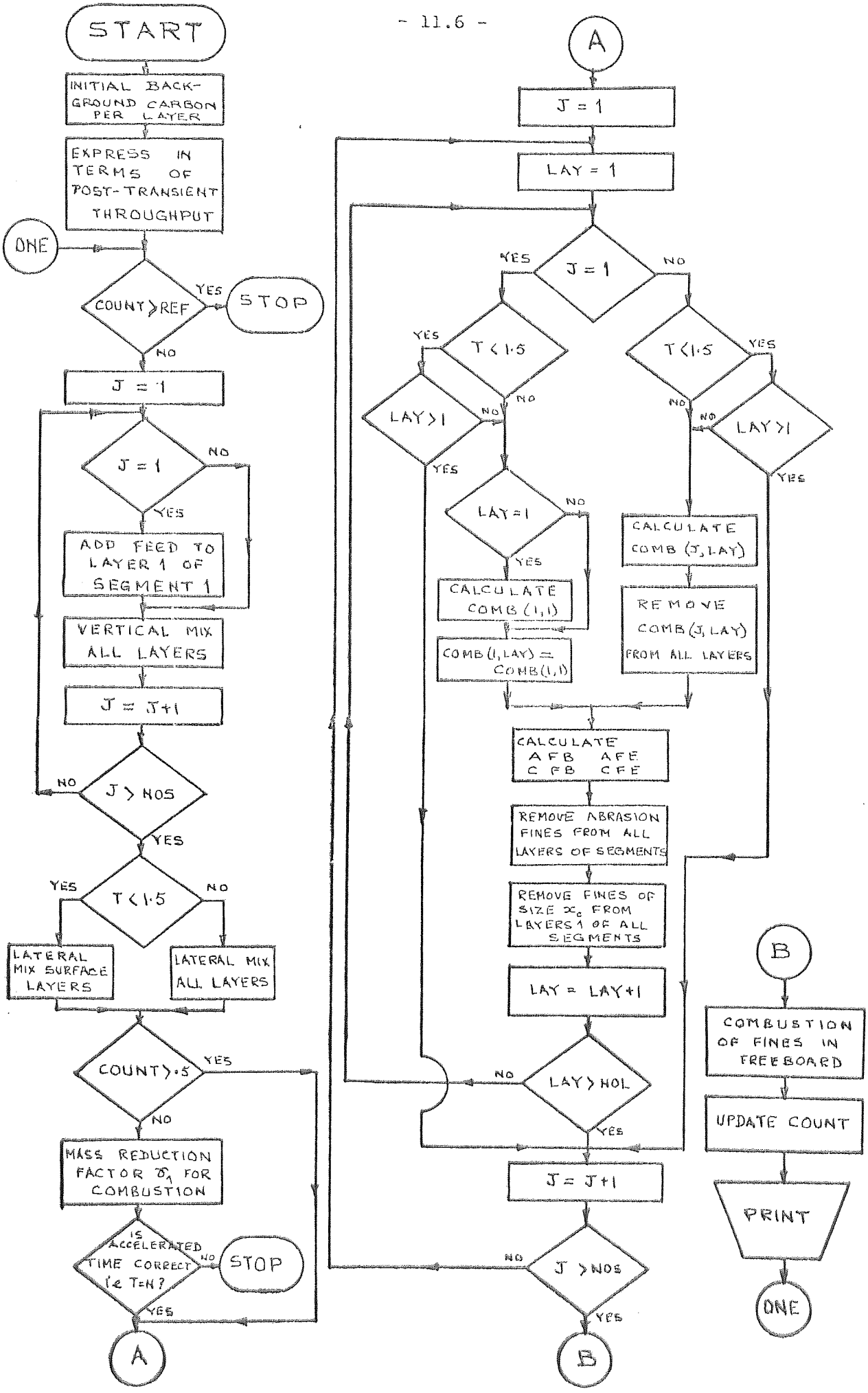

FIG. A 11.1 FLOWCHART OF TRANSIENT MODE — FLUTRA

TABLE A11.1 TYPICAL PRINTOUT FROM FLUTRA FOR THE TRANSIENT MODE (N = 7)

COARSE COMB	FINES COMB	BED COMB	FRB COMB	ELUT	TOT CARBON
COUNT= 1.00000E+00;					
J= 1	SEGKOL= 5.24322E+01;				
J= 2	SEGKOL= 3.05109E+01;				
J= 3	SEGKOL= 1.65909E+01;				
J= 4	SEGKOL= 1.12115E+01;				
6.7366E-01	1.5973E-02	6.8963E-01	3.2153E-02	1.9740E-01	9.1884E-01
COUNT= 2.00000E+00;					
J= 1	SEGKOL= 5.26447E+01;				
J= 2	SEGKOL= 3.04620E+01;				
J= 3	SEGKOL= 1.65825E+01;				
J= 4	SEGKOL= 1.12001E+01;				
6.6905E-01	1.5858E-02	6.8491E-01	3.1932E-02	1.9716E-01	9.1366E-01
COUNT= 4.00000E+00;					
J= 1	SEGKOL= 5.30734E+01;				
J= 2	SEGKOL= 3.03654E+01;				
J= 3	SEGKOL= 1.65662E+01;				
J= 4	SEGKOL= 1.11816E+01;				
6.6190E-01	1.5679E-02	6.7758E-01	3.1588E-02	1.9678E-01	9.0562E-01
COUNT= 8.00000E+00;					
J= 1	SEGKOL= 5.38975E+01;				
J= 2	SEGKOL= 3.01982E+01;				
J= 3	SEGKOL= 1.65363E+01;				
J= 4	SEGKOL= 1.11588E+01;				
6.5152E-01	1.5422E-02	6.6704E-01	3.1092E-02	1.9624E-01	8.9405E-01
COUNT= 1.60000E+01;					
J= 1	SEGKOL= 5.53387E+01;				
J= 2	SEGKOL= 2.99866E+01;				
J= 3	SEGKOL= 1.64761E+01;				
J= 4	SEGKOL= 1.11281E+01;				
6.4865E-01	1.5339E-02	6.6399E-01	3.0927E-02	1.9607E-01	8.9066E-01

TABLE A11.1 (CONT.) FLUTRA

COUNT= 3.20000E+01;					
J= 1	SEGKOL= 5.76028E+01;				
J= 2	SEGKOL= 2.98920E+01;				
J= 3	SEGKOL= 1.63619E+01;				
J= 4	SEGKOL= 1.10589E+01;				
6.4585E-01	1.5262E-02	6.6111E-01	3.0774E-02	1.9592E-01	8.8747E-01
COUNT= 6.40000E+01;					
J= 1	SEGKOL= 6.06101E+01;				
J= 2	SEGKOL= 3.03588E+01;				
J= 3	SEGKOL= 1.62048E+01;				
J= 4	SEGKOL= 1.09397E+01;				
6.4496E-01	1.5252E-02	6.6021E-01	3.0762E-02	1.9589E-01	8.8653E-01
COUNT= 1.28000E+02;					
J= 1	SEGKOL= 6.39559E+01;				
J= 2	SEGKOL= 3.18653E+01;				
J= 3	SEGKOL= 1.65729E+01;				
J= 4	SEGKOL= 1.09674E+01;				
6.5301E-01	1.5494E-02	6.6850E-01	3.1256E-02	1.9637E-01	8.9579E-01
COUNT= 2.56000E+02;					
J= 1	SEGKOL= 6.73648E+01;				
J= 2	SEGKOL= 3.42740E+01;				
J= 3	SEGKOL= 1.78105E+01;				
J= 4	SEGKOL= 1.17187E+01;				
6.7865E-01	1.6182E-02	6.9483E-01	3.2610E-02	1.9778E-01	9.2487E-01
COUNT= 5.12000E+02;					
J= 1	SEGKOL= 7.05268E+01;				
J= 2	SEGKOL= 3.68487E+01;				
J= 3	SEGKOL= 1.96206E+01;				
J= 4	SEGKOL= 1.30833E+01;				
7.1499E-01	1.7122E-02	7.3211E-01	3.4440E-02	1.9973E-01	9.6591E-01
COUNT= 1.02400E+03;					
J= 1	SEGKOL= 7.24665E+01;				
J= 2	SEGKOL= 3.84571E+01;				
J= 3	SEGKOL= 2.08226E+01;				
J= 4	SEGKOL= 1.40203E+01;				
7.3968E-01	1.7760E-02	7.5744E-01	3.5683E-02	2.0105E-01	9.9379E-01

TABLE A11.2. DATA FORMAT FOR FLUTRA

e, C(1), C(2), ... C(NOS), S(1), S(2), ... S(NOS), B, PFFE,

PFFB, SCOMB(1), SCOMB(2), ... SCOMB(NOS), V, F, AFB(1),

AFB(2), ... AFB(NOS), AFE(1), AFE(2), ... AFE(NOS),

CFB(1), CFB(2), ... CFB(NOS), CFE(1), CFE(2), ... CFE(NOS),

XE, XC, PROP2, T, P, REF

LISTING A11.2 XLATE - TRANSLATION PROGRAM (FLUMX/FLUTRA)

```
GET LIST(N);
NOS=TRUNC((N+1)*.5+.5);
DECLARE FE(1) CONTROLLED , CFE(1) CONTROLLED , FB(1) CONTROLLED , X(1) CONTROLLED , Y(1) CONTROLLE
O R I N G C )
DECLARE cfe(1) CONTROLLED , afe(1) CONTROLLED , cfb(1) CONTROLLED afb(1) CONTROLLED ;
ALLOCATE FE(NOS),CFE(NOS),FB(NOS),X(NOS),Y(NOS),D(NOS),cfe(NOS),afe(NOS),cfb(NOS),afb(NOS);
EVEN=MOD(N+1,2);
GET LIST(PFFB,PFFE);
GET LIST(FE,CFE,FB);
FB(1)=FB(1)-PFFB;
cfe=CFE;
cfe(NOS)=cfe(NOS)*(EVEN+1);
afe=FE;
afe(1)=afe(1)-PFFE;
afe(NOS)=afe(NOS)*(EVEN+1);
D=afe+CFE;
D(NOS)=D(NOS)+CFE(NOS)*EVEN;
X=afe/D;
Y=CFE/D;
Y(NOS)=Y(NOS)*(EVEN+1);
afb=FB*X;
afb(NOS)=afb(NOS)*(EVEN+1);
cfb=FB*Y;
cfb(NOS)=cfb(NOS)*(EVEN+1);
PUT LIST('');
PUT LIST('    N=',N);
PUT LIST('');
PUT LIST('afb',afb);
PUT LIST('afe',afe);
PUT LIST('cfb',cfb);
PUT LIST('cfe',cfe);
PUT LIST('');
FREE FE,CFE,FB,X,Y,D,cfe,afe,cfb,afb;
```

TABLE A11.3. FORMATS FOR XLATE

Data from FLUMX

N

PFFB, PFFE

FE(1), FE(2), ... FE(NOS)

CFE(1), CFE(2), ... CFE(NOS)

FB(1), FB(2), ... FB(NOS)

Ouput from FLUTRA

N

AFB(1), AFB(2), ... AFB(NOS)

AFE(1), AFE(2), ... AFE(NOS)

CFB(1), CFB(2), ... CFB(NOS)

CFE(1), CFE(2), ... CFE(NOS)

APPENDIX 12

NOMENCLATURE

Symbol	Description
A	Heat transfer surface area of tubes
H	Heat transfer coefficient
M	Mass of ash in segment
	Mass of ash per layer of segment
n	Number of layers in segment
Q	Heat of combustion released in time T
q	Quantity of heat transfer to tubes in time T
S	Specific heat of bed material
T	Incremental time equal to bubble plug flow through bed height
ψ	Temperature of bed
θ	Steam temperature

APPENDIX 12

HEAT TRANSFER FROM BED TO TUBES

Consider the effect of heat flow by solids movement over a small interval T of time equal to one bubble mix time (T ≈ 0·5 s). T is the time for bubbles to travel through the bed height. Initially, assume all layers to have uniform temperature, so that the initial conditions set the temperature ψ_r of the r th layer as $\psi_r = \psi$.

The heat transfer q_r in a time T from layer r if it contains tubes with steam at temperature Θ is

$$q_r = HA(\psi_r - \Theta) \qquad \ldots\ldots (A12.1)$$

The total heat transferred in time T from n layers with tubes is

$$\sum_{r=1}^{n} q_r = HA \sum_{r=1}^{n} (\psi_r - \Theta) \qquad \ldots\ldots (A12.2)$$

In transferring a quantity q_r of heat in a time T the temperature of layer r having tubes drops by $\Delta\psi_r$ given by

$$q_r = m.s.\ \Delta\psi_r \qquad \ldots\ldots (A12.3)$$

The layer temperature ψ_r' after heat transfer is thus

$$\psi_r' = \psi_r - \Delta\psi_r \qquad \ldots\ldots (A12.4)$$

For thermal conservation the amount Q_1 of heat released by combustion in time T in layer 1 is such that

$$Q_1 = \sum_{r=1}^{n} q_r \qquad \ldots\ldots (A12.5)$$

This heat of combustion when added to layer 1 raises its temperature from ψ_1 to ψ_1'

$$\psi_1' = \psi_1 + Q_1/m_1.s. \qquad \ldots\ldots (A12.6)$$

The temperature of all layers is now defined after heat absorbtion and heat evolution. A bubble mix over the incremental time T results in a fresh set of temperatures for all layers.

TABLE 12.1

Steady state temperature profile through bed height
(after 480 mixes)

Layer	Steam temperature Θ = 356°C				Vertical mixing parameter f = 0·4		
	Vertical mixing parameter f				Steam temperature Θ °C		
	0·1	0·2	0·4	0·8	300	356	500
1	844,06	847.21	856.57	929.27	800.81	856.57	999.96
2	843.33	845.54	852.13	902.60	796.37	852.13	995.52
3	844.07	845.54	849.94	883.20	794.18	849.94	993.33
4	843.72	844.21	846.40	862.71	790.64	846.40	989.79
5	844.36	844.55	845.09	848.93	789.33	845.09	988.48
6	843.91	843.55	842.44	833.77	786.67	842.44	985.83
7	844.95	844.21	842.01	825.13	786.25	842.01	985.20
8	844.65	843.55	840.25	815.20	784.49	840.25	983.64
9	845.85	844.54	840.69	811.53	784.93	840,69	984.08
10	845.69	844.21	839.81	806.60	784.05	839.81	983.20

TABLE 12.2

Dynamic response of vertical heat flow in segment

Time		All combinations of f and Θ considered
mixes	min	1 - response/step
1	0	1·0
481	2	0·52
961	4	0·27
1441	6	0·14
1921	8	0·07
2401	10	0·037
2881	12	0·019

TABLE 12.3

Relevant parameters used in the computation

Area of segment		9 ft^2
Bed height		$2\frac{1}{2}$ ft
Mass of ash in segment	M	1000 lb
Number of layers	NOL	10
Number of layers with tubes	NOTUBE	5
Area of heat transfer surface of tubes	AREA	5·66 ft^2
Rate of heat release in combustion layer per bubble run time T_1	Q	113·38 Btu/T (0·815 x 10^6 Btu/h)
Specific heat of ash	SP	0·17
Heat transfer coefficient	HC	8·2 x 10^{-3} CHU/degC ft^2 T^1 (100 Btu/degF ft^2 h)

LISTING 12. PROGRAM OF HEAT TRANSFER TO TUBES

```
XSTEP:  PROC OPTIONS(MAIN);
        DCL (TEMPI,TEMP,TUBE,QQ)(15) BINARY FLOAT (53) CONTROLLED;
        DCL(Q,SUM,JDASH,G,R,MEAN,J,F,S,D,M)BINARY FLOAT(53);
        DCL SUMQ(20);
        GET LIST(Q,HC,AREA,THETA,NOL,M,SP,NOTUBE,F);
        ALLOCATE TEMP (NOL),TUBE (NOTUBE),QQ (NOTUBE), TEMPI (NOL) ;
        AREA=AREA/NOTUBE;
        GET LIST(TEMPI)SKIP;
        GET LIST(TUBE)SKIP;
REP:    GET DATA(X)SKIP; IF X<0 THEN STOP;
        PUT SKIP;
        TEMP=TEMPI;
        F=X;
        PUT DATA(AREA,F,HC,M,NOL,NOTUBE,Q,SP,THETA)SKIP;
        Q1=Q;
        JJ=0;
REP2:   PRINT=1;
        N=0;
CYCLE:  SUM=0;
        N=N+1;
L1:     DO I=1 TO NOTUBE;
        QQ(I)=HC*AREA*(TEMP(TUBE(I))-THETA);          Equation 1
        SUM=SUM+QQ(I);                                Equation 2
        END L1;
        TEMP(1)=TEMP(1)+Q1/(M*SP);                    Equation 6
        JDASH=TEMP(1);
        G,R=0;
        MEAN=0;
L2:     DO L=1 TO NOL-1;                              }
        J=F*JDASH;                                    }
        S=F*(G+R);                                    }
        D=(1-F)*TEMP(L+1);                            }  vertical
        TEMP(L)=J+S+D;                                }  mixing
        JDASH=(1-F)/F*J;                              }  algorithm
        G=(1-F)/F*S;                                  }
        R=F*TEMP(L+1);                                }
        MEAN=MEAN+TEMP(L);                            }
        END L2;                                       }
        TEMP(NOL)=JDASH+G+R;
        MEAN=(MEAN+TEMP(NOL))/NOL;
L3:     DO I=1 TO NOTUBE;
        TEMP(TUBE(I))=TEMP(TUBE(I))-QQ(I)/(M*SP);     Equations 3 & 4
        END L3;
        IF JJ>=1 THEN GO TO J2;
        IF N<4000 THEN GO TO CYCLE;
        PUT LIST(TEMP)SKIP;
        PUT EDIT('N          SUM          MEAN')(SKIP,X(8),A(27));
```

LISTING 12. (CONTD) XSTEP

```
XSTEP:  PROC OPTIONS(MAIN);                                          CREOOC
                  JJ,PRINT=1;
                  Q1=Q*1.1;
                  MN=0;
                  GO TO CYCLE;
             J2:  MN=MN+1;
                  IF MOD(MN,PRINT)¬=0 THEN GO TO CYCLE;
                  PRINT=480*PRINT;
                  JJ=JJ+1;
                  SUMO(JJ)=SUM;
                  PUT EDIT(MN,SUM,MEAN)(SKIP,X(6),F(5,0),2 F(13,4));
                  IF MN<5000 THEN GO TO CYCLE;
                  PUT SKIP;
                  DO I=2 TO JJ;
                  E=(SUMO(JJ)-SUMO(I))/(SUMO(JJ)-SUMO(1));
                  PUT LIST(E);
                  END;
                  GO TO REP;
                  END XSTEP;
```